

PROJECT ADMINISTRATION DATA SHEET

ORIGINAL REVISION NO. _____

Project No. E-25-M06(R6152-0A1) GTRC/ XXX DATE 7/11/86

Project Director: Dr. Ramond P. Vito School/ XXX ME _____

Sponsor: American Heart Association

Type Agreement: Grant-In-Aid Agreement dated 7/1/86

Award Period: From 7/1/86 To 6/30/87 2/31/87 (Performance) 6/30/87 (Reports)

Sponsor Amount:	<u>This Change</u>	<u>Total to Date</u>
Estimated: \$	<u>17,380</u>	\$ <u>17,380</u>
Funded: \$	<u>17,380</u>	\$ <u>17,380</u>

Cost Sharing Amount: \$ NONE Cost Sharing No: N/A

Title: Bi-Axial Mechanical Properties of Canine Pericardium

ADMINISTRATIVE DATA OCA Contact Brian J. Lindberg ext. 4820

1) Sponsor Technical Contact: _____ 2) Sponsor Admin/Contractual Matters: _____

~~Mr. Robert B. Copeland, President~~
~~American Heart Association~~
~~Georgia Affiliate~~ see Rev #1
~~Broadview Plaza, Level C~~
~~2581 Piedmont Road, N.E.~~
~~Atlanta, Georgia 30324~~

Defense Priority Rating: N/A Military Security Classification: N/A
(or) Company/Industrial Proprietary: N/A

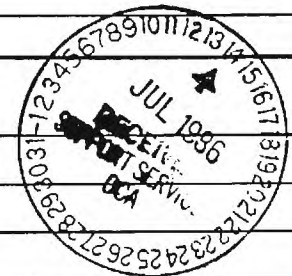
RESTRICTIONS

See Attached N/A Supplemental Information Sheet for Additional Requirements.

Travel: Foreign travel must have prior approval - Contact OCA in each case. Domestic travel requires sponsor approval where total will exceed greater of \$500 or 125% of approved proposal budget category.

Equipment: Title vests with None proposed or anticiapted.

COMMENTS:



COPIES TO: _____ SPONSOR'S I. D. NO. 02.500.011.86.002

Project Director	Procurement/GTRI Supply Services	GTRC
Research Administrative Network	Research Security Services	Library
Research Property Management	Reports Coordinator (OCA)	Project File
Accounting	Research Communications (2)	Other <u>Jones</u>

SPONSORED PROJECT TERMINATION/CLOSEOUT SHEET

Date 2/24/88

Project No. E-25-M06 School/Lab ME

Includes Subproject No.(s) n/a

Project Director(s) R. Vito GTRC/GITX

Sponsor American Heart Association

Title Bi-axial Mechanical Properties of Canine Pericardium

Effective Completion Date: 12/31/87 (Performance) 1/15/88 (Reports)

Grant/Contract Closeout Actions Remaining:

- None
- Final Invoice or Copy of Last Invoice Serving as Final
- Release and Assignment
- Final Report of Inventions and/or Subcontract:
Patent and Subcontract Questionnaire sent to Project Director
- Govt. Property Inventory & Related Certificate
- Classified Material Certificate
- Other _____

Continues Project No. _____ Continued by Project No. _____

COPIES TO:

Project Director
 Research Administrative Network
 Research Property Management
 Accounting
 Procurement/GTRI Supply Services
 Research Security Services
 Reprts Coordinator (OCA)
 Program Administration Division
 Contract Support Division

Facilities Management - ERB
 Library
 GTRC
 Project File
 Other _____

BI-AXIAL MECHANICAL PROPERTIES OF
CANINE PERICARDIUM

by

Raymond P. Vito
Associate Professor
School of Mechanical Engineering
Georgia Institute of Technology
Atlanta, Georgia 30332

SUBMITTED TO:

American Heart Association
Georgia Affiliate
1685 Terrell Mill Road
Marietta, Ga. 30067

Final Report Grant #E25-M06
January 18, 1988

I Investigator
Raymond P. Vito, Ph.D.

Project Title
"Bi-axial Mechanical Properties of Canine Pericardium"

Period of Support
July 1, 1986 - present

II Project Report
Scientific Summary

Abstract

Our key findings may be briefly summarized:

1. We developed a new method for measuring the thickness of pericardial tissue.

2. We were able to measure, for the first time, shear strains in pericardium subjected to in-plane bi-axial deformation.

3. We developed a new experimental technique for determining the material symmetry axis of the pericardium prior to mechanical testing.

4. We were able to reduce the data in sets thereby avoiding the problem of protocol dependent material properties usually associated with bi-axial mechanical testing.

In the following, we elaborate on each of these points. More complete details may be found in Choi (1987) (copy attached).

Methods

Knowledge of mechanical properties is fundamental to the mechanical modeling of the heart in health and disease and also to the design of pericardial heart valves and patches. Accordingly, the bi-axial mechanical properties of canine pericardium were studied in-vitro.

Fresh specimens were obtained from animals used for experimental work not expected to affect the pericardium and stored in cold saline until use; usually within four hours of removal. Specimen dimensions were measured and the specimens mounted in a computer controlled bi-axial testing device. All experiments were conducted in saline at room temperature.

Thickness Measurement

The specimen thickness is difficult to measure accurately and its measurement represents a significant experimental challenge. Accurate measurement of the thickness is important as stresses are calculated using the thickness and measured forces.

Previously reported methods exhibit a large variance in the thickness measurements. A novel technique, utilizing the electrical resistance micrometer shown in Figure (1), was developed during this grant period and seems to eliminate the large effect that fluid surface tension has on such measurements. The basic idea behind this technique is illustrated in Figure (2). The micrometer is advanced until contact with the saline film on the tissue is made. The voltmeter shown indicates when the circuit is complete. When the micrometer is withdrawn from the tissue, a second reading is taken when contact with the saline film is broken. The difference between these two readings is a measure of the surface tension effect. As the saline film evaporates, this effect diminishes. However, some saline must always be present on the tissue to prevent drying and the associated change in mechanical properties. Thus measurements taken over the first ten to twenty minutes may be extrapolated using linear regression to accurately determine the thickness of the tissue. Representative results are shown in Figure (3). The technique has been used on seven specimens and has a measurement to measurement variance of 0.01mm when using the same point of the same tissue. Table (1) shows the point to point thickness variation in a representative specimen (#3).

Strain Measurement

Five particles, placed on the tissue (diam = 250 micron) as shown in Figure (4), are tracked with an image digitizer interfaced to a minicomputer (PDP-11-34). Using this technique, strain measurement is redundant and shear strains can be measured for the first time in any laboratory. Shear strains are always present when the stretching axis and the material axis (assuming orthotropy) do not coincide. Representative results are shown in Figure (5).

Material Symmetry Axis

Shear strains are present almost always since the material axis are not known a-priori and are therefore not likely to coincide with the stretching axis. This is a fundamental problem in bi-axial testing of soft tissues. However, in previous works, this problem is ignored leading to material constants which are incorrect. We attempted to remedy this using two basic approaches:

1. In the first method, the shear strain measurements and the theory are used to determine the unknown angle between the orthotropic axis of the material and the stretching axis. The method relies on the fact that shear strains result from the non-coincidence of the material axis and the stretching axis. Details of this somewhat complex scheme may be found in Choi (1987) (attached).

2. In the second method, we attempted to develop an experimental technique to determine the orthotropic axis of the pericardium and then perform a bi-axial test using coincident material and stretching axis.

We have been unsuccessful to date in implementing option one; probably due to the non-uniqueness inherent in many non-linear problems.

For option two, several different protocols were attempted. We were successful in one of these which we now describe. The pericardium was laid undeformed on a lexan plate and a 7.0 cm circle stamped on the tissue. Careful dissection resulted in a circular specimen to which 000 silk sutures were attached, using magnetic recording tape and super glue, at 15° increments as shown in Figure (6). Note that the sutures form diameters of the specimen at 15° intervals.

Next the specimen was mounted in the bi-axial testing device and 10 gm applied to one diameter and 100 gm applied to the diameter orthogonal to it. After applying these forces, two marks 5 cm apart were placed on the tissue along the diameter subjected to 100 gm. The tissue was then rotated 15° and the procedure repeated until all possible diameters were loaded with 100 gm and marked. When the tissue was allowed to return to the stress free state, the marks placed on the tissue form an ellipse with major and minor axis identical to the unknown material symmetry axis. A 4 cm X 4 cm specimen was then cut from the tissue for use in the bi-axial testing in which the material and the stretching axis coincide. The specimen, mounted in the apparatus, is shown in Figure (7).

Analysis of Results

Our results indicate that the pericardium is orthotropic, nonlinear viscoelastic and relatively strain rate insensitive. Figure (8) and (9) are plots of representative data illustrating these points.

The data analysis was done using several possible strain energy density functions taken from the literature. The details behind the individual models may be found in Choi (1987) (attached).

A major problem in reducing bi-axial experimental data is that the material constants so determined are protocol dependent. This is because of the situation indicated in Figure (10) and referred to in statistics as multi-colinearity. Accordingly, we attempted to reduce the data in sets. These sets are taken by applying differing ratios of the strains in the two preferred material directions determined as outlined above. Thus all strain states expected in-vivo are in a data set. Figure (11) shows representative plots of the strains E_{11} versus E_{22} . Table (2) indicates the corresponding material constants obtained for the model shown in the Table. (Note that the stress strain law follows directly from the function W shown.) Experimental and

theoretical predictions of the stress S_{11} are shown in Figures (12) and (13) respectively. The agreement between theory and experiment is good.

Lay Summary

The mechanical nature of the pericardium is unknown. It is important to understand how the pericardium responds to forces like the ones it experiences in the body. This information may be important in modelling the heart. Such models can serve as a guide to diagnosis and treatment. The pericardium also serves a mechanical role when it is made into a prosthetic heart valve or a "patch".

III Collaborators

Dr. Hilmi Demiray, a visiting professor, helped in the development of the mechanical model. Dr. Demiray is an internationally recognized expert on the theoretical aspects of tissue mechanics.

Mr. Hwa Soon Choi is conducting this research as his thesis dissertation. He has completed his thesis proposal and successfully defended it before the Faculty. He will complete his Thesis this spring. A copy will be forwarded to the Association.

Dr. Andre Churchwell served as a medical consultant.

IV Publications

Choi, H.W. and Vito, R.P., The bi-axial mechanical properties of canine pericardium. Proceedings, 40th Annual Conference on Engineering in Medicine and Biology (1987)

Also presented at the Symposium on Cardiovascular Research sponsored by the GHA and held in Athens, Ga. on August 7, 1987.

Dr. Vito has been invited to present this work at the Society of Engineering Science meeting, Berkeley, Ca. in June 1988.

Expected: One and perhaps two journal papers resulting from Mr. Choi's Thesis.

V This work is continuing using Institute support.

Table (1). Thickness measurement data for the specimen #03.

Point No.		# 1		# 2	
Stage		Contact	Lost-contact	Contact	Lost-contact
	(min.)	(mm)	(mm)	(mm)	(mm)
T	0.0	0.3734	0.5715	0.3175	0.6045
	2.0	0.3708	0.5258		
	2.5			0.3073	0.5410
i	3.5	0.3454	0.5105		
	4.5			0.3022	0.5080
m	5.5	0.3302	0.4623		
	6.5			0.2819	0.4927
e	8.0	0.3124	0.4166		
	8.25			0.2743	0.4217
Linear regression $h = -\alpha t + \beta$		$\alpha = 0.008265$ $\beta = 0.3778$	$\alpha = 0.019208$ $\beta = 0.5703$	$\alpha = 0.005413$ $\beta = 0.3202$	$\alpha = 0.020149$ $\beta = 0.6012$
Thickness		0.232 mm		0.217 mm	

Table (1). Comparison of the material constants of [MODEL 4] * determined from the individual data set and determined from the complete data set (Specimen #05 , canine pericardium).

Protocol	a1	B0	b1	b2	b3
P1	1.82222	0.00017	-221.9719	55.8146	48.0009
P2	1.86187	0.00034	-104.7934	50.8625	39.8545
P3	1.52789	0.01288	-74.6157	9.7404	20.5505
P4	1.71814	0.00029	54.7648	112.8587	50.2555
P5	1.46838	0.00030	53.2002	-1726.8939	71.0944
P1+P2+P3 +P4+P5	1.92430	0.00100	44.9223	43.5682	30.4653

* Model 4 refers to a particular choice for the strain energy density function W; namely:

$$W = 1/2 a_1(E_{11}^2 + E_{22}^2 + E_{11}E_{22}) + B_0 \{ \exp(1/2b_1E_{11}^2) + \exp(1/2b_2E_{22}^2) + \exp(b_3E_{11}E_{22}) \}$$

The stresses, which follow from W (Choi 1987), are:

$$S_{11} = a_1(E_{11} + 1/2E_{22}) + B_0 \{ b_1E_{11}\exp(1/2b_1E_{11}^2) + b_3E_{22}\exp(b_3E_{11}E_{22}) \}$$

$$S_{22} = a_1(1/2E_{11} + E_{22}) + B_0 \{ b_3E_{11}\exp(b_3E_{11}E_{22}) + b_2E_{22}\exp(1/2b_2E_{22}^2) \}$$

These equations are used to give the theoretical plots in Figures (12) and (13).

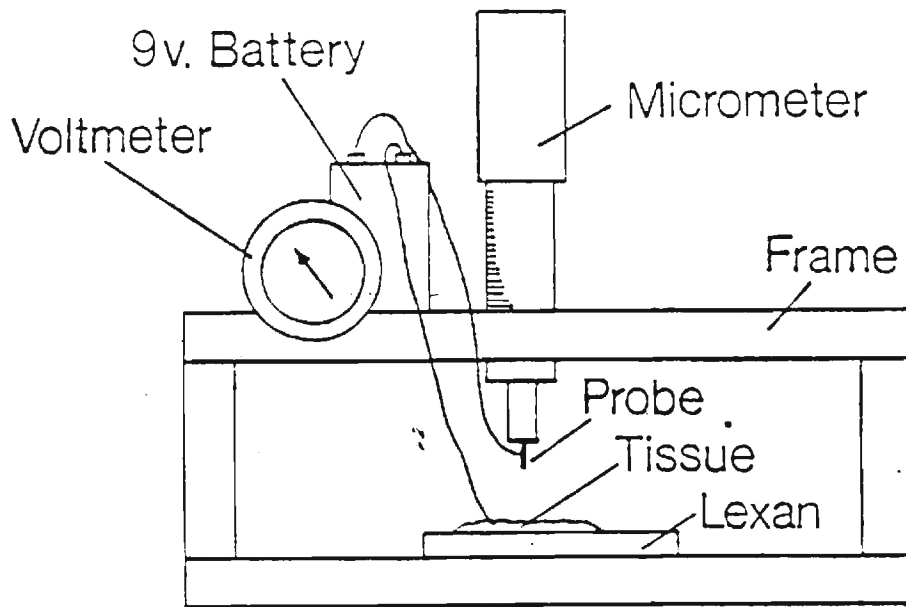


FIGURE (1) The electrical resistance micrometer can be read to 0.0001". Contact with the tissue closes the circuit as indicated by the meter.

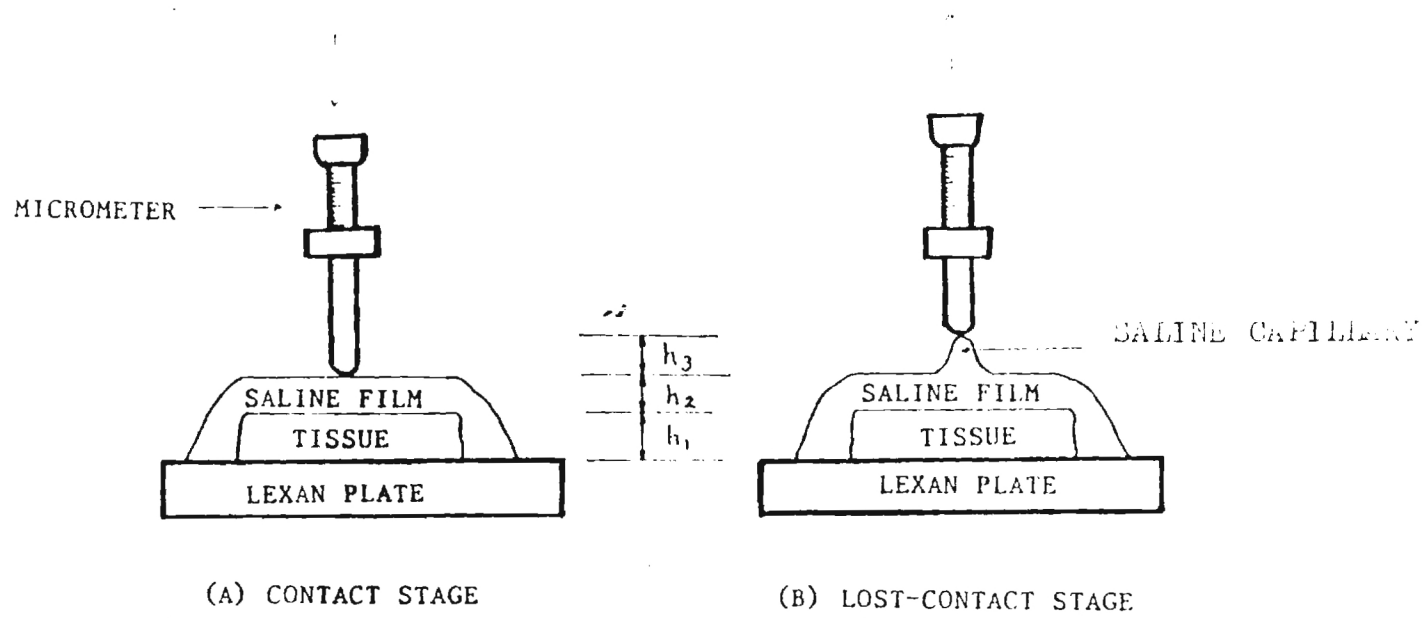


Figure (2) Schematic diagram of two reading stage for thickness measurement: (a) contact stage (b) lost-contact stage.

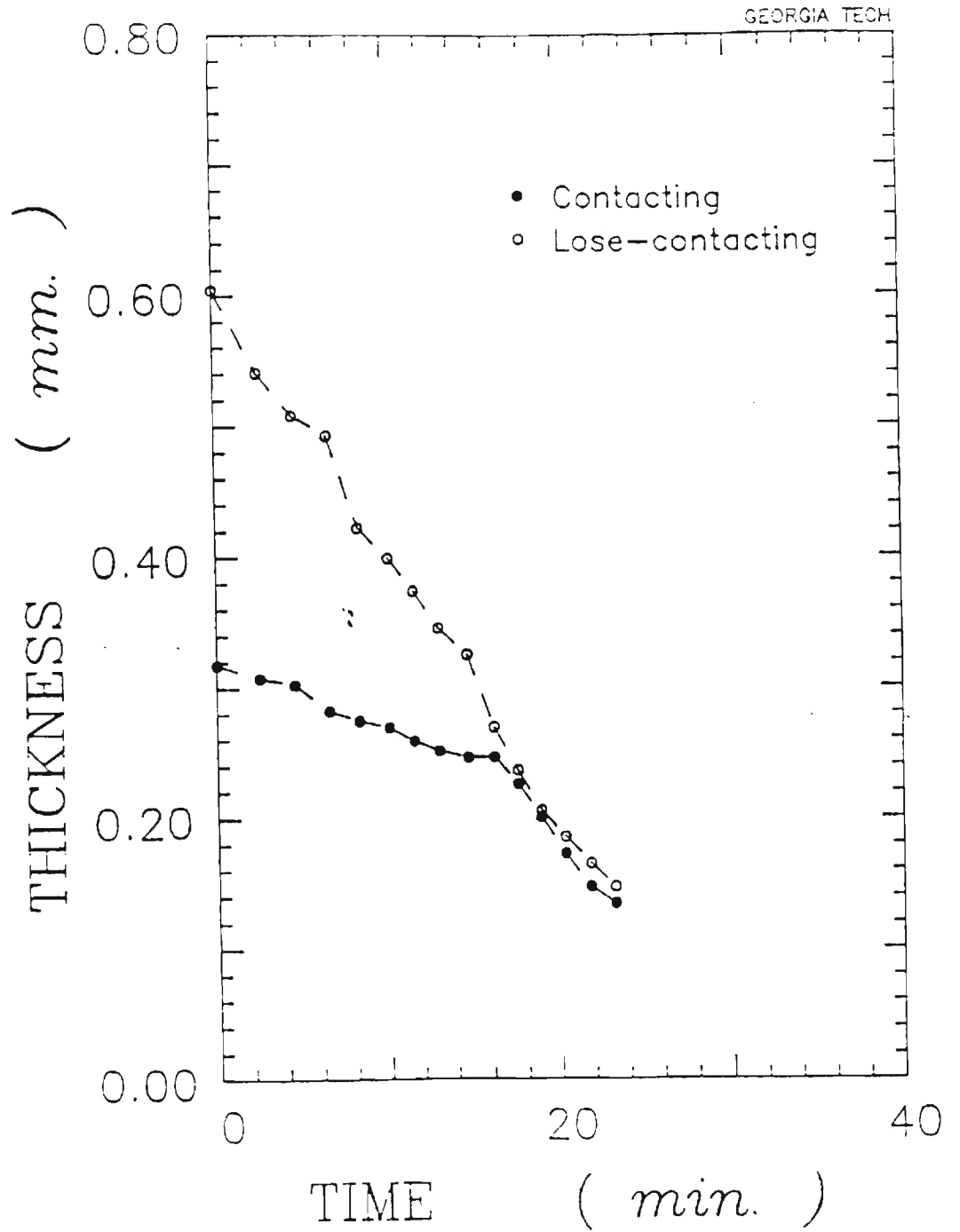


FIGURE (3) The "contact" and "lost contact" readings of the micrometer are plotted vs. time for specimen #02. Note the convergence of the two lines as the saline film evaporates.

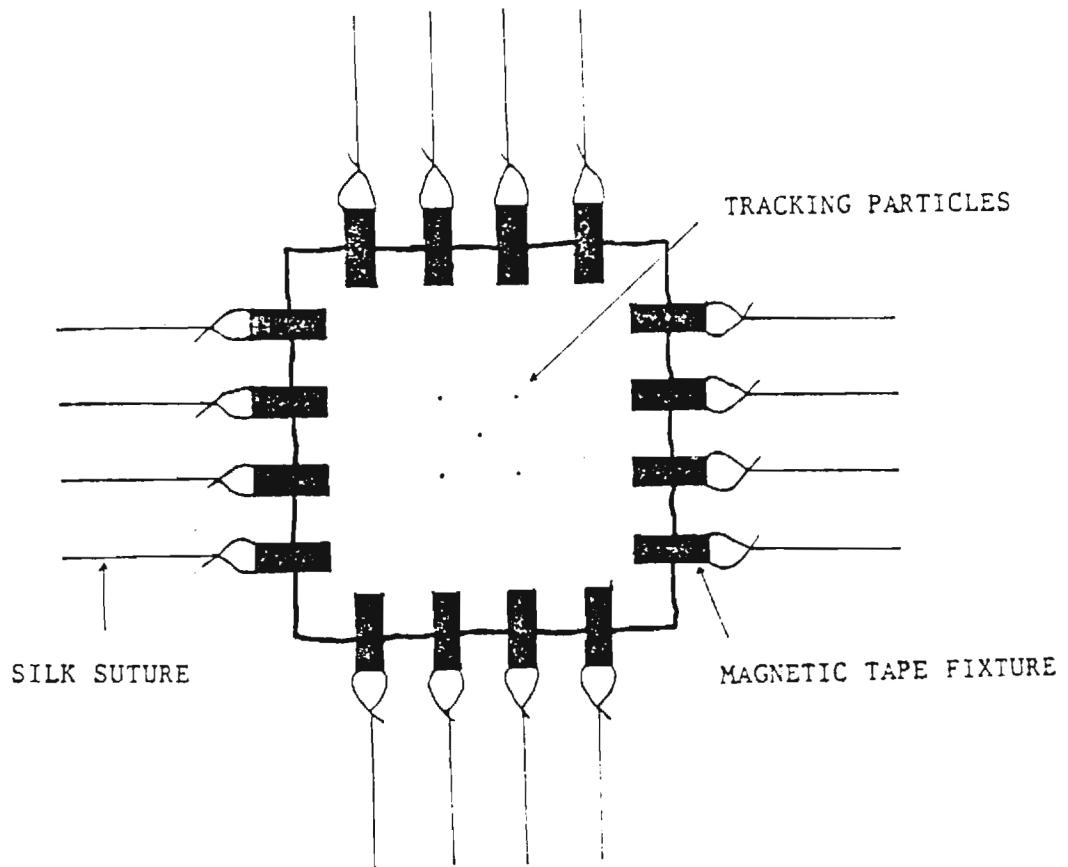


FIGURE (4) The specimen is mounted using surgical silk attached to small pieces of magnetic tape. The tape is attached to the tissue using super glue. Note the small tracking particles at the center of the specimen.

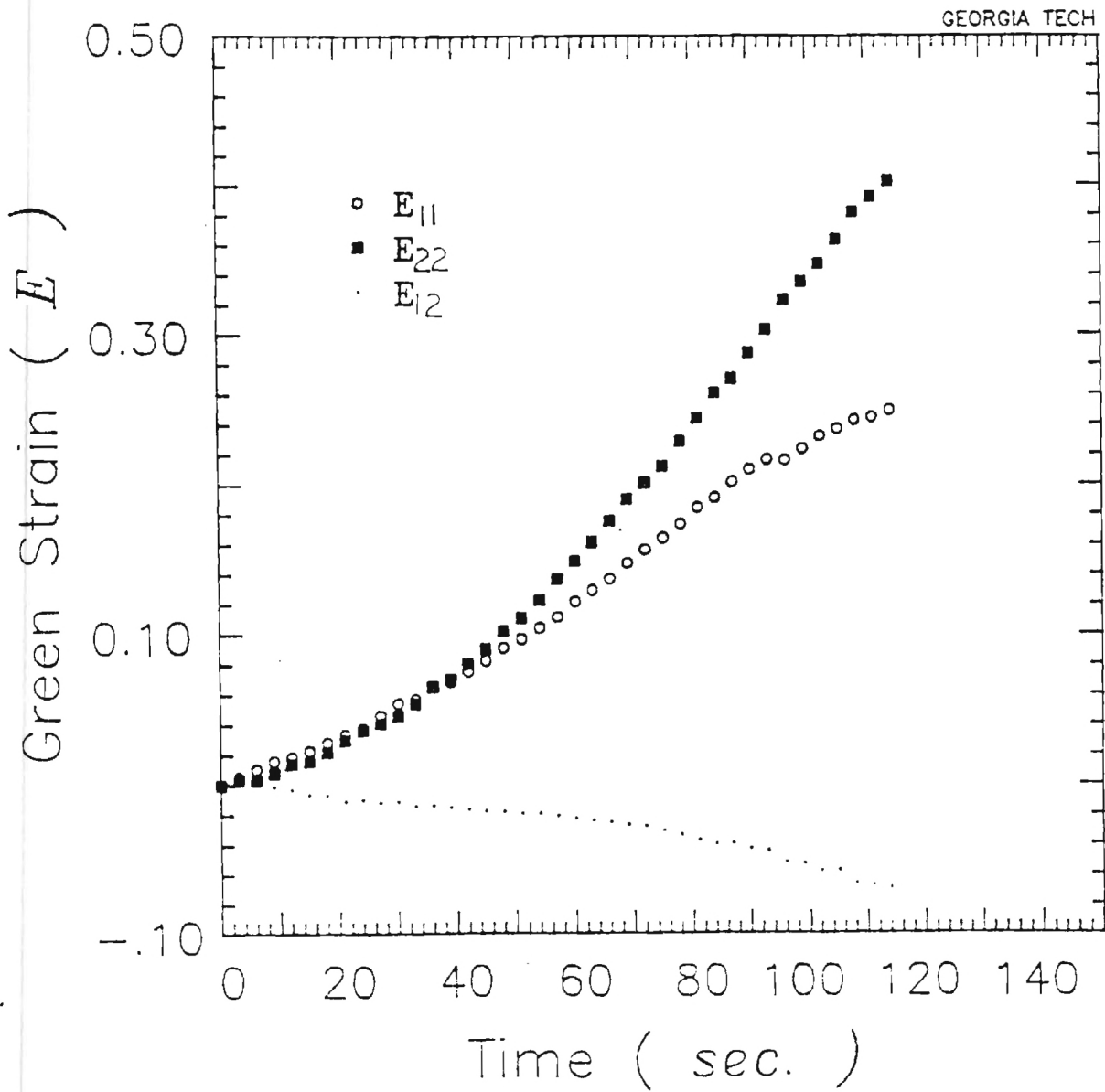


FIGURE (5) This figure shows the extensional strains E_{11} and E_{22} and the shear strain E_{12} vs time. The non-zero shear strain indicates that the material axis and the stretching axis do not coincide.

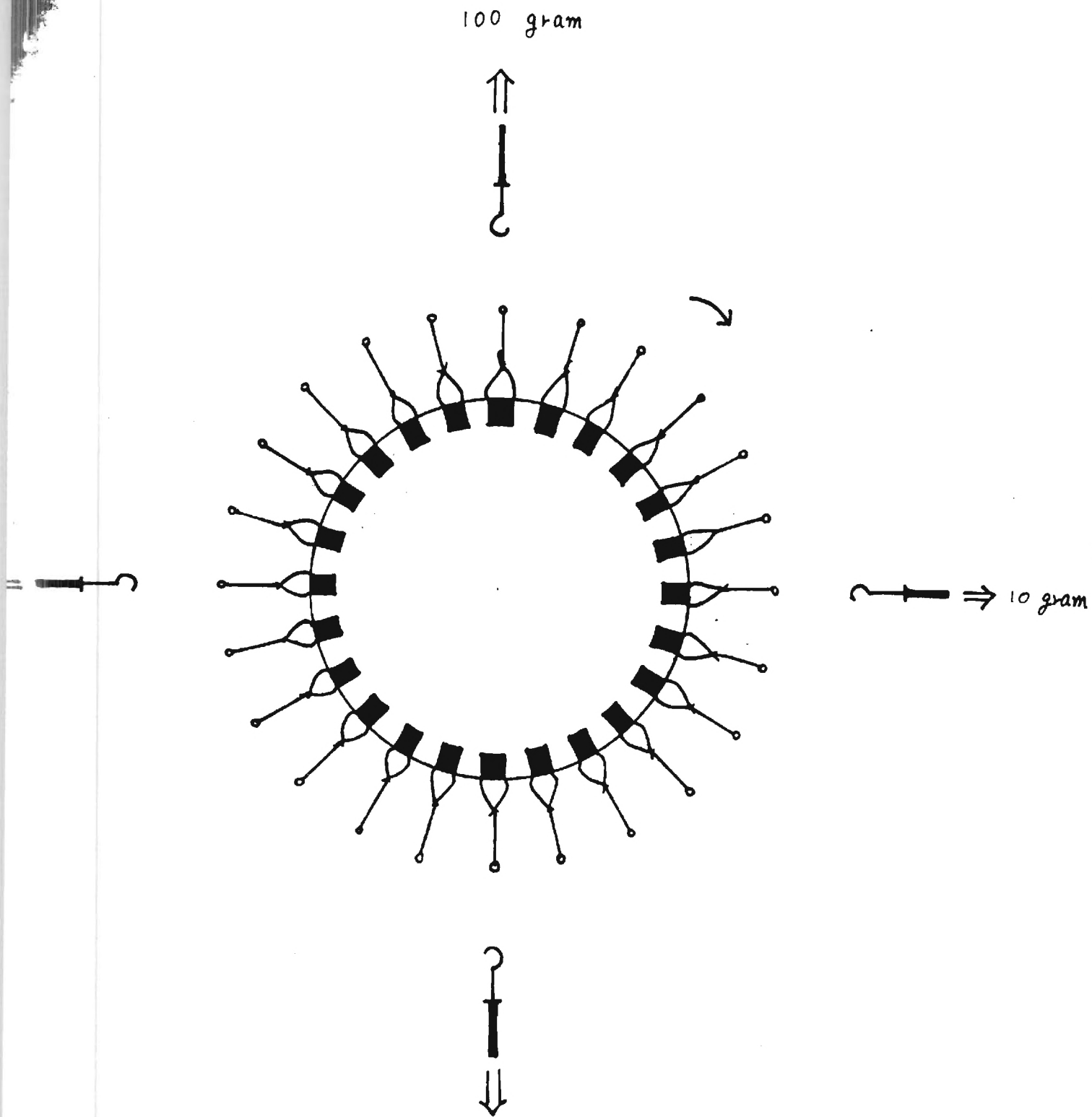


FIGURE (6) The circular specimen is prepared with surgical silk attachments along diameters 15° apart. Such a specimen can be used to determine the material symmetry axis as described in text.

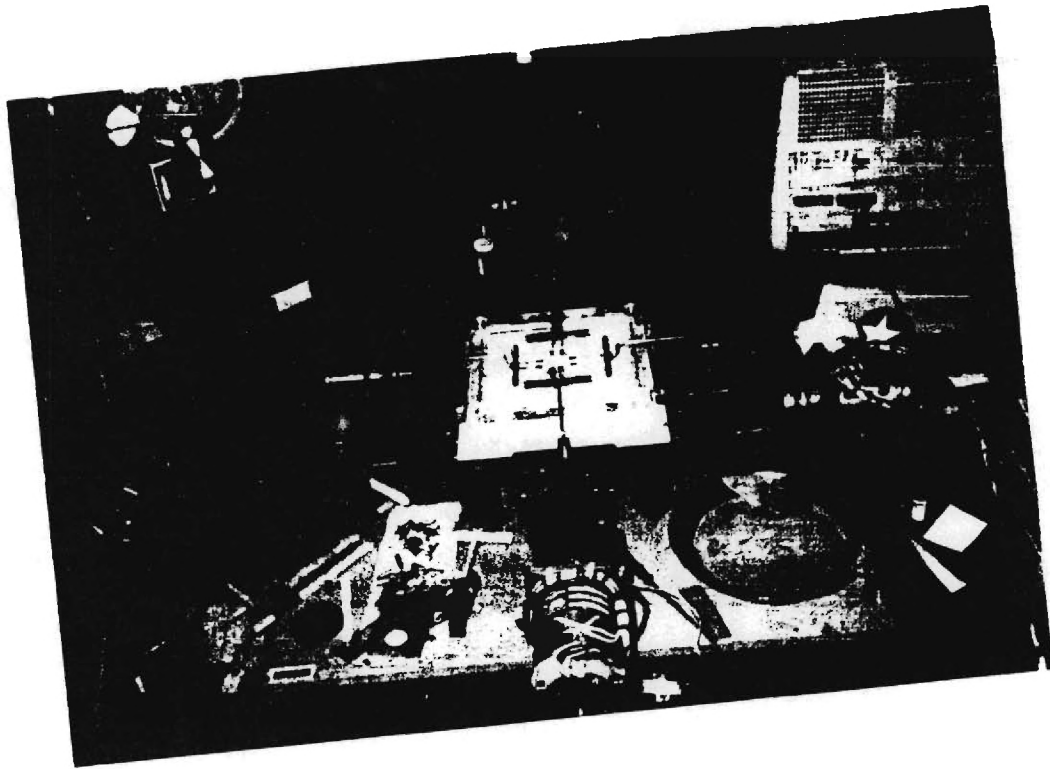


FIGURE (7) The specimen as mounted in the bi-axial mechanical testing device.

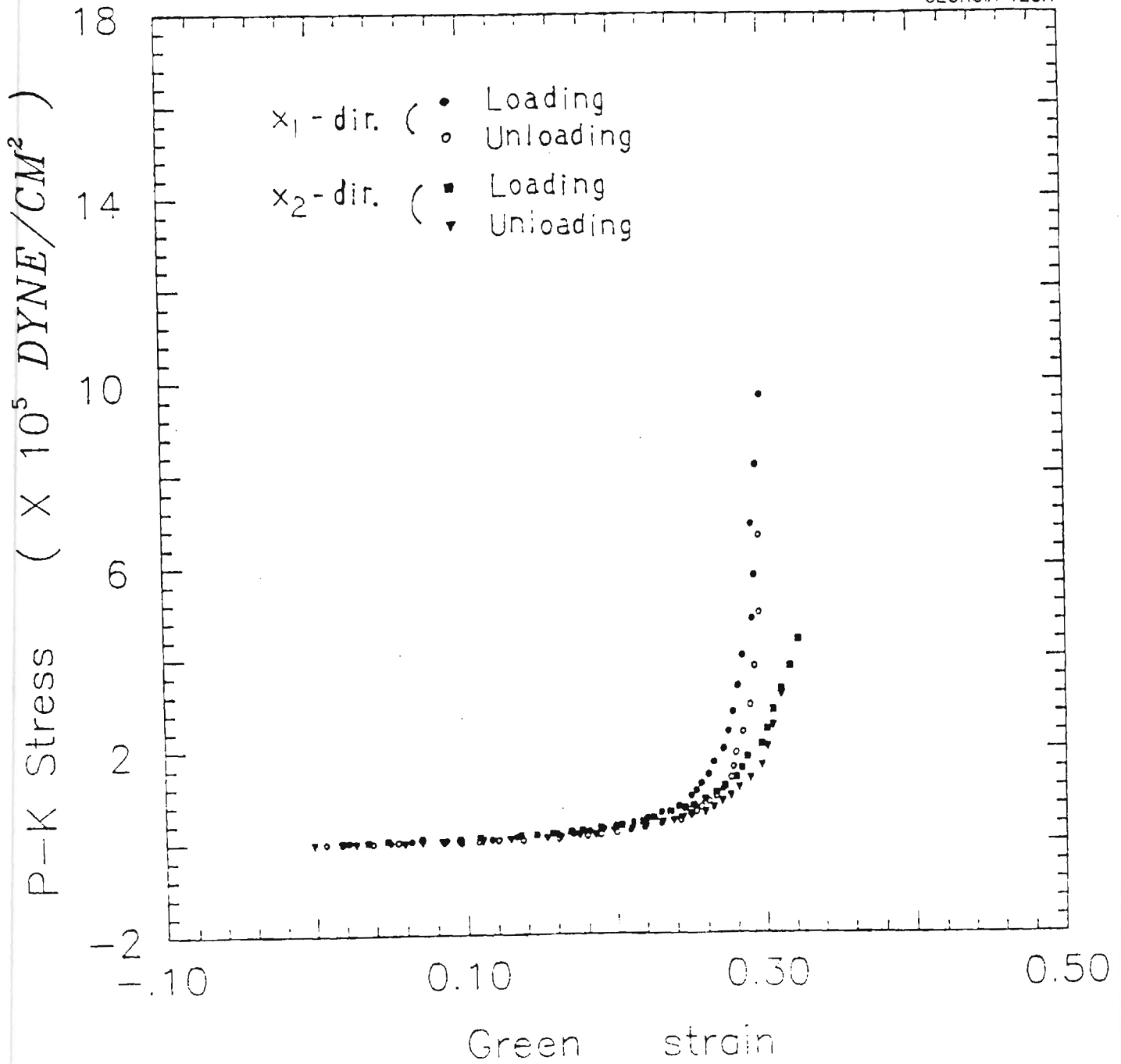


FIGURE (8) The pericardium is nonlinear viscoelastic and orthotropic as shown by these results for specimen #02.

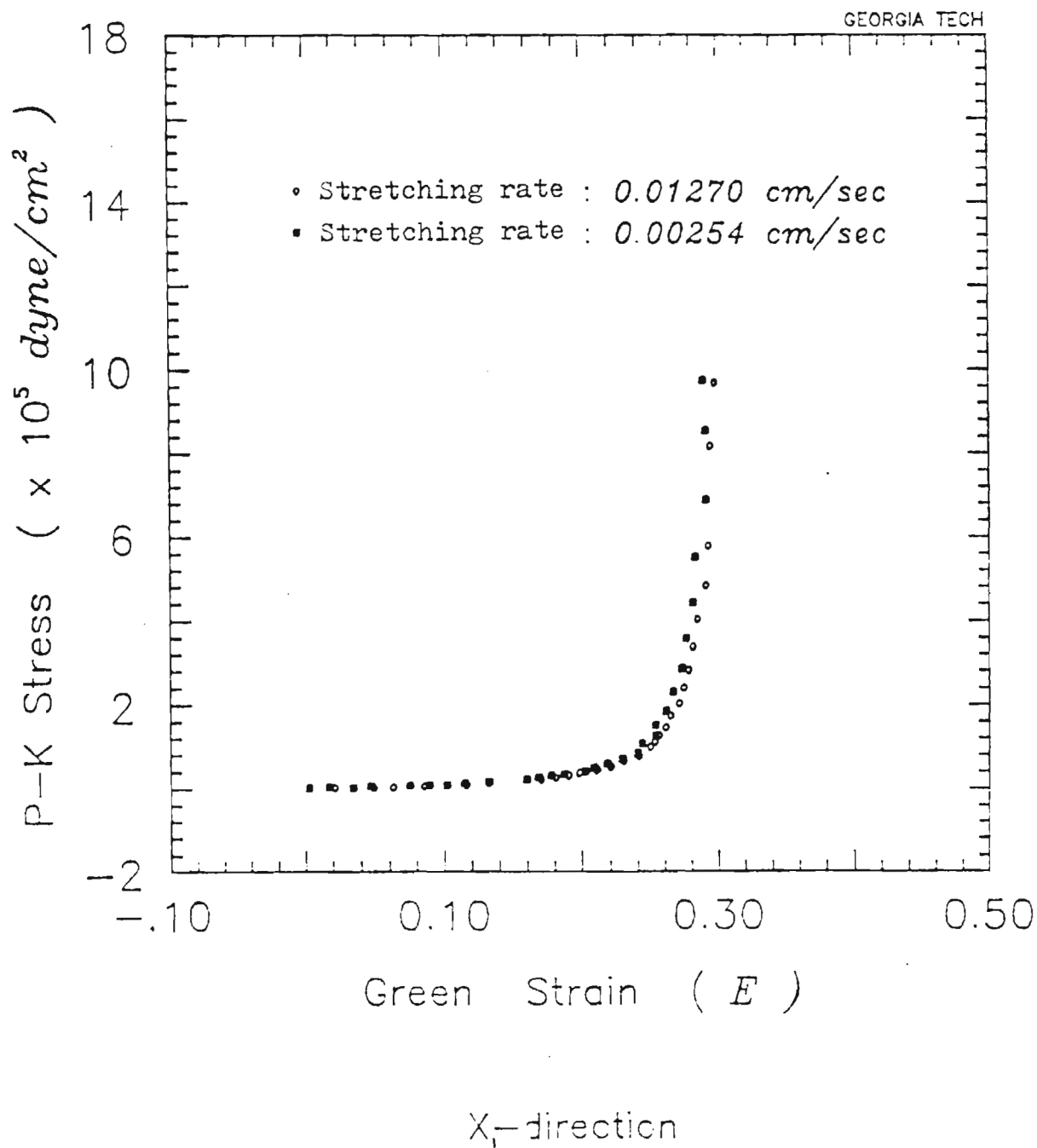


FIGURE (9) Changing the strain rate by a factor of 20 has little effect on the experimental data. This is a result typical of soft tissues.

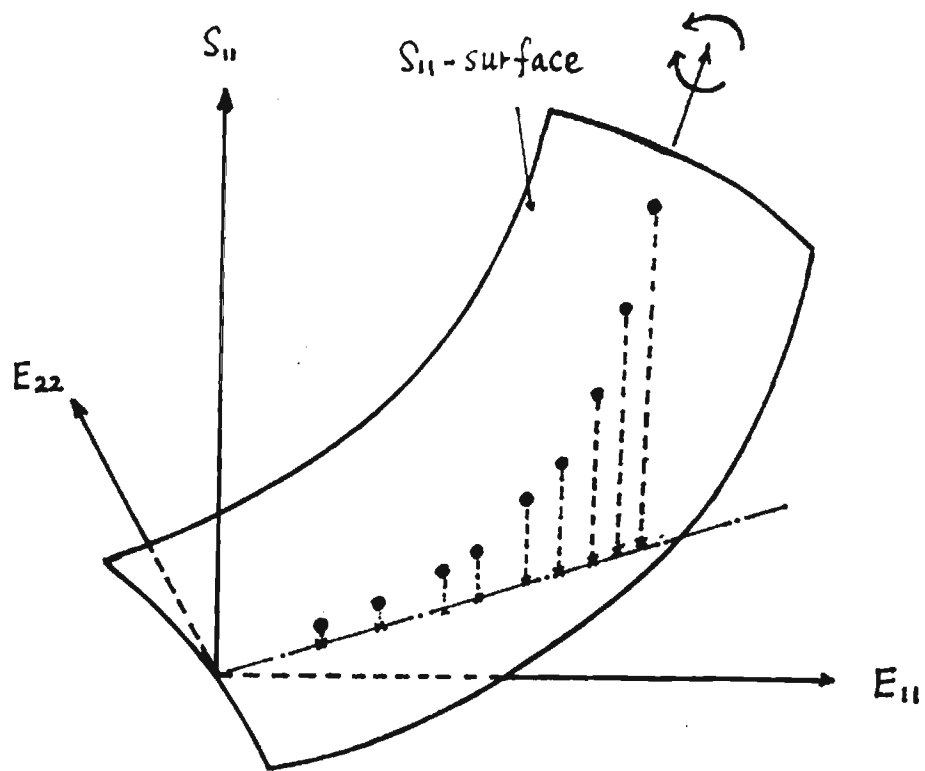
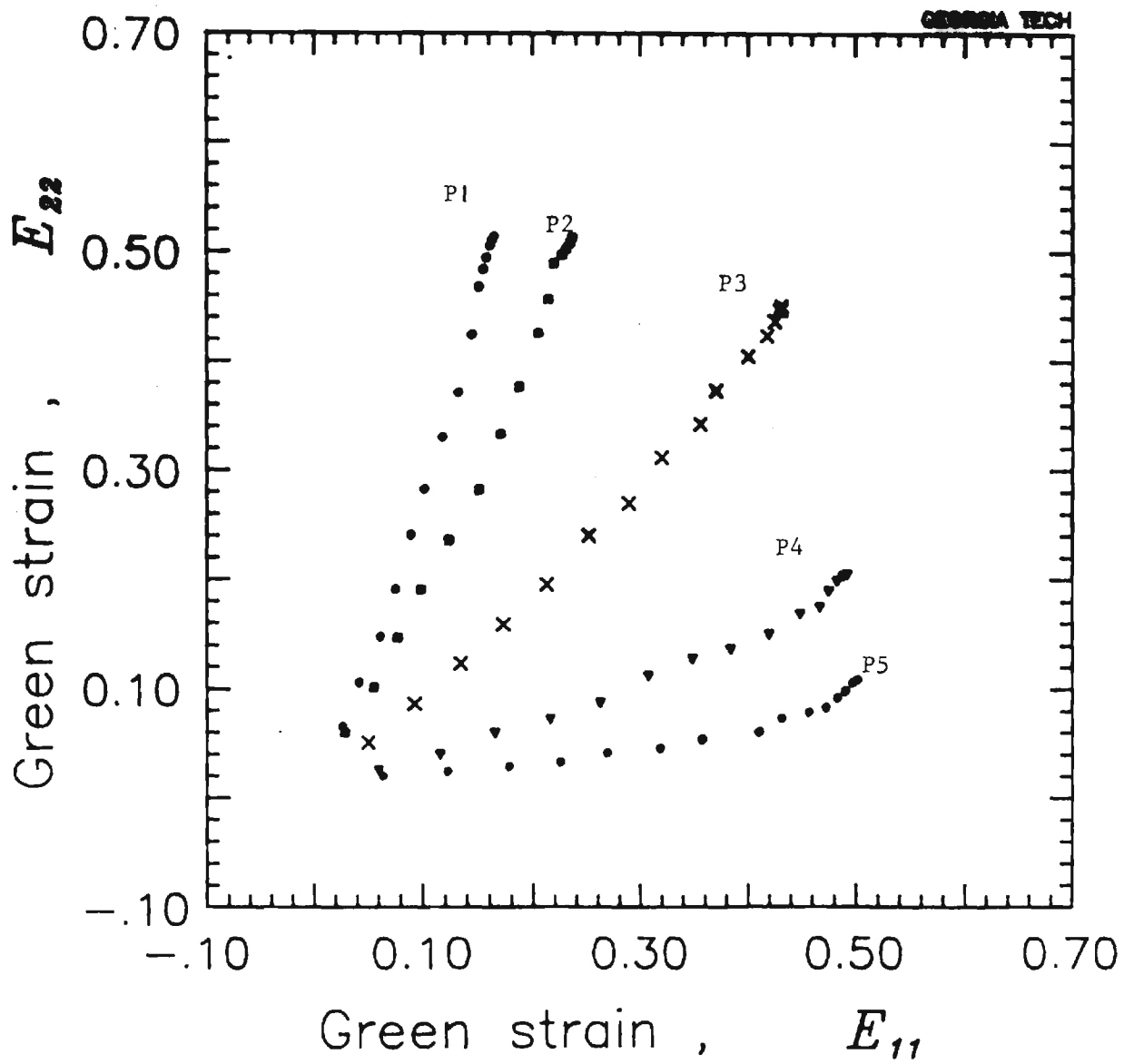


Figure (10) Instability of the fitting surface due to the multicollinearity.



Strain Trajectories

Data : *dogdat5*

Figure (1). Five different strain-trajectories included in a complete set of data.

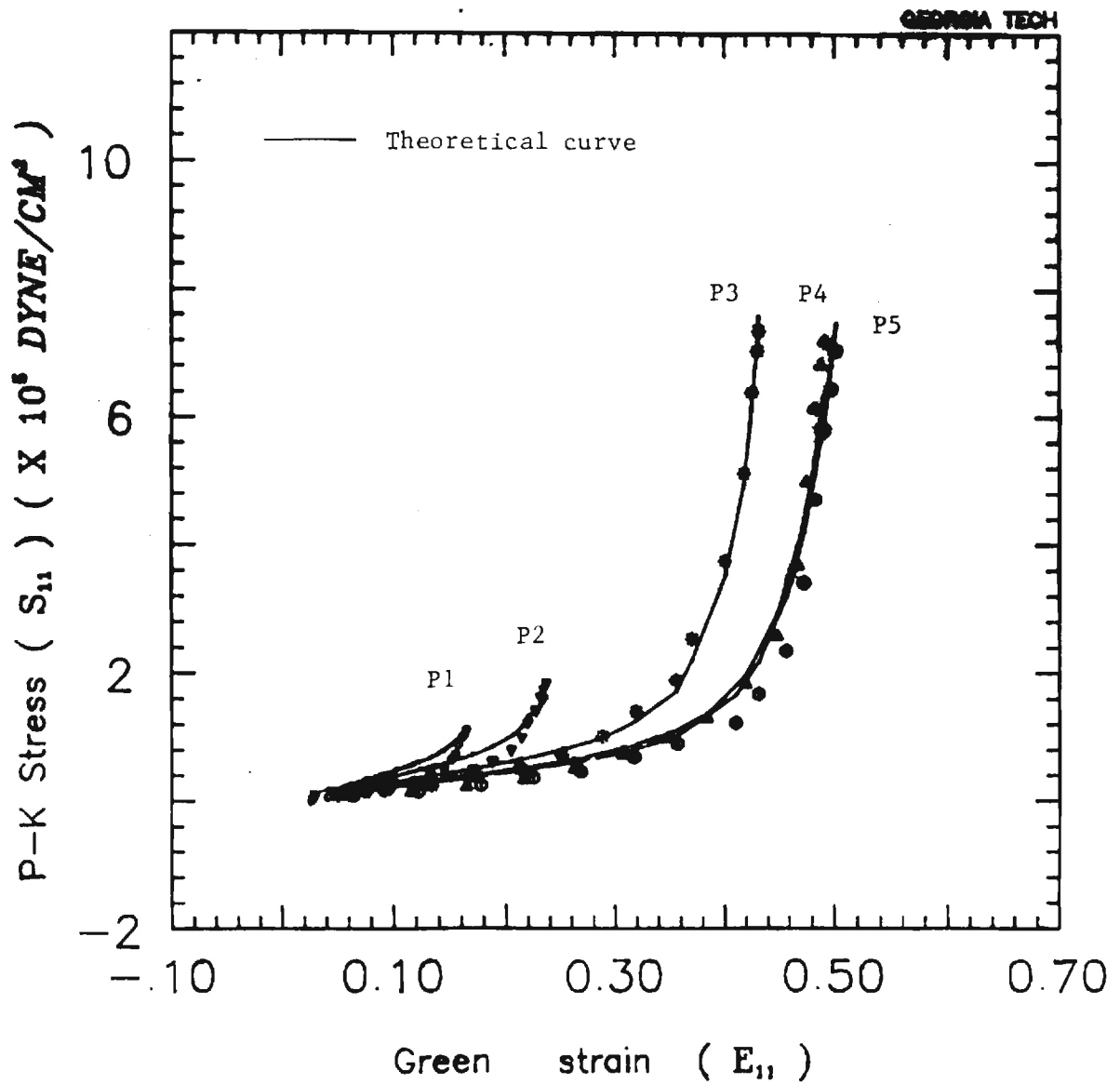


FIGURE (12) The theoretical and experimental values of the stress S_{11} and strain E_{11} for the various protocols. The theoretical values are computed using the protocol independent material constants given in Table (2).

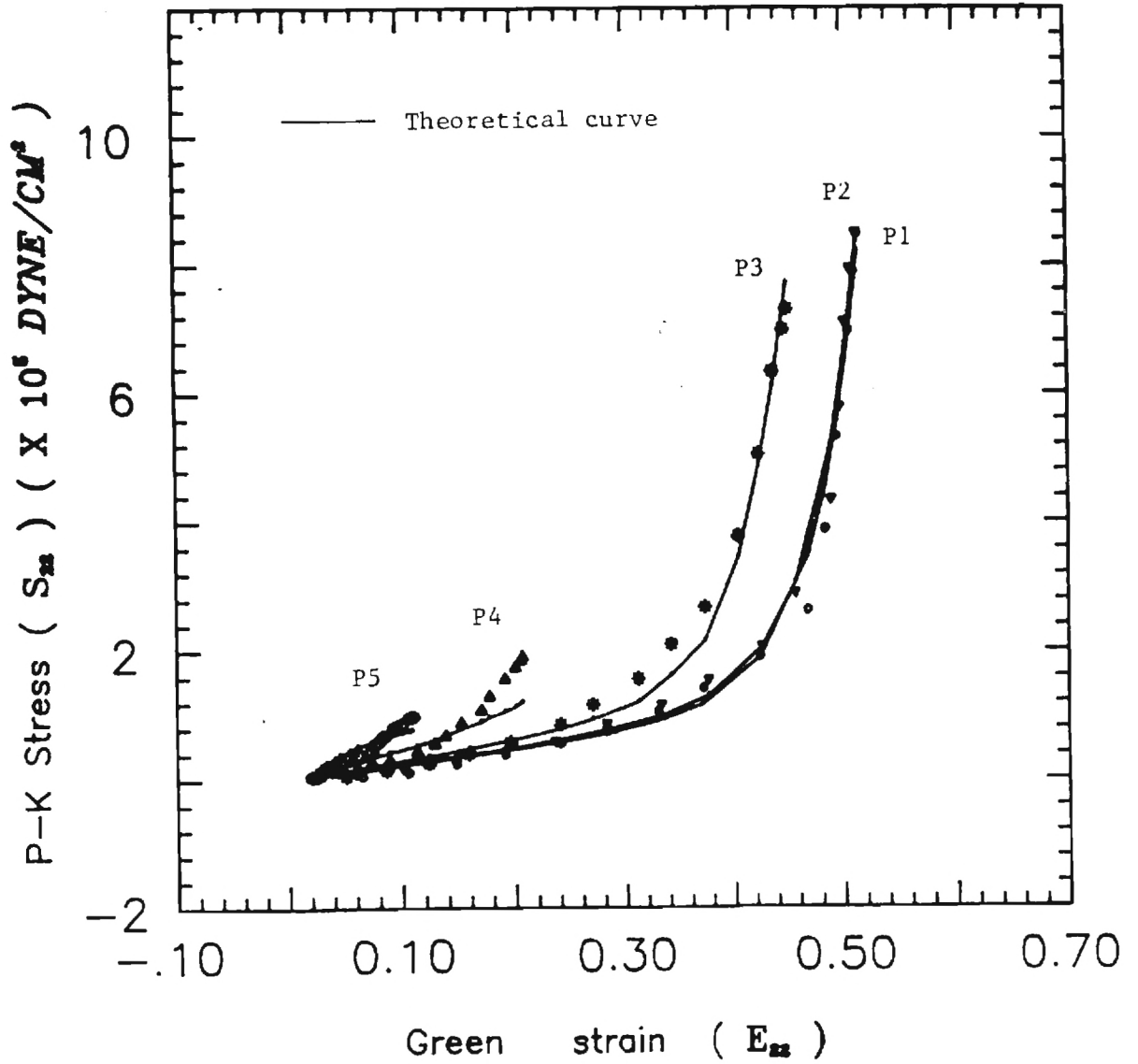


FIGURE (13) The theoretical and experimental values of the stress S_{22} and strain E_{22} for the various protocols. The theoretical values are computed using the protocol independent material constants given in Table (2).

MECHANICAL PROPERTIES OF CANINE
PERICARDIUM

A Thesis Proposal

Submitted to the Faculty of
Engineering Science and Mechanics
School of Civil Engineering
Georgia Institute of Technology
Atlanta, Georgia 30332

by

Hwa-Soon Choi

February 12, 1987

TABLE OF CONTENTS

	Page
i. Nomenclature.....	4
1. Introduction.....	6
1.1 Description of the Pericardium.	
1.2 Function of the Pericardium.	
1.3 Significance of Pericardial Mechanics.	
1.4 Review of the Literature.	
a. Soft Tissue Mechanics	
b. Mechanics of the Pericardium.	
1.5 Brief outline of Objectives.	
2. Experimental Methods.....	18
2.1 Introductory Comments	
2.2 Experimental System.	
2.3 Specimen Acquisition.	
2.4 Specimen Preparation.	
a. Measurement of Initial Dimensions	
a.1 In-plane Measurements.	
a.2 Thickness Measurement.	
b. Specimen Mounting.	
2.5 Specimen Testing.	
a. Strain Measurement.	
b. Stress Measurement.	
c. Bi-axial Testing Protocols.	
3. Pseudo-elastic Analysis.....	39
3.1 Stress-strain Law.	
3.2 Strain Energy Function.	
3.3 Bi-axial Test Formulation.	
a. Formulation with respect to the Fixed Stretching Axis.	
b. Formulation with respect to the Material Symmetry Axis.	
3.4 Data Analysis.	
4. Microstructural Observations.....	49
4.1 Objectives of Microstructural Observation.	
4.2 Specimen Preparation for Light Microscopy.	
4.3 Stereological Analysis.	
a. The Volume Fraction.	
b. Waviness of Fiber Bundles.	
5. Preliminary Results.....	55
5.1 Thickness Measurement.	
5.2 Uniform Bi-axial Test.	
5.3 Non-uniform Bi-axial Test.	
5.4 Constant Lateral Displacement Test.	
Appendix 1.....	73
References.....	77

Captions for Figures.....	90
Headings for Tables.....	92

NOMENCLATURE

A (A_{ijkl} , A_{mn} , A_i)	
a (a_{ij} , a_i)	Pseudo-elastic material constants.
B (B_0 , B_{ijkl})	
b (b_{ijkl} , b_{mn} , b_i)	
C (C_{ij})	Displacement gradients referred to x_i axis.
C' (C'_{ij})	Displacement gradients referred to x'_i axis.
E (E_{ij})	Green's strain tensor.
\mathcal{E} (\mathcal{E}_{ij})	Eulerian infinitesimal strain tensor.
f(...)	Function of variables ...
h (h_0, h_1, h_2, h_3)	Thickness.
H (H_n)	Interpolation functions.
I (I_1, I_2, I_3)	Green's strain invariants.
L	Length.
l (l_{ij})	Direction cosines.
P	Hydro-static pressure.
S (S_{ij})	Second Piola-Kirchhoff stress tensor.
T (T_{ij})	Lagrangian stress tensor.
t	Time.
u (u_1, u_2)	Displacements referred to x_i axis.
V_V	Volume fraction.
W	Strain energy density function per unit volume of undeformed state.
x'_i (x'_1, x'_2, x'_3)	Undeformed coordinates along axis of orthotropy.

$x_i(x_1, x_2, x_3)$

Undeformed coordinates
along the stretching axis.

$y_i^1(y_1^1, y_2^1, y_3^1)$

Deformed coordinates along
the axis of orthotropy.

$y_i(y_1, y_2, y_3)$

Deformed coordinates along
the stretching axis.

ϕ

Angle between x_i^1 axis
and x_i axis

θ

Angle between y_i^1 axis
and y_i axis

σ (σ_{ij})

Cauchy stress tensor.

λ

Stretch ratio.

ρ_0

Density of material in
undeformed state.

ρ

Density of material in
deformed state.

η (η_1, η_2)

Natural coordinates

1. Introduction

1.1 Description of the Pericardium

The pericardium is normally found in vertebrates, including man. The pericardium consists of a tough, fibro-collagenous outer coat (the parietal pericardium) with discrete attachments to the sternum, great vessels, and diaphragm, and a thin inner membrane (the visceral pericardium) as shown in Figure (1). The pericardial cavity, that space between the visceral and parietal pericardium, contains a small volume of fluid which serves to lubricate the outer surface of the heart. The pericardium holds the heart in a fixed geometric position and isolates the heart from other thoracic structures [Holt,1970].

Histologically, the human parietal pericardium is composed of three layers: the serosa, the fibrosa, and an outer layer of epi-pericardial tissue. The serosa consists of a surface layer of mesothelial cells and of a narrow sub-mesothelial space. The fibrosa is composed of connective tissue cells, small vessels, variously oriented layers of collagen fibrils and small elastic fibers. The epi-pericardial connective tissue layer contains mainly large coarse bundles of collagen, blood vessels, nerves, lymphatics and connective tissue cells. A part of the pericardiosternal ligaments consists of some of these collagen bundles [Ishihara et al.,1980]. The major constituent of the parietal pericardium is the fibrosa, the chief ingredient of which is compactly arranged collagen fibers disposed in three layers oriented approximately 120° with respect to each other. The elastic fibers are small and often oriented at right angles to the collagen bundles [Shabetai,1985].

The canine parietal pericardium has a multilayered network of collagen fibers [Wiegner and Bing,1981]. However, the histological study on the orientation of fibers in each layer has not been reported.

1.2 Function of the Pericardium

The functions of the pericardium have long been mysterious as stated by Shabetai [1985] :

The pericardium is known not to be essential to life; its congenital absence or surgical removal is usually not followed by adverse consequences. On the other hand, laboratory investigations have furnished convincing evidence that the pericardium influences cardiac function. This paradox arises because the modulation of cardiac function by the pericardium is subtle, and because cardiac function adapts to the absence of the pericardium.

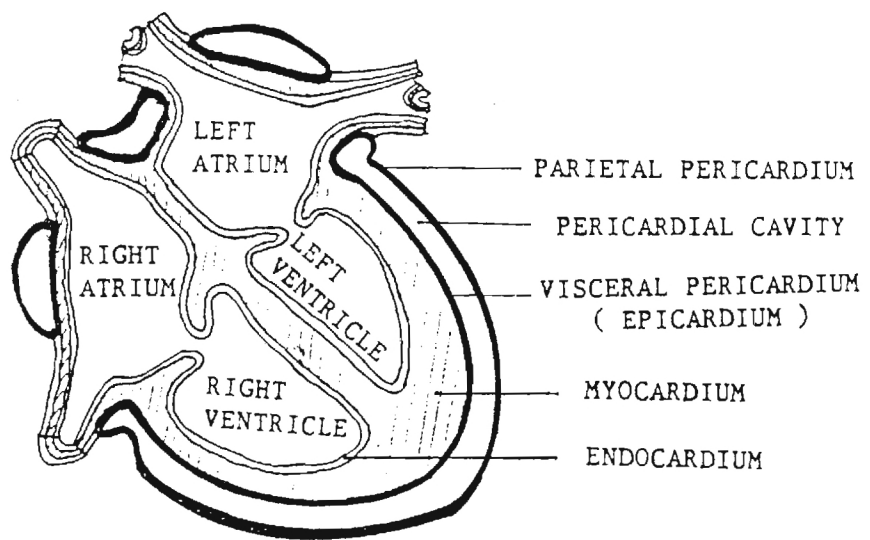


Figure (1) The pericardium and heart wall.

However, in the absence of the pericardium there may be significant long term effects such as cardiac hypertrophy and myocardial scarring. After removal of the pericardium, the heart may attach to the sternum and diaphragm. Thus at least the local contractility of the heart may be adversely affected [Fowler, 1970].

The pericardium serves to hold the heart, and isolates the heart from other structures in the thorax, thus preventing adhesions and spread of infection.

The pericardium also serves the following functions:

- 1) Moderates diastolic filling of the ventricles.
- 2) Prevents hypertrophy of the heart under conditions of strenuous exercise [Holt,1970].
- 3) Restrains the volume of the heart in the face of acute volume overloads and more chronic volume overloads [Bhargava et al.,1983].
- 4) Plays an important role in the diastolic interaction between the two chambers [Maruyama et al.,1982 ; Hess et al.,1983].

Also, the pericardial fluid reduces friction on the epicardium and equalizes the gravitational, inertial and hydrostatic forces over the surface of the heart [Avasthey and Wood,1974].

Because the pericardium surrounds the heart, its constrictive function can have fatal consequences in pathological situations such as cardiac tamponade and constrictive pericarditis. Cardiac tamponade is the impairment of diastolic filling of the heart caused by an unchecked rise in intrapericardial pressure. Constrictive pericarditis is the inflammation of the pericardium resulting in constriction of the heart [Fowler,1985].

1.3 Significance of Pericardial Mechanics

Within the last decade, pericardial diseases have become increasingly common. Therefore, the understanding of pericardial physiology is becoming recognized as one of the basic concepts in the physiology of the circulation. As aforementioned, The pericardium has significant influences on cardiac function and diastolic interaction between the two chambers of heart. For the better interpretation of clinical measures (e.g., pressure-volume relations, electrocardiogram) of cardiac function, the development of a mechanical model of the intact heart with pericardium in health and disease has to be done. Although there have been numerous efforts to develop a mechanical model of the intact heart [e.g., Demiray,1976 a,b; Ghista and Sandler,1969; Gould et al.,1972; Mchale and Greenfield,1973; Mirsky,1969,1973; Moskowitz,1982; Wang and Sonnenblick,1979; Wong and Rautaharju, 1968; Voukydis,1972 a,b,c], the effects of the pericardium have been almost disregarded in those studies except the work of Vito [1979] and Vito and Demiray [1980]. Prior to developing a mechanical model of the heart, it is essential to know the mechanical properties of pericardium. That is, we have to know the constitutive relationships of the pericardium.

Another important aspect of the pericardium is the heart valve replacement. Bioprosthetic valves are made of porcine or bovine pericardium. When using the bio-prosthetic valves in the heart valve replacement, problems associated with material degradation [Ferrans et al.,1978] have been important factors limiting the long-term success of cardiac valve replacement [Schoen et al.,1982].

The pericardium is useful in other cardiac surgery as well. For example, porcine pericardium was used as a patch to repair intra-cardiac defects [Radegran and Bjork,1979]. The pericardium used in cardiac surgery is usually treated with glutaraldehyde or formaldehyde to improve the durability by producing cross-linking between collagen fibers [Woodroof,1979], and to make the tissue biologically inert.

From the above discussion, it appears that the understanding of microstructural changes due to mechanical and chemical factors is important to the development of cardiology.

In summary, the long-term aims of the pericardial mechanics are:

- 1) To understand the constitutive relationships of the pericardium.
- 2) To construct a mechanical model of the intact heart and prosthetic heart valves.
- 3) To understand quantitatively the relationship between material properties and microstructure of the pericardium.
- 4) To apply all these knowledge to the real clinical problems.

1.4 Review of the Literature

a) Soft Tissue Mechanics

Soft tissue may be considered in several basic categories: soft connective tissues (lung tissue, skin, blood vessels, ligaments, tendons, mesentery, pericardium, and other membranes), muscles, organs, and the brain. Thus mechanics of soft tissues covers a vast area.

The tissue's capacity to withstand and transmit the loads through deforming appropriately can be characterized in health and disease. Knowledge of such 'load-deformation' relations of the tissues can serve as a basis for diagnosis [Kenedi et al., 1975]. Therefore, identification of the constitutive equations of living tissues has been a major activity in recent years [Fung ,1983].

Generally, soft biological tissues are regarded as nonhomogeneous, anisotropic, nearly incompressible materials, and they are usually subjected to large deformations. Thus the stress-strain relationships are usually nonlinear and history dependent. But attempts to include all of these factors in a single theory would likely lead to intractable mathematical and experimental complexity. Therefore, most studies up to now are based on the certain assumptions such as homogeneity, isotropy

and incompressibility, even though little or no evidence exists for these assumptions.

The studies for identification of the constitutive equations can be divided into two basic groups, that is, macroscopic analysis [e.g., Blatz,1969; Fung,1972,1973,1979,1981; Hildebrandt et al.,1969 a,b.; Veronda and Westmann,1970; Vito, 1973,1979,1980 a,b] and microscopic analysis [e.g., Broom,1978; Comninou and Yannas,1976; Decreamer et al., 1980 a,b; Lanir, 1979 a,b, 1983 a,b]

Macroscopic analyses are based on the various mathematical methods of continuum mechanics such as finite elasticity and viscoelasticity. We can separate this approach into two groups; pseudo-elastic approach and viscoelastic approach.

First, pseudo-elastic approach assumes implicitly the existence of the pseudo-strain energy density functions. We know that living tissues are not perfectly elastic. Therefore, they cannot have a strain energy density function in the thermodynamic sense. But the biological tissues usually show the strain rate insensitivity, then the loading curve and the unloading curve can be separately treated as a uniquely defined stress-strain relationship, which is associated with a strain energy density function [Fung,1981]. Therefore, the characterization of soft tissues reduces to discovering the pseudo-strain energy density functions which can yield desired agreement between theory and experiments. But in this approach, the viscoelastic behaviors such as creep and relaxation are ignored.

Although many different mathematical expressions have been used to describe the experimental results of uniaxial and biaxial tests, only two forms of strain energy density function are used widely, the exponential form [e.g. Fung,1967; Blatz et al.,1968; Gou,1970; Vito,1973; Demiray,1972,1975; Tong and Fung,1976; Yin et al.,1986] and the power series form [e.g. Patel and Vaishnav ,1972; Haut and Little,1969; Vito,1980]. These function forms are briefly shown in Table (1).

Table (1) The previously suggested strain energy function forms

(Author)	(Strain energy function)	(material)
1941 : Mooney	$W = A_1(I_1 - 3) + A_2(I_2 - 3)$	rubber
1951 Rivlin and Saunders	$W = A_1(I_1 - 3) + A_2(I_2 - 3) + A_3(I_2 - 3)^2$	rubber
1967 Vainis and Landel	$W = w_1(\lambda_1) + w_2(\lambda_2) + w_3(\lambda_3) = \frac{3}{2n} f(2n\lambda_i)$	rubber
1967 Tucker and Sacks	$W = A_1(I_1 - 3) + A_2(I_2 - 3) + A_3(I_3 - 1) + A_4(I_1 - 3)^2 + A_5(I_2 - 3)^2 + A_6(I_3 - 1)^2 + A_7(I_1 - 3)^3 + A_8(I_2 - 3)^3 + A_9(I_3 - 1)^3$	rubber
1967 Hart-Smith	$W = B \left[\int e^{A_1(I_1 - 3)^2} dI_1 + A_2 \ln \left(\frac{I_2}{3} \right) \right]$	rubber
1967 Fung	$W = \frac{1}{ba} \log \frac{1 + (\frac{b}{A}) e^{ax}}{1 + (\frac{1}{B}) e^a}$	soft tissues
1968 Alexander	$W = A_1 \int e^{b_1(I_1 - 3)^2} dI_1 + A_2 \ln \left\{ \frac{(I_2 - 3) + b_2}{b_2} \right\} + A_3(I_2 - 3)$	
1968 Blatz et al.	$W = \frac{A}{2b} [e^{b(I_1 - 3)} - 1]$	soft tissues
1970 Veronda and Westmann	$W = A_1 [e^{b(I_1 - 3)} - 1] + A_2(I_2 - 3) + f(I_3)$	skin
1970 Gou	$W = A_1 [e^{b I_1 (I_1^2 - 3 I_2)} - 1]$	soft tissues
1972 Patel and Vaishnav	$W = A_1 E_{11}^2 + A_2 E_{11} E_{22} + A_3 E_{22}^2 + A_4 E_{11}^3 + A_5 E_{11}^2 E_{22} + A_6 E_{11} E_{22}^2 + A_7 E_{22}^3 + A_8 E_{11}^4 + A_9 E_{11}^3 E_{22} + A_{10} E_{11}^2 E_{22}^2 + A_{11} E_{11} E_{22}^3 + A_{12} E_{22}^4$	blood vessel
1973 Vito	$W = A_1 [e^{b_1(I_1 - 3)} - b_2(I_2 - 3) - 1]$	artery
1974 Kasyanov and Knet	$W = A_1 (e^{a_1} - 1) + A_2 (e^{a_2} - 1)$	blood vessel
1974 Fung et al.	$W = \frac{1}{2} [\lambda I_1^2 + 2\mu I_2] \{ b_1 + \exp(b_2 I_1 + b_3 I_2) \}$	lung
1976 Tong and Fung	$W = \frac{1}{2} [A_1 E_{11}^2 + A_2 E_{22}^2 + 2A_3 E_{11} E_{22}] + B \exp \{ b_1 E_{11}^2 + b_2 E_{22}^2 + b_3 E_{11}^2 + 2b_4 E_{11} E_{22} + b_5 E_{11}^3 + b_6 E_{22}^3 + b_7 E_{11}^2 E_{22} + b_8 E_{11} E_{22}^2 \}$	skin
1980 Vito	$W = A_1(I_1 - 3) + A_2(I_1 - 3)^2 + \dots$	artery
1983 Chuong and Fung	$W = \frac{3}{2} \exp (b_1 E_{11}^2 + b_2 E_{22}^2 + 2b_4 E_{11} E_{22})$	artery

Second, viscoelastic approach is based on the linear or nonlinear viscoelasticity of continuum mechanics. Usually, biological tissues show the features of hysteresis, relaxation, creep and strain rate insensitivity [Fung,1972]. To explain these characteristics of soft tissues, a number of viscoelastic models have been suggested. For oscillations of small amplitude about an equilibrium state, the discrete type linear models such as Voigt, Maxwell, and Kelvin models have been applied [e.g., Galford and McElhaney,1970; Sanjeevi,1982].

For finite deformation, the nonlinear stress-strain characteristics of the tissues must be considered. Therefore, the quasilinear viscoelastic model [Fung,1967], finite linear model [Lianis,1963; Dehoff,1978], and many forms of nonlinear models [Lockett,1972; Vaishnav,1980; Wu and Lee,1984] have been suggested. Among them, the quasilinear viscoelastic model was most frequently applied to several tissues including tendons [Haut and Little,1972], mesentery [Chen and Fung,1973], heart muscle [Pinto and Fung,1973], ligaments [Woo et al.,1981; Jenkins and Little,1974], articular cartilage [Woo et al.,1980], papillary muscle [Pinto and Patitucci,1980], smooth muscle [Price et al.,1979], and heart valves [Rousseau et al.,1983]. The quasilinear viscoelastic model requires that the reduced relaxation function must be independent of strain level, and relaxation function is assumed to be factorable into a function of the time times the stress.

In macroscopic analysis, it is very difficult to verify the physical meaning of the parameters in the constitutive equations. This fact results in difficulties in its application to the real physiological situations. To understand the interactive nature of macroscopic behavior with the constituents at the microscopic level, the microscopic analyses [e.g. Lanir and Fung,1974 a,b; Lanir,1979,1980,1983 a,b; Comninou and Yannas,1976; Decreamer et al.,1980 a,b; Wu and Yao,1976] and morphological observations [e.g. Broom,1978; Viidik and Ekholm,1968] have been performed. In microscopic analysis, all parameters in the constitutive equations are closely related to the measurable physical quantities such as volume fraction of each component, stiffness of fiber, orientation and waviness of fibers. But the microscopic analysis has been limited in its application, mainly due to the lack of data about the collagen and elastin fibers in the tissue [Fung,1982].

Microscopic analyses are based on the theory of the fiber reinforced composite material. Soft biological tissues consist of collagen fibers, elastin fibers, and ground substance. The mechanical properties of soft tissue depend on the response of its constituents and their structure. Thus, soft tissues may be treated as fiber reinforced composites. Adkins [1956], Green and Adkins [1970], Adkins and Rivlin [1955], and Spencer [1972] developed the theory of large deformations of elastic materials reinforced by inextensible cords. Wu and Yao [1976] investigated the mechanical properties of human lumbar fibrosus, and the fibers were considered to be extensible and nonlinearly elastic. Lanir [1979,1980,1983 a,b] proposed two conceptual models of the tissue's structure; 'High density cross links version' and 'Low density cross links version'. Based on these two structural

models, he presented several constitutive equations which have material constants and fiber distribution functions as variable parameters.

To understand the tissue's microstructure, the morphological observations such as the light microscopy [Weibel,1963], phase contrast microscopy [Broom,1977,1978], the scanning and transmission electron microscopy [Ishihara et al.,1980; Ferrans et al.,1978] have to be made on tissues. For the better understanding of the relationship of microstructure to function, simultaneous morphological and stress-strain studies have been carried out. For example, Broom [1978] carried out uniaxial tension test on porcine tricuspid leaflets, and simultaneously observed the geometric changes of elastin and collagen fibers using the optical technique known as 'Nomarski differential interference contrast'. He observed that the wave form of collagen bundles showed the uncrimping response to the increased load. Broom did not quantify the microstructure. To quantify the microstructure, stereologic techniques [Underwood,1970] can be used. Stereology is the science of deducing 3-dimensional structure from 2-dimensional observations. Quantification of the volume fractions, fiber orientation, fiber length and fiber waviness is important to mechanical modelling of soft tissue which attempt to account for structural variables [e.g.;Comminou and Yannas,1976; Lanir,1978,1979 a,b,1980; Decraemer,1980 a,b]. The quantifications of microstructure from the stereologic point of view have been applied to the myocardium [Anversa et al., 1979], the skeletal muscle [Eisenberg,1974] and the lung tissues [Weibel,1979]. But the stereological technique was not applied to the pericardium. Therefore, the combined studies of microstructural analysis and macroscopic analysis are recommended for the better understanding of mechanical properties of soft tissues.

b) Mechanics of the Pericardium

To understand the effects of the pericardium on cardiac function, we have to know the mechanical properties of the pericardium. But very little is known about the mechanical properties of the pericardium.

Barnard [1898] first examined the mechanical properties of the pericardium. Unfortunately, his comment, "Pericardium is practically inextensible" is incorrect in the range of small physiological loading.

Nelemans [1940] studied the elastic and plastic properties of pericardium. However, the plasticity of pericardium has been a controversial point up to now [Lee and Boughner,1981; Trowbridge and Crofts,1986].

Hildebrandt, et al. [1969 a,b] reported a constitutive equation form for several animal tissues including the canine pericardium. They adopted the assumption of incompressibility and isotropy without justification, and applied the nonlinear elastic theory to obtain the constitutive relations under the uniaxial and uniform biaxial deformations. They conducted inflation tests and used membrane theory to compute the stresses from the measured inflating pressure, radius of curvature and

tension. In inflation test, the principal strains cannot be varied independently. This fact restricts the use of the inflation test to determine the constitutive law. They used single-sided manometer to measure the inflation pressure, and marker granules to measure the strains. They proposed the following constitutive equation for mesentery and pericardium :

$$\sigma = B \left(\lambda^2 - \frac{1}{\lambda} \right) \left[\frac{1}{(\lambda_{max} - \lambda)^{b_1}} + \frac{1}{(\lambda - \lambda_{min})^{b_2}} \right] \quad (1.1)$$

where, σ is Eulerian stress and λ is the extension ratio. The λ_{max} and λ_{min} are the uniaxial strain asymptotes. The material constants B , b_1 , b_2 , λ_{max} and λ_{min} have to be determined from the experimental data.

Rabkin, et al. [1974] conducted several uniaxial loading tests on canine pericardium at room temperature, and reported the results about the incremental modulus, relaxation stress and hysteresis. They observed that the pericardium had the similar nonlinear stress-strain relationships, strain rate insensitivity and viscoelastic behaviors as other soft tissues.

Using these experimental data, Rabkin and Hsu [1975] constructed the one-dimensional stress-strain law of the pericardium as an exponential form:

$$T = B(e^{b\epsilon} - 1) \quad (1.2)$$

where, T is Lagrangian stress, strain ϵ is defined as the length changes per unit initial length, and B and b are material constants. Also, they proposed the mechanical model for the pericardium which is composed of two parallel springs and one dashpot, representing the collagen and elastic fibers. But usefulness of their mechanical model is questionable. In their model, the springs and dashpots are arranged in the normal direction to the plane of pericardium, this may be far from the real structure of the pericardium.

Vito [1979] carried out twenty constant strain rate uniaxial test on canine pericardium at 37°C. He assumed the pericardium as a homogeneous, isotropic, incompressible and elastic material. From the concepts of hyperelasticity, he postulated a stress-strain law using the strain energy function of the following form:

$$W = A(I_1 - 3)^b \quad (1-3)$$

where, I_1 is the strain invariant ($I_1 = \lambda^2 + \frac{2}{\lambda^2}$), and A and b are material constants. These material constants were determined for a least squared fit to the data. Also, he proposed a mechanical model of cardiac function including the effects of pericardium. Using this model, he showed that the effects of pericardial thickness changes were significant to the pericardial fluid pressure of the deformed heart. One year later, Vito [1980] reported one biaxial testing result on the canine pericardium. A software based, biaxial testing system was used in this constant stretching rate test. The result indicated that the anisotropic and viscoelastic effects might be significant in the pericardium.

Wiegner and Bing [1981] investigated the elastic and viscoelastic properties of the canine pericardium at 37°C, and particularly at low stresses. Constant stretching rate, creep and relaxation tests were performed on the pericardial strips. They used the following form of stress-strain equation to fit the experimental data:

$$\sigma = \sum_{i=1}^2 2 \frac{B_i}{A_i} \left(\lambda^{A_i - 1} - \lambda^{\frac{A_i}{2} - 1} \right) \quad (1.4)$$

where, σ is the Eulerian stress and A_i , B_i are material constants. They tried to combine the analysis of mechanical properties with microstructure observation. Only the general comments were given, without sophisticated analysis.

Lee and Boughner [1981] performed the uniaxial tests on the canine pericardia in different test environments. They explained the changes of mechanical properties caused by different environments, and emphasized the importance of preconditioning, the effects of temperature and the degree of wetness. They used the same form of stress-strain equation as the equation (1.2), to fit the stress-strain data. Several years later [1985], they performed a series of tests on human pericardium, and compared these results with their previous test results of canine pericardium. They showed that the mechanical behaviors of both pericardia were quantitatively similar, whereas human pericardium displayed significantly greater viscous effects. Their results suggest that the experimental results of canine pericardium may not be directly applicable to human pericardium.

Shoemaker [1984] developed a two-dimensional constitutive model for membranous soft tissues, based on the microstructural consideration. This model was applied to experimental stress-strain data from canine pericardium. Its applicability to pericardium was not so good.

Lee et al. [1985] investigated the two-dimensional elastic and viscoelastic properties of the pericardium in normal and volume overload dogs. They reported only qualitative aspects of the pericardial mechanics, and didn't suggest any constitutive equation. They observed the anisotropic characteristics, strain rate insensitivity, creep and stress relaxation of pericardium. But no analysis was given. They observed the rightward shift of tension-stretch curve in dogs with chronic volume enlargement, and concluded that chronic cardiac dilatation resulted in a more compliant pericardium without thickness change. They measured the two orthogonal dimensions of a central grid placed on the specimen electrooptically using a pair of television cameras and video dimension analyzers. They measured thickness with an instrument consisting of a micrometer and a force transducer, when the pressure was 4.0 g/cm². However, they did not explain the reason why this value was taken. They pointed out that the anisotropy of pericardium resulted in difficulties when comparing the biaxial test data from one specimen with another.

Trowbridge and Crofts [1985] performed the cyclic uniaxial load tests on natural pericardium and chemically modified bovine pericardium which is used in the construction of heart valve substitutes. They observed significant increases in length in

both the preconditioned natural and chemically fixed pericardium. They stated that the deformations caused by preconditioning were not permanent, but the deformations caused by chemical fixation were permanent. From these reasons, they suggested that the original tissue length in its undeformed state should be used as a reference gauge length for the mechanical testings.

Yin et al. [1986] performed biaxial tests on canine pericardium. They showed how to quantify the biaxial stress-strain data, using the regression analysis [Belsley et al. 1980] and bootstrapping method [Efron 1979]. Main emphasis was given to the data analysis method. They proposed a two-dimensional strain energy density function with five-parameter:

$$W = B_1 (E_{11}^2 + E_{22}^2) + B_2 E_{11} E_{22} + 0.5 A [\exp (b_1 E_{11}^2 + b_2 E_{22}^2) - 1] \quad (1.5)$$

where, E_{11} and E_{22} are Green strains, and B_1 , B_2 , A , b_1 and b_2 are material constants. They also found that the pericardial mechanics might be strain-history dependent and anisotropic. However, they didn't perform any viscoelastic analysis.

In summary, the previous studies on pericardium show that the pericardium has the similar load-deformation characteristic, strain rate insensitivity and viscoelastic behaviors as other soft tissues. Although many tests such as uniaxial stretching tests, uniform biaxial stretching tests, relaxation tests and creep tests were performed on the pericardium, the constitutive equation was not identified.

Most studies show that the pericardium is anisotropic. However, all studies were based on the assumption of isotropy or transverse-isotropy. And the biaxial strains were measured by applying a grid system to the surface of a two dimensional structure and observing deformations of the grid. However, the grid methods allow for quantification of only average tensile strains within the grid, and it is sufficient for an isotropic material. For an anisotropic material, we need to know the shear strains, and the strain energy density function has to contain shear effects. Therefore, new studies on the pericardium which account for anisotropic effects are in order.

1.5 Brief Outline of Objectives

The proposed study is a systematic study of the mechanical properties of canine pericardium. There are two main objectives in this study.

The first is to identify the stress-strain law of the pericardium via the concepts of pseudo-elasticity and hyperelasticity. The pericardium is assumed as an incompressible, orthotropic material with unknown material symmetry axes. Several forms for strain energy density function are proposed, and used to quantify the biaxial test data. The stress-strain law is formulated with respect to stretching axis and material symmetry axis. By performing the biaxial testing completely under the software control, the orientation of material symmetry axis and the material constants will be

quantified. The tensile strains and shear strains are measured by tracking particles placed on the specimen using a video digitizer. For the first time, shear strains measured from video digitizer are included in the stress-strain law, and the material symmetry axis may be determined approximately.

The second is the microstructure observation to give some insight on understanding the relationship between material properties and microstructure of the pericardium. Tissues are fixed in formalin at various stress level, and after the process of dehydrating, clearing, embedding in paraffin, sectioning and staining, the series of specimen slides are obtained. The number, orientation and shape of the collagen and elastin fibers are observed from these slides using the light microscope. The stereologic techniques will be used to quantify the microstructure of the pericardium. It may be possible to infer the orientation of the material symmetry axis from the histological observations. Some explanations may thus be given to the correlations of microstructural and mechanical measurements in biaxial tests.

2. Experimental Methods

2.1 Introductory Comments

In biomechanical studies on soft tissues, the various tests are used as the following:

- (1) uniaxial test
- (2) uniform and non-uniform biaxial test
- (3) triaxial test
- (4) shear test
- (5) torsional test
- (6) inflation test
- (7) indentation test

✓ In general, the three-dimensional constitutive law cannot be deduced from the biaxial data alone. It requires the complete sets of triaxial test data. But it is very difficult to perform the triaxial tests. Therefore, the biaxial tests combined with another tests such as shear and torsion tests are commonly recommended. Before performing tests, we have to keep in mind some common experimental difficulties and concerns.

a) In Vivo and in Vitro

The experimental results obtained in vivo and in vitro, may be significantly different from with each other. The differences result from the changes in dimensions, mechanical or chemical properties, boundary conditions, moisture, temperature etc. Therefore, we have to be cautious to apply the test results obtained in vitro to the in vivo condition.

b) The Reference State

In the pseudo-elastic analysis, a "natural" or "stress-free" state is assumed to exist. However, finding and quantifying the "stress-free" state of a soft tissue is one of the most difficult task in biomechanics [Fung,1981]. This is because the response is history dependent and load history prior to experiment is unknown, and the tissue is very compliant at a low stress level.

c) Preconditioning

Preconditioning is a repetition of the same procedure a number of times until a state of homeostasis is obtained. Preconditioning is necessary for each experiment in order to obtain repeatable results. Since the pericardium in vivo is subjected to cyclic loading, the specimen is preconditioned by sequentially loading and unloading it until the response become reproducible. However, the effects of preconditioning on the mechanical properties are uncertain.

d) Edge Effect

It is very difficult to provide the uniform stress fields on the edge. Disturbances due to the application of fixtures result in complex stress-strain states at the point of application. Usually guided by the Saint-Venant's principle, the data of the region sufficiently far from edges are used to quantify the mechanical properties.

2.2 Experimental System

A computer-controlled biaxial test system as shown in Figure (2) is used for the study of the mechanical properties of pericardium. The main components of the system are described below.

a) Tissue Bath

Tissues are immersed in a jacketed plexiglass chamber containing a physiologic solution. As a physiologic solution, we use the 0.9% saline solution. This solution can be expected to minimize the osmotic swelling of the tissues. The solution is maintained at 37°C (or at room temperature) using both a refrigeration unit and pump-thermo-control unit to circulate continuously ethylene glycol of fixed temperature through the jacket.

b) Stretching Mechanism

The stretching mechanism consists of two identical, orthogonally positioned axes, each driven by a digital DC servo motor as shown in Figure (3). Each axis consists of two coupled, double-nut, preloaded ball screws, one with a left and one with a right hand thread. The servo system accepts the velocity and position information through a customized controller units and sixteen bit parallel interfaces which are connected to the computer. The servos can be run in either of two modes: the step mode or the phase-locked mode. The phase-locked mode will be used in constant stretch rate tests, and the step mode will be used in the relaxation test. The velocity range of the servos are 0.000127 to 4.16 cm/s, and the position accuracy is 5.08 microns.

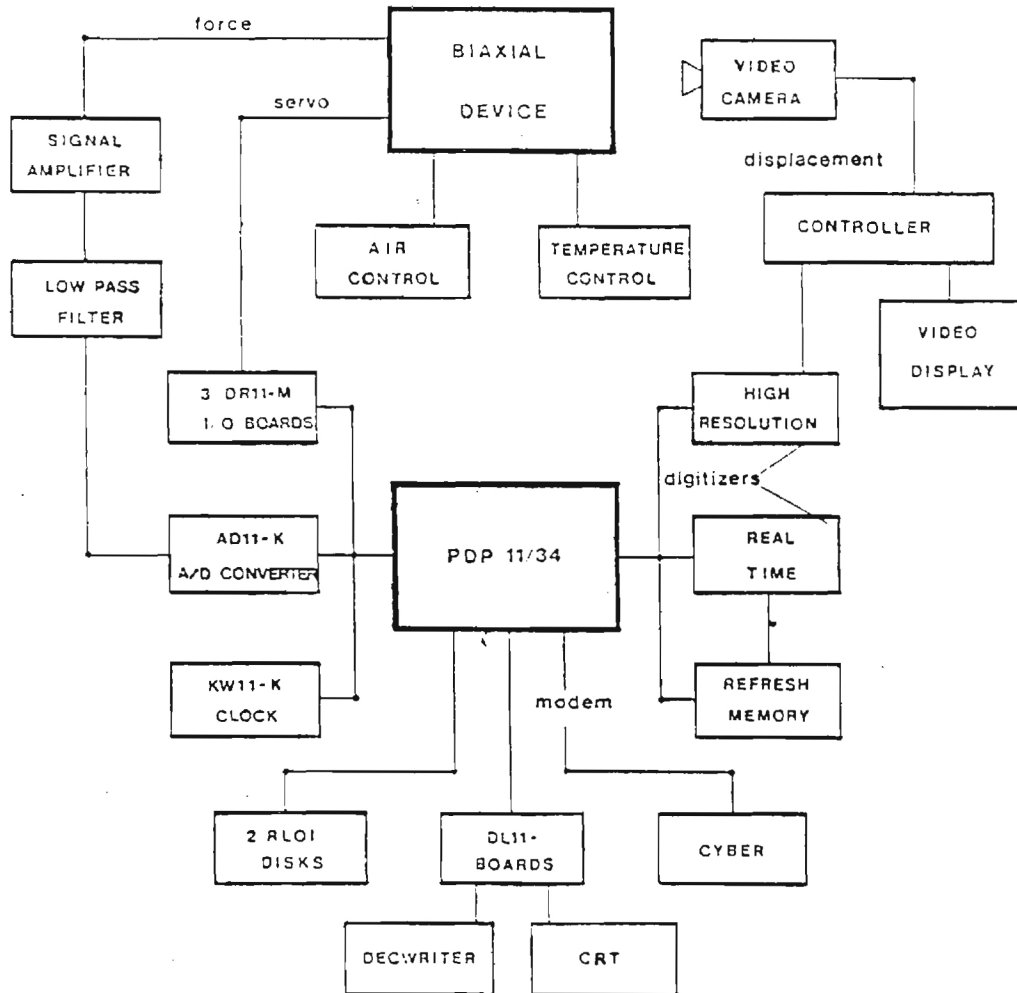


Figure (2) Flow chart of the bi-axial test system.

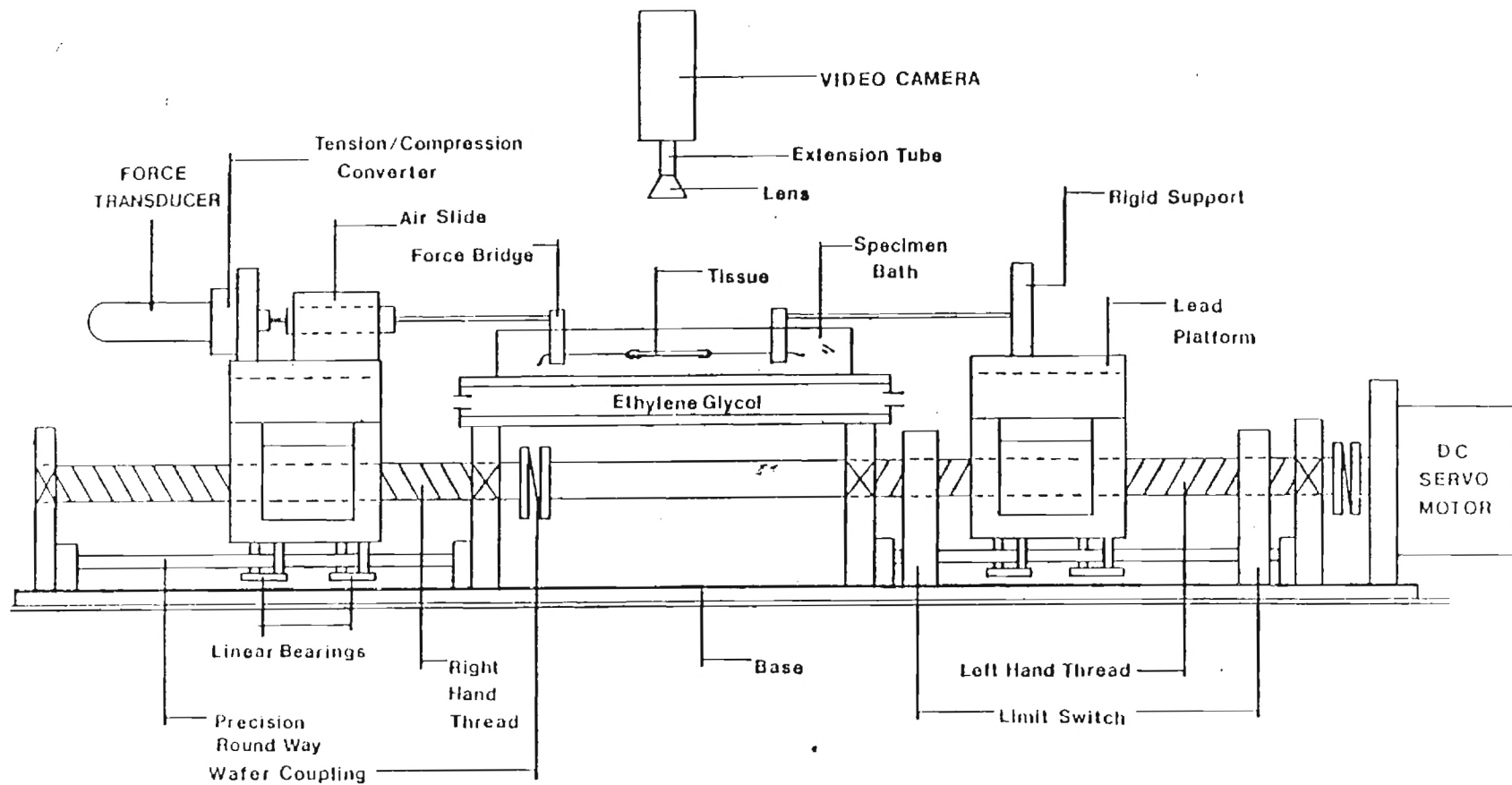


Figure (3) Sideview of the bi-axial test equipment.

c) Force Measurement System

The Statham gold cell with a tension-to-compression converter is used as a force transducer. The load measurement is linear in the range of 0 to 200 grams. The load cell signal is conditioned with a Honeywell Accudata 218 strain gage amplifier and filtered by a 10 Hz low pass filter. Force data is digitized with a twelve bit A/D converter interfaced to the PDP-11/34. The load cell is connected to the force plate which rides in an air slide to eliminate the frictional forces.

d) Dimension Measurement System

The in-plane dimensions of the specimen are measured and monitored by a video digitizer interfaced to the PDP-11/34. The system consists of a video camera, a controller unit, a picture displayer, low and high resolution digitizer as shown in Figure (4). This system is completely controlled by the software. A picture frame is digitized into a 640 column by 480 row pixel grid. Each pixel is identified by an x-y position and a light intensity value. Five tracking particles (1 at center, 4 at corners of 1.5x1.5cm square) of the central region of the specimen may be identified by concentrations of small or zero light intensity values. These points are tracked by computer software using the algorithm described in section 2.5. The locations of the particles at the reference state are determined by using a joystick cursor.

During testing, the initial search region is defined by locating the particles with the joystick cursor. Subsequent search regions and particle locations are determined using the algorithm described in section 2.5.

e) Thickness Measurement System

The thickness can be measured by the electrical resistance method. The thickness measurement device consists of an aluminum frame, a micrometer, a 9 volt battery, a voltmeter and a removable lexan plate as shown in Figure (5). The specimen from the tissue bath will be placed on the lexan plate in a near initial reference state after removing much of the physiologic solution. A gold probe with a wire to the battery will be used as the micrometer tip. A second wire will be placed on the specimen surface. The electrical circuit remains open and the voltmeter shows no voltage until the probe comes into contact with the specimen surface. Taking the difference between the micrometer readings corresponding to the lexan surface and specimen yields the tissue thickness.

The techniques used to measure the thickness are described in detail in section 2.4.

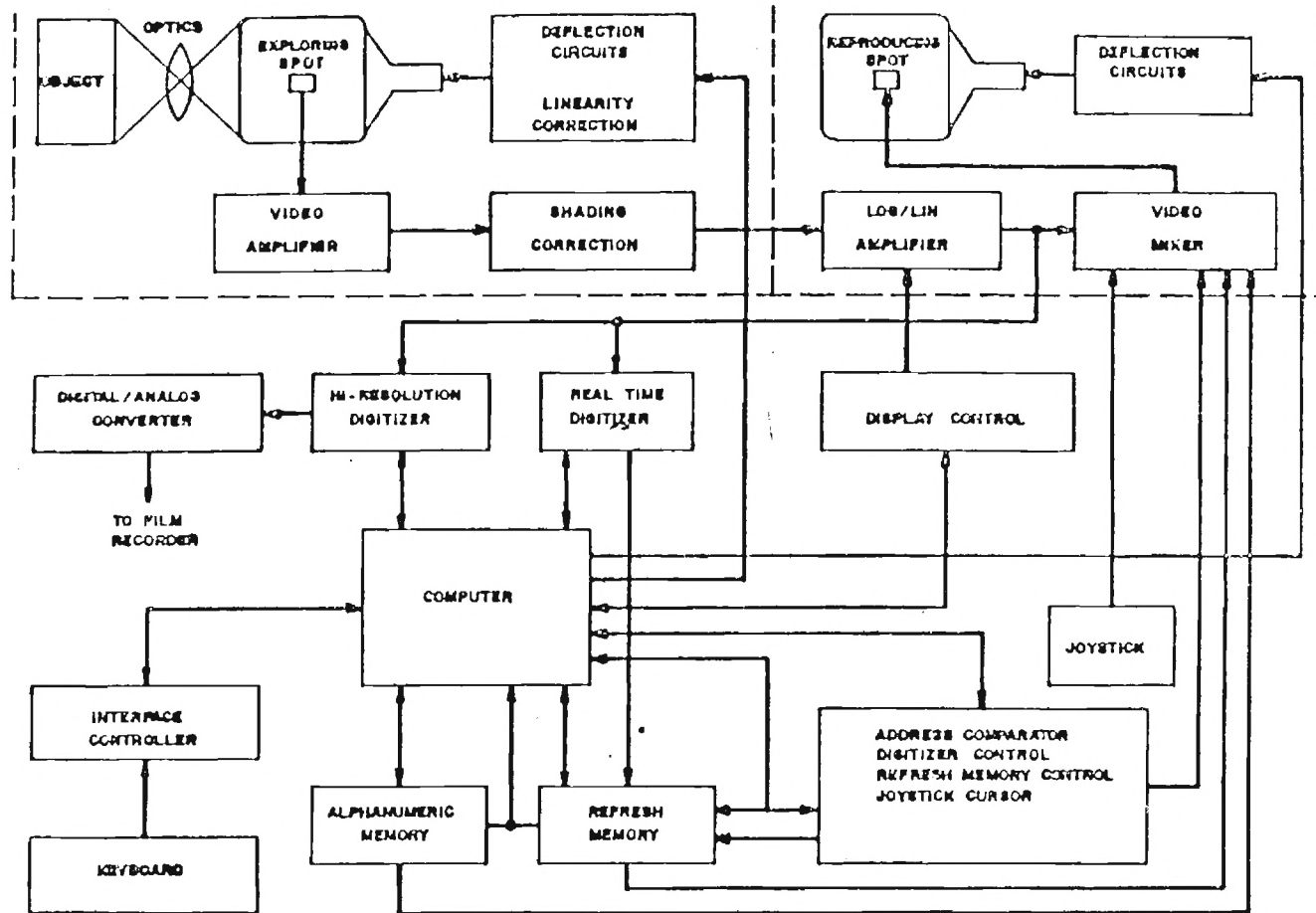


Figure (4) Flowchart of the video digitizing system.

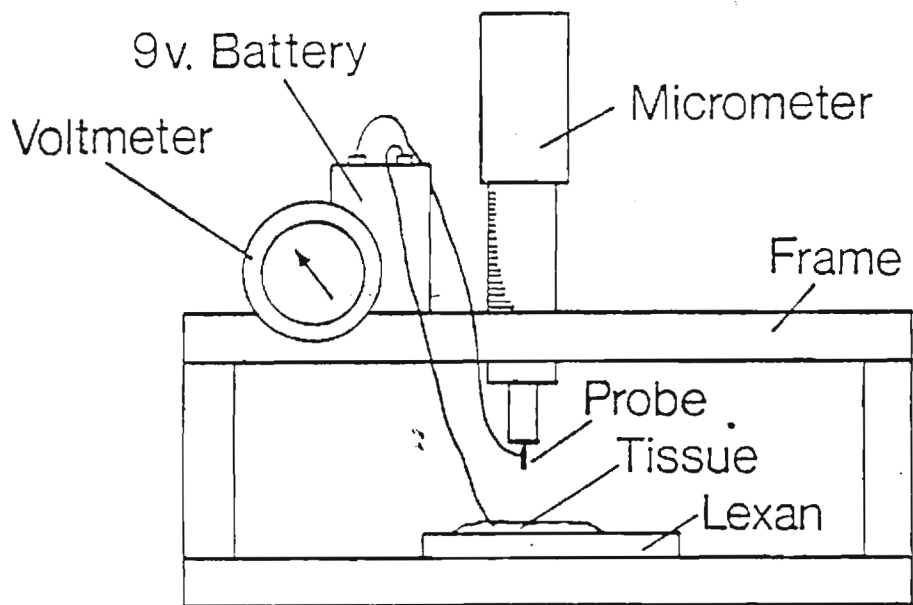


Figure (5) Electrical resistance thickness measuring device.

2.3. Specimen Acquisition

Specimens were acquired at the dog lab of Crawford Long Hospital of Emory University. Most animals were sacrificed by exsanguination. However, some were sacrificed using an overdose of anesthetic. In many cases, the animals were used for other experiments. However, the pericardium was unlikely to have been affected in any way either by the method of sacrifice or the experimental protocols used prior to our acquiring the specimen.

The pericardium was marked with a dye or suture to indicate anatomical orientation. The specimen was then either removed in the dog lab or the whole heart, including the pericardium, was brought back to Georgia Tech for dissection. The pericardium was maintained at 4^o C in saline until used less than 48 hrs. later.

2.4 Specimen Preparation

a. Measurement of Initial Dimensions

a.1 In Plane Dimensions

After isolating the specimen from canine parietal pericardium, it was placed on the lexan plate with sufficient saline around it to prevent sticking. The initial dimensions of the outer edge region were measured using a ruler. The in-plane measurements of the central tracking region were made by floating the specimen in saline and using the image digitizer to measure the distance between the particles on the tissue. The particles were located as accurately as possible using the joystick cursor, and the pixel values of the cursor position were recorded. By repeating this procedure four times, the average pixel values of each particle were taken as the exact location of the particles at the initial reference state.

a.2 Thickness Measurement

The thickness of pericardium has to be measured accurately, because the constants of the constitutive equation may be sensitive to the small changes in thickness value. However, it is not easy, since the pericardium is very thin and soft. The thickness of canine pericardium was reported as the range of 0.14 to 0.28 mm [Wiegner et al., 1981; Freeman and LeWinter, 1984; M.C. Lee et al., 1985]. We employed the electrical resistant method to measure the thickness. The measurement device is described in detail in section 2.2. After the initial dimensions were measured but prior to specimen mounting, the specimen was placed on the lexan plate and restored to its undeformed dimensions. The lexan plate and specimen were then placed on the frame under the micrometer tip. The micrometer tip was then connected to the battery with a wire. A second wire was then placed on the specimen surface. The electrical circuit remains open, and the voltmeter showed no voltage until the micrometer tip came into contact with the specimen surface. When the micrometer tip

touched the specimen surface, the electrical circuit closed, and voltmeter showed some voltage. At that instance, we took the thickness readings.

However, these readings were the combination of specimen thickness and saline film thickness. To minimize the saline film effects, the following protocol was employed. The specimen was removed from the saline bath with forceps and placed on a towels, first on one side and then the other, to remove much of the excess saline. The specimen was then placed on the lexan plate within the electrical-resistance device. Measurements were taken at one point on the surface at even time increments. We recorded two readings: one at initial contact stage, the other at lost-contact stage. As shown in Figure (6), the micrometer tip first contact the surface saline film, then the electrical circuit closed, and we recorded one reading value at this initial contact stage. When releasing the micrometer tip slowly, the electrical circuit remained closed because of the surface tension effect. After a while, it suddenly lost the contact, and we recorded another reading value at this lost-contact stage. The difference between these two readings is mostly due to the surface saline film effects. We expect that the differences between the two readings will decrease with time as the saline film evaporates. The reason for this is that the reading at initial contact stage might be a combination of the tissue thickness (h_1) and saline film thickness (h_2). And the reading at lost-contact stage might be a combination of the tissue thickness (h_1), saline film thickness (h_2) and saline capillary height (h_3) due to surface tension as shown in Figure (6). Since we want to determine the tissue thickness (h_1) alone, we may take the reading value at $h_2=0$ and $h_3=0$ as a tissue thickness. We may assume that h_1 is constant (no tissue thickness change) as long as some saline remains on the tissue surface. If no saline remains on the surface, the tissue begins to dry out and the thickness decreases rapidly. Therefore, the slope of the curve (h_1+h_2) changes greatly at the point of $h_2=0$ as shown in Figure (7). Figure (7) is the real thickness measurement data of the specimen #03. Practically, this point could be determined as a cross-point of two curves h_1+h_2 and $h_1+h_2+h_3$ by extrapolating initial readings in 8 minutes.

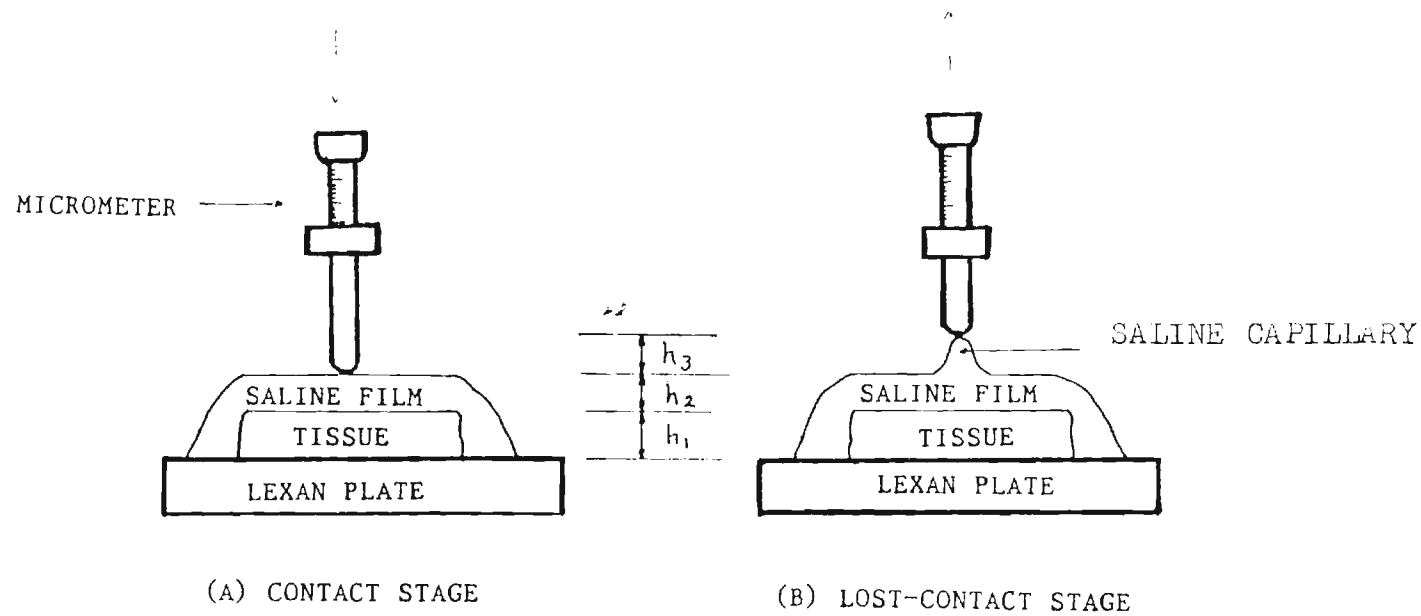


Figure (6) Schematic diagram of two reading stage for thickness measurement: (a) contact stage (b) lost-contact stage.

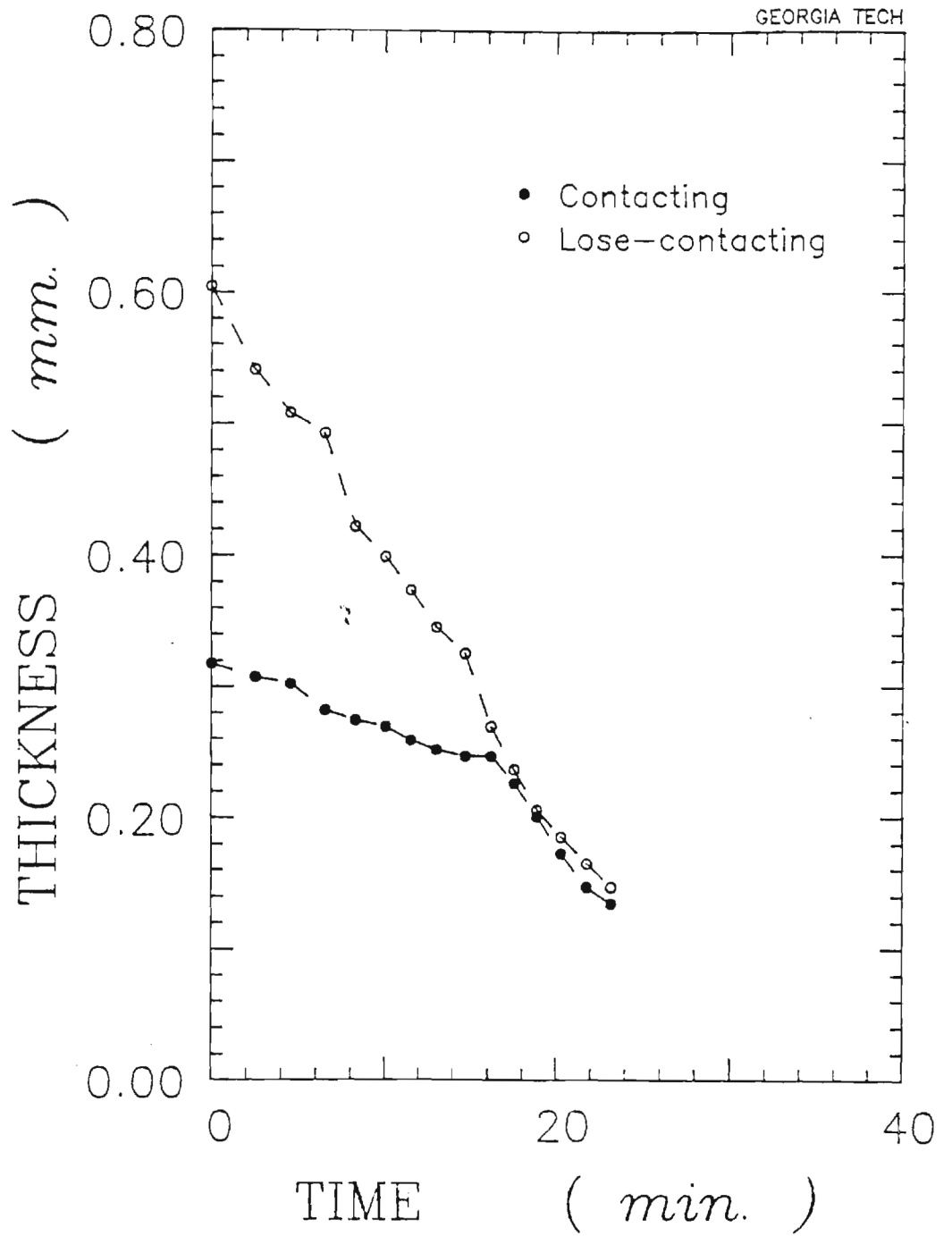


Figure (7) Thickness measurement - the change of two stage reading values with time for specimen #02.

b. Specimen Mounting

Approximately 5cmx5cm squared specimen isolated from the canine pericardium using a scalpel and scissors. To get a good specimen, the relatively uniform portion (with not too much excess fat attached) of pericardium was chosen.

To measure the initial dimensions and the strains, 0.025cm-diameter black particles were glued on the 1.5cmx1.5cm squared center region of the specimen surface using cyanoacrylate ester adhesive. The position histories of these particles were used to calculate the shear and tensile strains at each data collecting time increment. To apply relatively uniform stress field on the boundary, 2cm half-folded magnetic tapes were glued to the upper and lower surfaces of specimen by using the cyanoacrylate ester. And the magnetic tapes were connected to the force-distribution bridges by means of silk sutures as shown in Figure (8). We made the sutures 3cm long so as not to impose the shear stress on the specimen boundaries.

2.5 Specimen Testing

a. Strain Measurement

Reduction of the particle position histories into strain measures is fundamental for examining the deformation field. The displacements of the marker centroids are directly measured using a video digitizer as described below. Given the locations of the four particles, the extensional and shear strains can be calculated using the interpolation function method of Hoffman [1984].

During testing, the initial search region is defined by locating the particles with the joy-stick. Subsequent search regions are determined by the computer by predicting the expected location of a marker based on the known speed of the servos, the direction of travel, the specimen dimensions, and the time of travel since the last search. In this search region, the computer search for a pixel value which is below a user-defined threshold. Once a lower-than-threshold value is found, then the computer adds the contents of rows and columns in a localized region to determine the center of particle. This process is repeated for each of the four corner particles at each time t . A similar technique was used by Humphrey [1985].

We introduce interpolation functions to approximate the displacement field in the central region of the specimen. Hence, we can compute shear and extensional strains at any point within the central region [Hoffman, 1984].

Consider a mapping of four particles from global (x_1, x_2) coordinates into natural (η_1, η_2) coordinates as shown in Figure (9).

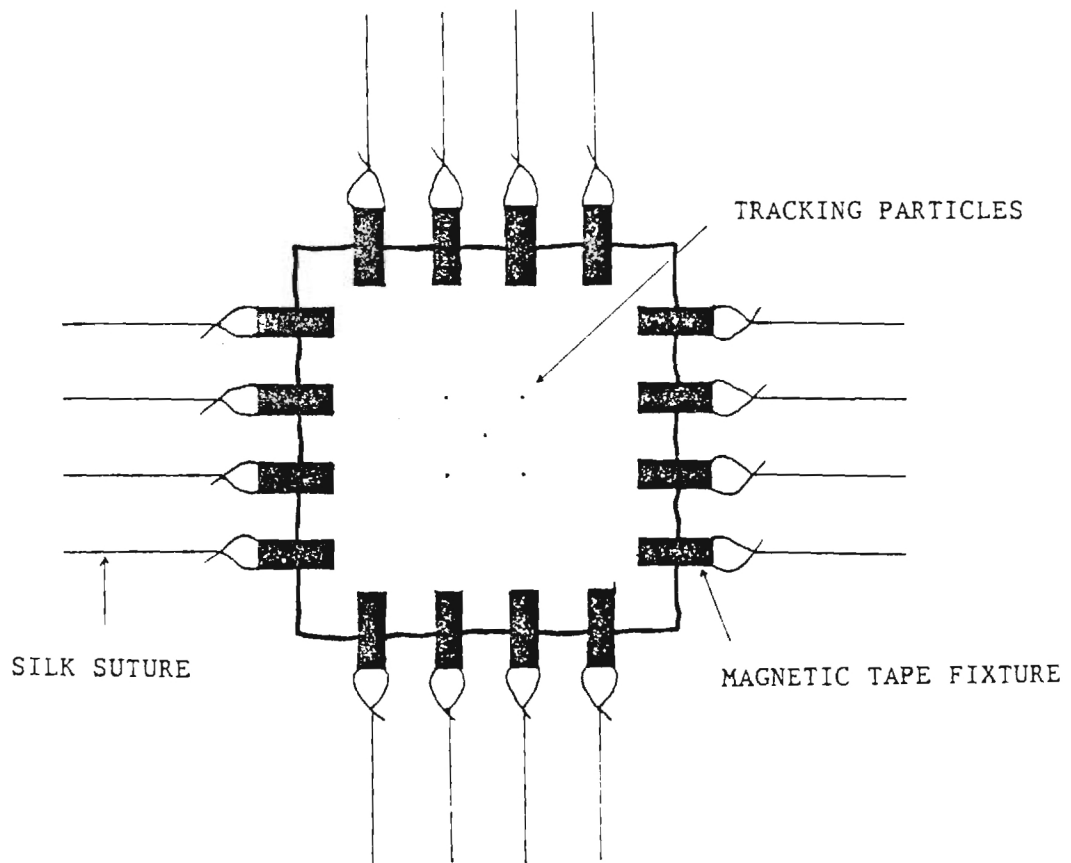


Figure (8) Specimen mounting.

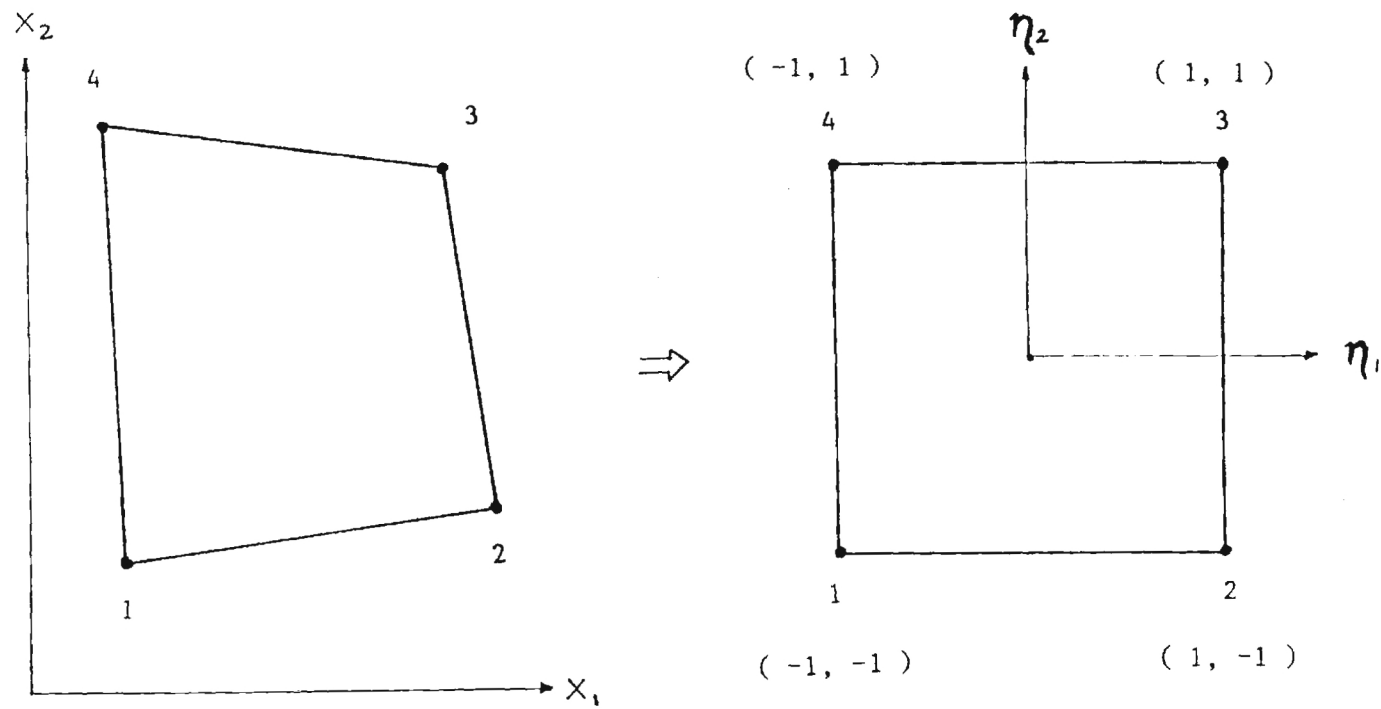


Figure (9) Mapping of tracking particle position from global coordinates to natural coordinates.

We can measure the positions of four particles at undeformed state (x_1, x_2) and deformed state (y_1, y_2) . Thus, the displacement (u_1, u_2) of each of four tracking particles are measured:

$$\begin{aligned} (u_1)_n &= (y_1)_n - (x_1)_n \\ (u_2)_n &= (y_2)_n - (x_2)_n \end{aligned} \quad (\text{where, } n=1, 2, 3, 4) \quad (2.1)$$

The displacement components u_1 and u_2 of any point within the central region can be represented as the functions of the normalized coordinates η_1, η_2 by using the interpolation functions $H_n(\eta_1, \eta_2)$ and the measured constants $(u_1)_n, (u_2)_n$:

$$\begin{aligned} u_1(\eta_1, \eta_2) &= \sum_{n=1}^4 (u_1)_n \cdot H_n(\eta_1, \eta_2) \\ u_2(\eta_1, \eta_2) &= \sum_{n=1}^4 (u_2)_n \cdot H_n(\eta_1, \eta_2) \end{aligned} \quad (2.2)$$

where, the interpolation functions $H_n(\eta_1, \eta_2)$ are given as

$$\begin{aligned} H_1(\eta_1, \eta_2) &= \frac{1}{4} (1 - \eta_1)(1 - \eta_2) \\ H_2(\eta_1, \eta_2) &= \frac{1}{4} (1 + \eta_1)(1 - \eta_2) \\ H_3(\eta_1, \eta_2) &= \frac{1}{4} (1 + \eta_1)(1 + \eta_2) \\ H_4(\eta_1, \eta_2) &= \frac{1}{4} (1 - \eta_1)(1 + \eta_2) \end{aligned} \quad (2.3)$$

Also, the (x_1, x_2) coordinates of any point within the central region can be expressed as a function of η_1, η_2 :

$$\begin{aligned} x_1(\eta_1, \eta_2) &= \sum_{n=1}^4 (x_1)_n \cdot H_n(\eta_1, \eta_2) \\ x_2(\eta_1, \eta_2) &= \sum_{n=1}^4 (x_2)_n \cdot H_n(\eta_1, \eta_2) \end{aligned} \quad (2.4)$$

Hence, the displacement u_1, u_2 and the undeformed state coordinates (x_1, x_2) of any point within the central region are expressed as the functions of η_1 and η_2 .

Using the chain rule, we can write the partial derivatives of the displacement components with respect to η_1 and η_2 :

$$\begin{Bmatrix} \frac{\partial u_1}{\partial \eta_1} \\ \frac{\partial u_1}{\partial \eta_2} \end{Bmatrix} = \begin{Bmatrix} \frac{\partial x_1}{\partial \eta_1} & \frac{\partial x_2}{\partial \eta_1} \\ \frac{\partial x_1}{\partial \eta_2} & \frac{\partial x_2}{\partial \eta_2} \end{Bmatrix} \begin{Bmatrix} \frac{\partial u_1}{\partial x_1} \\ \frac{\partial u_1}{\partial x_2} \end{Bmatrix} \quad (2.5)$$

and similarly for u_2 .

Inverting these relationships, we can get the partial derivatives of u_1 and u_2 with respect to x_1 and x_2 which are used to calculate the Lagrangian finite strains (Green's strains). That is,

$$\begin{pmatrix} \frac{\partial u_1}{\partial x_1} \\ \frac{\partial u_1}{\partial x_2} \end{pmatrix} = \frac{1}{\frac{\partial x_1}{\partial \eta_1} \frac{\partial x_2}{\partial \eta_2} - \frac{\partial x_1}{\partial \eta_2} \frac{\partial x_2}{\partial \eta_1}} \begin{pmatrix} \frac{\partial x_2}{\partial \eta_2} & -\frac{\partial x_2}{\partial \eta_1} \\ -\frac{\partial x_1}{\partial \eta_2} & \frac{\partial x_1}{\partial \eta_1} \end{pmatrix} \begin{pmatrix} \frac{\partial u_1}{\partial \eta_1} \\ \frac{\partial u_1}{\partial \eta_2} \end{pmatrix} \quad (2.6)$$

and similarly for u_2 .

If we know the (η_1, η_2) coordinates of any point in the central region, we can compute $\frac{\partial u_1}{\partial x_1}$, $\frac{\partial u_1}{\partial x_2}$, $\frac{\partial u_2}{\partial x_1}$ and $\frac{\partial u_2}{\partial x_2}$.

The Lagrangian finite strains (Green's strains) with respect to x_1, x_2 axes are given by:

$$\begin{aligned} E_{11} &= \frac{\partial u_1}{\partial x_1} + \frac{1}{2} \left[\left(\frac{\partial u_1}{\partial x_1} \right)^2 + \left(\frac{\partial u_2}{\partial x_1} \right)^2 \right] \\ E_{22} &= \frac{\partial u_2}{\partial x_2} + \frac{1}{2} \left[\left(\frac{\partial u_2}{\partial x_2} \right)^2 + \left(\frac{\partial u_1}{\partial x_2} \right)^2 \right] \\ E_{12} &= \frac{1}{2} \left[\frac{\partial u_1}{\partial x_2} + \frac{\partial u_2}{\partial x_1} + \left(\frac{\partial u_1}{\partial x_1} \right) \left(\frac{\partial u_1}{\partial x_2} \right) + \left(\frac{\partial u_2}{\partial x_1} \right) \left(\frac{\partial u_2}{\partial x_2} \right) \right] \end{aligned} \quad (2.7)$$

and the deformation gradients are:

$$\begin{aligned} C_{ij} &= \frac{\partial y_i}{\partial x_j} = \frac{\partial u_i}{\partial x_j} + \delta_{ij} \\ C_{11} &= \frac{\partial u_1}{\partial x_1} + 1 \\ C_{12} &= \frac{\partial u_1}{\partial x_2} \\ C_{21} &= \frac{\partial u_2}{\partial x_1} \\ C_{22} &= \frac{\partial u_2}{\partial x_2} + 1 \end{aligned} \quad (2.8)$$

b. Stress Measurement

The resultant forces applied to the specimen can be measured by the force transducer. Assuming that the central region of the specimen is subject to the uniformly distributed force field, we can measure the stresses. It is shown that Cauchy's stress tensor and the second Piola-Kirchhoff stress tensor (Kirchhoff stress tensor) are symmetric, whereas the first Piola-Kirchhoff stress tensor (Lagrangian stress tensor) is not. For laboratory work on large deformations, it is simple to use the Lagrangian stress tensor (T_{ij}) and Green strain tensor (E_{ij}). But since T_{ij} is not symmetric, it is inconvenient in the stress-strain relationship. Cauchy stresses (σ_{ij}) are the true stresses felt by the body, and are convenient to use in equations of equilibrium. Kirchhoff stresses (S_{ij}) are directly related to the strain energy function. Thus we use Kirchhoff stresses (S_{ij}) and Green Strains (E_{ij}) in the stress-strain law. Clearly these three stresses are convertible to each other by following relationships [Fung, 1981]:

$$T_{ij} = S_{im} \frac{\partial Y_j}{\partial X_m} = \frac{\rho_0}{\rho} \frac{\partial X_i}{\partial X_m} \sigma_{mj} \quad (2.9)$$

$$S_{ij} = \frac{\partial X_i}{\partial Y_m} T_{jm} = \frac{\rho_0}{\rho} \frac{\partial X_i}{\partial Y_m} \frac{\partial X_j}{\partial Y_n} \sigma_{nm} \quad (2.10)$$

ρ_0 and ρ are the densities of the material in the undeformed and deformed states, respectively.

Referring to Figure (10), we see that the Lagrangian stresses are:

$$T_{11} = \frac{F_1}{L_{20} h_0} \quad (2.11)$$

$$T_{22} = \frac{F_2}{L_{10} h_0} \quad (2.12)$$

$$T_{12} = T_{21} = 0 \quad (2.13)$$

where L_{10} and L_{20} are the initial lengths in x_1 , x_2 direction, respectively. h_0 is the initial thickness of the specimen. F_1 and F_2 are resultant forces in x_1 , x_2 direction, respectively. All these quantities can be measured, we obtain the Lagrangian stresses from equations (2.11), (2.12), and (2.13). From equations (2.9) and (2.13), we obtain

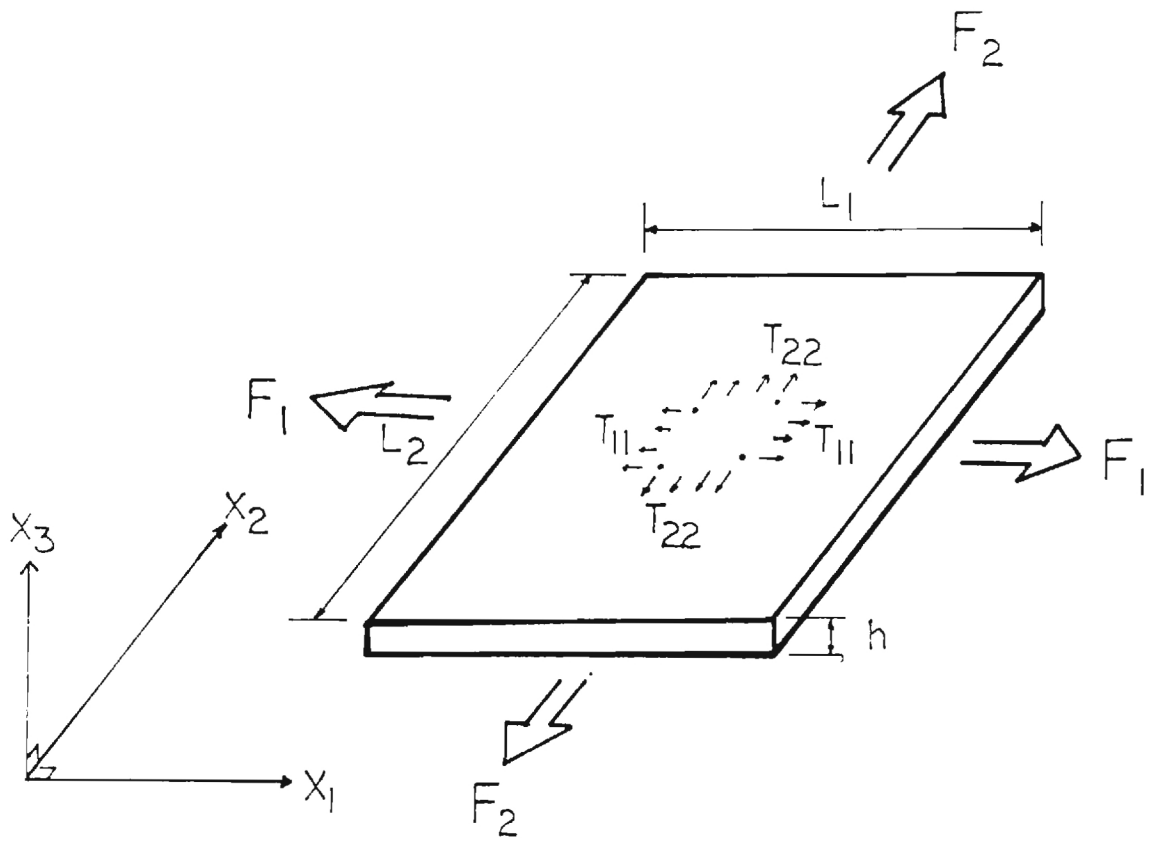


Figure (10) Schematic diagram of a bi-axially stretched specimen for stress measurement.

$$\begin{aligned}
T_{11} &= S_{11}C_{11} + S_{12}C_{12} \\
T_{22} &= S_{21}C_{21} + S_{22}C_{22} \\
T_{12} &= S_{11}C_{21} + S_{12}C_{22} = 0 \\
T_{21} &= S_{21}C_{11} + S_{22}C_{12} = 0
\end{aligned}
\tag{2.14}$$

where C_{ij} are displacement gradients, which can be measured by equation (2.8). Hence, we obtain the Kirchhoff stresses from equation (2.14).

$$S_{11} = \frac{C_{22}}{C_{11}C_{22} - C_{12}C_{21}} T_{11} \tag{2.15}$$

$$S_{22} = \frac{C_{11}}{C_{11}C_{22} - C_{12}C_{21}} T_{22} \tag{2.16}$$

$$S_{12} = S_{21} = \frac{-C_{21}}{C_{11}C_{22} - C_{12}C_{21}} T_{11} = \frac{-C_{12}}{C_{11}C_{22} - C_{12}C_{21}} T_{22} \tag{2.17}$$

Note that the symmetry of kirchhoff tensor gives the following relationship:

$$C_{21}T_{11} = C_{12}T_{22} \tag{2.18}$$

Therefore, equation (2.18) may be used in cross-checking the assumption of homogeneous deformation and uniform stress field. In summary, we can measure the Lagrangian stresses using equations (2.11), (2.12), and (2.13), and convert these values to Kirchhoff stresses using equations (2.15), (2.16), and (2.17).

c) Biaxial Testing Protocols

The specimen was immersed in 0.9 % saline solution at room temperature. After mounting the specimen in experimental device, some set-up procedures were inevitable, to ensure the correct light levels, to position the specimen to the center region of video camera, to impose the relatively uniform stress fields on the specimen. The initial reference state was defined when no force was imposed on the specimen. By stretching the specimen slowly from the fully relaxed state, we observed the change of output voltages from force transducers. On beginning to change the output voltages (from the already known 0-force output voltages), we stopped the stretching. This state was defined as the initial reference state, and initial locations of tracking particles were determined using joystick cursor.

To get the relatively general stress-strain law, the following four classes of biaxial testing were conducted on each specimen:

1. Uniform stretching mode in which both axes were cyclically stretched at equal stretching rates.
2. Non-uniform biaxial stretching mode in which both axes were cyclically stretched at different stretching rates.

3. Lateral displacement mode in which one direction was cyclically stretched at a constant rate while the displacement in the second direction was held constant.
4. Lateral force mode in which one direction was cyclically stretched at a constant rate while the force in the second direction was maintained at a prescribed level.

Test were performed at various stretching rates between 0.000635 and 0.0635 cm/sec. These stretching rates yielded Green strain rates approximately from 0.00016 to 0.016 cm/cm/sec.

To cover the physiological range of loading on pericardium, the maximum load 70-130 g was chosen. The stresses to be expected in the canine pericardium were estimated from the law of Laplace for a thin-walled spherical sac model:

$$\sigma = \frac{P r}{2 t} \quad (2.19)$$

where σ is the stress in the pericardium, P is the transpericardial pressure, r is the sac radius, and t is the wall thickness. The transpericardial pressure is the difference between the pericardial pressure and the pleural pressure. According to Tyson, et al. [1984], transpericardial pressure remains low (2.3mm Hg - 4.9mm Hg) over the entire physiological range in the normal conscious dogs. However, the transpericardial pressure increased to 10.3 ± 0.6 mmHg in the volume overload dogs. Taking the values, $P=12$ mmHg (0.16×10^5 dyne/cm²), $r=4.0$ cm, and $t=0.2$ mm, we obtained maximum stress $\sigma_{\max} = 16 \times 10^5$ (dyne/cm²). This stress value corresponds to an equal biaxial load of 130g on a 5.0x5.0cm square specimen (4.0x4.0cm square effective loading region).

First, a series of uniform biaxial stretching tests were conducted. Twenty initial preconditioning cycles were performed in uniform biaxial stretching mode with gradually increasing maximum loads and stretching rates. After the initial preconditioning was completed, both axes were cyclically stretched five times at equal rates of 0.00127 cm/sec. The force-extension results of each cycle were graphed on the video display immediately following the completion of each cycle. Once the curves became coincident, three more cycles were performed at the stretching rate of 0.00127 cm/sec, and the data of the third cycle were stored. This procedure was repeated three times more, after changing the stretching rate to 0.00254, 0.00508 and 0.0127 cm/sec respectively in each test.

The second series of tests consisted of non-uniform biaxial stretching tests. Both axes were cyclically stretched at different rates. These tests were performed to approximate equal maximum force on both directions (as a simulation of uniform biaxial force tests). From the uniform biaxial stretching test data, we may discern between the stiff direction and the compliant direction. The maximum loads of both directions may thus be equalized by increasing the stretching rate of compliant direction. The stiff direction was stretched at the rate of 0.00254 cm/sec, and the compliant direction was stretched at the rate of 0.00381 cm/sec. After watching the response, the stretching rate of compliant direction was adjusted appropriately

to equalize the maximum loads of both directions. If we got the appropriate combination of stretching rates, then two cycles of loading and unloading were performed. After then, the data of the third cycle were stored.

The third series of tests consisted of constant lateral displacement tests. Ten preconditioning cycles were performed, in which the constant-lateral-displacements were increased stepwise. Again three cycles at lateral stretch ratios of 1.0, 1.1, 1.2 and 1.3 were executed, and the data of the third cycle in each test were stored.

The fourth series of tests were performed in constant lateral force mode. The specimen was again preconditioned five cycles with gradually increasing constant-lateral-loads. As before, three cycles of the constant-lateral-loads of 0, 10, 20 and 30 g were performed, and the data of the third cycle in each test were stored.

Finally, ten cycles of preconditioning in the uniform stretching mode were performed, and data collected for each cycle at stretching rates of 0.00127, 0.00254, 0.00508 and 0.0127 cm/sec. The last test in each set of experiments was a uniform stretching test for comparison with data taken earlier in the day. One additional uniform biaxial stretching test was performed after rotating the specimen 90° in the tissue bath, and the result was compared with the same kind of test in order to check the errors caused by different tissue orientations.

3. Pseudo-elastic Analysis

3.1 Stress-strain Law

Before any mechanical analysis of the pericardium or any of its components can be performed, the constitutive relationships which characterized individual material behaviors under applied loads must be known. Based on the previous studies [Vito,1980; Lee et al.,1985; Yin et al.,1986], it appears that the pericardium behaves like most biological soft tissues, and is nonlinearly viscoelastic, anisotropic and undergoes large deformation. Thus the stress-strain relationship is nonlinear and history dependent. However, the pericardium shows that the stress and strain are uniquely related in each branch (loading and unloading) of a specific process after preconditioning, and they are strain-rate insensitive. Therefore, we can treat the pericardium as one elastic material in loading, and another elastic material in unloading (we call it pseudoelastic). Further simplification can be gained by assuming the existence of a strain energy function (we call it hyperelastic).

The elastic medium is described in its undeformed or material state B_0 by the coordinates $\{ x_i \}$ and in its deformed or spatial state B by the coordinates $\{ y_i \}$. Here, both $\{ x_i \}$ and $\{ y_i \}$ are referred to the same set of fixed rectangular Cartesian coordinates. Let the elastic body undergo the homogeneous deformation in which a typical particle initially at the point $\{ x_i \}$ moves to the point $\{ y_i \}$, then

$$y_i = C_{ij} x_j \quad (3.1)$$

and

$$\partial y_i / \partial x_j = C_{ij} \quad (3.2)$$

The deformation gradients C_{ij} are constants, and completely define the deformation. The Green strains are defined as the following [Green and Zerna,1968]:

$$E_{ij} = 1/2 (C_{ri}C_{rj} - \delta_{ij})$$

δ_{ij} is Kronecker delta function, and E_{ij} is the Green strain tensor. The strain energy function W (per unit volume of undeformed state) depends only on the state of deformation and is independent of the strain history. That is, for a homogeneous elastic material, we can write W as a function of the deformation gradients alone:

$$W = W (C_{ij}) \quad (3.3)$$

C_{ij} is the deformation gradient tensor. Upon imposing the requirement that W be frame indifferent, equation (3.3) can be restated in a more desirable form in terms of symmetric Green strain tensor:

$$W = W (E_{ij}) \quad (3.4)$$

The constitutive equation for a compressible, homogeneous, elastic solid is given as the following [Green and Adkins,1970]:

$$S_{ij} = 1/2 (\partial W / \partial E_{ij} + \partial W / \partial E_{ji}) \quad (3.5)$$

S_{ij} is the symmetric second Piola-Kirchhoff stress tensor. In the finite elasticity, there are many kinds of measures for stresses and strains. In this study, we use the Green strain (E_{ij}) and the Kirchhoff stress (S_{ij}), both are referred to the initial state.

3.2 Strain Energy Function

As aforementioned, two types of strain energy function (exponential and polynomial) have been used widely in the soft tissue mechanics area. Fung [1967] showed that the nonlinear material behavior of soft tissues could be conveniently described in terms of exponential. Later, Fung [1973] proposed the following three-dimensional pseudo-strain energy function form for soft tissues:

$$W = 1/2 A_{ijkl} E_{ij} E_{kl} + (B_0 + B_{mnl} E_{mn} E_{kl}) e^Q \quad (3.6)$$

$$Q = a_{ij} E_{ij} + b_{mnl} E_{mn} E_{kl} \quad (3.7)$$

A_{ijkl} , B_0 , B_{mnl} , a_{ij} and b_{mnl} are material constants. Over a period of years, Fung and colleagues have shown that the behavior of skin, arteries, lung parenchyma and mesentery are well described by equations (3.6) and (3.7). Later, they have shown that a better fit with experimental data can be obtained by dropping the first-order terms (B_0 , $a_{ij} E_{ij}$) in the equation (3.6) and (3.7). Moreover, the first term (A_{ijkl}) of the equation (3.6) has been dropped in the work on arteries [Chuong and Fung, 1983] or on lung parenchyma [Vawter et al., 1979]. However, the coefficient A_{ijkl} was retained in describing the skin [Tong and Fung, 1976] and the pericardium [Yin et al., 1986], and the A_{ijkl} was found to be useful in accounting for the mechanical behavior at a low stress level. Based on these results, the equation (3.6) can be refined as the following:

$$W = 1/2 A_{ijkl} E_{ij} E_{kl} + B (e^Q - 1) \quad (3.8)$$

where, $Q = 1/2 b_{ijkl} E_{ij} E_{kl}$ (3.9)

Recently, above form of W has been used the work on visceral pleura [Humphrey, 1985] and on pericardium [Yin et al., 1986].

Note that the strain energy function W includes the quadratic terms ($1/2 A_{ijkl} E_{ij} E_{kl}$ and $1/2 b_{ijkl} E_{ij} E_{kl}$) which is the exactly same form used in linear elasticity. Therefore, some of

the attractive analytical features of linear elasticity can be transferred to this nonlinear case. That is, we may use the arguments of the linear elasticity to reduce the number of material constants A_{ijkl} and b_{ijkl} . Using the strain energy function W given in the equation (3.8), we obtain the stress-strain relation as the following:

$$S_{ij} = \partial W / \partial E_{ij} = A_{ijkl} E_{kl} + B (b_{ijkl} E_{kl}) e^Q \quad (3.10)$$

$$Q = 1/2 b_{ijkl} E_{ij} E_{kl} \quad (3.11)$$

S_{ij} is the second Piola-Kirchhoff stress tensor, measured per unit area of the undeformed body. Since S_{ij} and E_{kl} are symmetric tensors, the coefficients A_{ijkl} and b_{ijkl} satisfy the following symmetry restrictions:

$$A_{ijkl} = A_{jikl} = A_{ijlk} = A_{klij} \quad (3.12)$$

$$b_{ijkl} = b_{jikl} = b_{ijlk} = b_{klij} \quad (3.13)$$

Therefore, each of A_{ijkl} and b_{ijkl} contains only 21 independent material constants respectively. Details of the above symmetry arguments are presented in Appendix 1.

If the material has certain elastic symmetry, then the number of constants can be reduced more. For an orthotropic material, the number of constants is reduced to 9 from 21. Also details of the elastic symmetry arguments can be found in Appendix 1. Therefore, the strain energy function W for an orthotropic material can be presented as the following:

$$W = 1/2 (A_1 E_{11}^2 + A_2 E_{22}^2 + A_3 E_{33}^2 + 4A_4 E_{12}^2 + 4A_5 E_{23}^2 + 4A_6 E_{31}^2 + 2A_7 E_{11} E_{22} + 2A_8 E_{22} E_{33} + 2A_9 E_{33} E_{11}) + B (e^Q - 1) \quad (3.14)$$

$$Q = 1/2 (b_1 E_{11}^2 + b_2 E_{22}^2 + b_3 E_{33}^2 + 4b_4 E_{12}^2 + 4b_5 E_{23}^2 + 4b_6 E_{31}^2 + 2b_7 E_{11} E_{22} + 2b_8 E_{22} E_{33} + 2b_9 E_{33} E_{11}) \quad (3.15)$$

Thus, we need a total of 19 material constants. From the equation (3.14) and (3.15), the two-dimensional strain energy function W for an orthotropic material is:

$$W = 1/2 (A_1 E_{11}^2 + A_2 E_{22}^2 + 4A_3 E_{12}^2 + 2A_4 E_{11} E_{22}) + B (e^Q - 1) \quad (3.16)$$

$$Q = 1/2 (b_1 E_{11}^2 + b_2 E_{22}^2 + 4b_3 E_{12}^2 + 2b_4 E_{11} E_{22}) \quad (3.17)$$

Because the second term in the equation (3.16) dominates at large strain, we may drop the first term as an approximation, then

$$W = B (e^Q - 1) \quad (3.18)$$

$$Q = 1/2 (b_1 E_{11}^2 + b_2 E_{22}^2 + 4b_3 E_{12}^2 + 2b_4 E_{11} E_{22}) \quad (3.19)$$

This 5-parameter strain energy function W may be the simplest form which can be tried to fit the biaxial test data. Also, the two-dimensional strain energy function W for an anisotropic material can be presented as the following:

$$W = 1/2 (A_1 E_{11}^2 + A_2 E_{22}^2 + 4A_3 E_{12}^2 + 2A_4 E_{11} E_{22} + 4A_5 E_{11} E_{12} + 4A_6 E_{22} E_{12}) + B (e^Q - 1) \quad (3.20)$$

$$Q = 1/2 (b_1 E_{11}^2 + b_2 E_{22}^2 + 4b_3 E_{12}^2 + 2b_4 E_{11} E_{22} + 4b_5 E_{11} E_{12} + 4b_6 E_{22} E_{12}) \quad (3.21)$$

As before, if we drop the first term in the equation (3.20), it becomes:

$$W = B (e^Q - 1) \quad (3.22)$$

$$Q = 1/2 (b_1 E_{11}^2 + b_2 E_{22}^2 + 4b_3 E_{12}^2 + 2b_4 E_{11} E_{22} + 4b_5 E_{11} E_{12} + 4b_6 E_{22} E_{12}) \quad (3.23)$$

3.3. Biaxial Test Formulation

The three-dimensional constitutive relationship uniquely defines its mechanical properties. For an isotropic incompressible material, the three-dimensional stress-strain law can be deduced from a complete two-dimensional test data, since any changes in the third dimension can be determined from the changes in the other two dimensions. In general, biaxial stretching tests have to be combined with another type of test such as an indentation test, torsion or shear test to identify the three-dimensional constitutive equation. In nature, pericardium exists as a sheet of tissue, hence the two-dimensional constitutive equation may have its own applicability.

Although the pericardium has been regarded as an anisotropic material, most studies up to now have adopted the assumption of isotropy or orthotropy without justification. Even when the pericardium was assumed to be orthotropic, the material symmetry axes were not determined a priori. For example, Lee et al.[1985] and Yin et al.[1986] performed biaxial stretching tests based on the assumption of orthotropy. However, their methodology did not allow them to measure shear strains and to determine the material symmetry directions of the specimen prior to mounting in the testing device. Therefore, they arbitrarily presumed that they stretched specimens along the material symmetry axes, even if they observed the deformation of the square target into a parallelogram. This means that their biaxial data were referred to arbitrary material directions, and the data from one specimen could not be compared with those from another specimen. To overcome these difficulties, shear strains have to be measured and the biaxial data can be referred to specific material directions.

Our immediate objective is to identify the two-dimensional stress-strain law of the pericardium, assuming the pericardium as

a homogeneous, and orthotropic thin membrane with unknown material symmetry axes. To accomplish our objective, shear strains are measured, and a methodology for the approximate determination of material orthotropic axes a posteriori is suggested.

However, some approximations are still inevitable due to the nonhomogeneity of tissue and experimental difficulties such as imposing uniform forces on the specimen boundaries. For our biaxial test formulation, following approximations are adopted.

At the specimen boundary, the largest shear force occurs at the largest extensional strain. The shear force exerted by the thread nearest from corner can be 10 % of the tensile force in the thread at the largest extensional strains. However, the shear force by the center thread is negligible. Therefore, shear stress in central target region is assumed to be negligible, at least on average.

Normal forces at the boundary are not uniform, if the stretching axes do not coincide with material orthotropic axes. However, the tensile force in the center thread is expected to be almost equal to the average value of tensile forces at the boundary. Although the exact verification of St. Venant's effect is not performed, we assume that the central target region of the specimen is far from the edge, and the stress is uniform in the central region.

Even if the whole specimen undergoes nonhomogeneous deformation, the variation of strains in the central region is not so large that the homogeneous deformation in the central region may be assumed.

Usually all biaxial test data are measured with respect to the fixed stretching axes. Using these data, we can formulate the constitutive equation in two ways. One is to formulate the stress-strain law with respect to stretching axis. In this case, we don't need any transformation equation, but need more complex form for W which accounts for general anisotropic behavior. Another is the formulation with respect to the material symmetry axis. In this case, we need the transformation equation, but can use more simple form for W by using material symmetry arguments.

a) Formulation With Respect to the Fixed Stretching Axis.

As aforementioned, the coordinates $\{ x_i \}$ and $\{ y_i \}$ are referred to the same set of rectangular Cartesian coordinates, which coincide with the stretching axes fixed in the testing device.

The two dimensional strain energy function is generally given as:

$$W = W (E_{11}, E_{22}, E_{12}) \quad (3.24)$$

Choosing W for an anisotropic material as the equation (3.22),

$$W = B \left[\exp \left(\frac{1}{2} b_1 E_{11}^2 + \frac{1}{2} b_2 E_{22}^2 + 2 b_3 E_{12}^2 + b_4 E_{11} E_{22} + 2 b_5 E_{11} E_{12} + 2 b_6 E_{22} E_{12} \right) - 1 \right] \quad (3.22)$$

From the equation (3.5), we obtain:

$$\begin{Bmatrix} S_{11} \\ S_{22} \\ S_{12} \end{Bmatrix} = \begin{Bmatrix} \partial W / \partial E_{11} \\ \partial W / \partial E_{22} \\ \frac{1}{2} \partial W / \partial E_{12} \end{Bmatrix} = \begin{bmatrix} b_1 & b_4 & b_5 \\ b_4 & b_2 & b_6 \\ b_5 & b_6 & b_3 \end{bmatrix} \begin{Bmatrix} E_{11} \\ E_{22} \\ 2E_{12} \end{Bmatrix} \quad B e^Q \quad (3.25)$$

$$\text{where, } Q = \frac{1}{2} b_1 E_{11}^2 + \frac{1}{2} b_2 E_{22}^2 + 2 b_3 E_{12}^2 + b_4 E_{11} E_{22} + 2 b_5 E_{11} E_{12} + 2 b_6 E_{22} E_{12}$$

If we choose another form for W as the equation (3.20), we get the following form of constitutive equation.

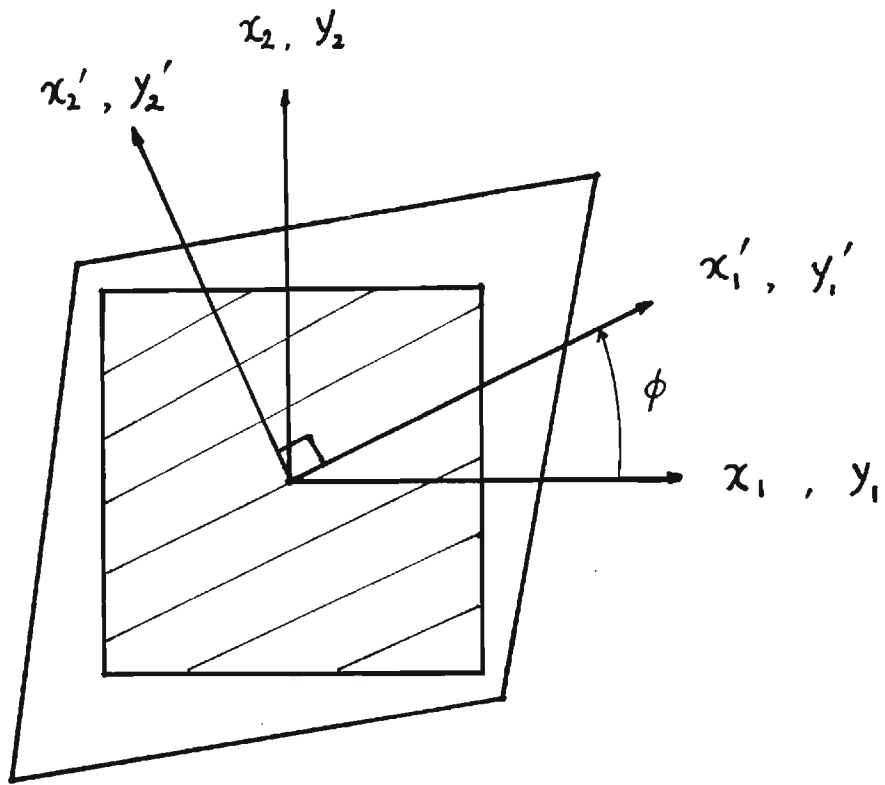


Figure (12). The orientation of the coordinates systems.

$$\begin{Bmatrix} S_{11} \\ S_{22} \\ S_{12} \end{Bmatrix} = \begin{Bmatrix} A_1 & A_4 & A_5 \\ A_4 & A_2 & A_6 \\ A_5 & A_6 & A_3 \end{Bmatrix} + B e^Q \begin{Bmatrix} b_1 & b_4 & b_5 \\ b_4 & b_2 & b_6 \\ b_5 & b_6 & b_3 \end{Bmatrix} \begin{Bmatrix} E_{11} \\ E_{22} \\ 2E_{12} \end{Bmatrix} \quad (3.26)$$

$$\text{where, } Q = 1/2 b_1 E_{11}^2 + 1/2 b_2 E_{22}^2 + 2 b_3 E_{12}^2 + b_4 E_{11} E_{22} + 2 b_5 E_{11} E_{12} + 2 b_6 E_{22} E_{12}$$

Therefore, we can use the above two equations (3.25) and (3.26) to fit the biaxial test data.

b) Formulation with respect to the Material Symmetry Axis.

Here, the elastic medium is described in its undeformed state by the coordinates $\{ x_i \}$ and in its deformed state by the coordinates $\{ y_i \}$. Both coordinates are referred to the same set of rectangular Cartesian coordinates, which coincide with the material symmetry axes at its undeformed state. The strain energy function form of the equation (3.18) is chosen to fit the biaxial data of pericardium. The similar forms were used in the works on arteries [Fung et al., 1979; Chuong and Fung, 1983] and lung tissues [Fung, 1975; Vawter et al., 1979]. Therefore, we try this form as a first choice for an orthotropic material:

$$W = B' (e^{Q'} - 1) \quad (3.27)$$

$$Q' = 1/2 b_1' E_{11}'^2 + 1/2 b_2' E_{22}'^2 + 2 b_3' E_{12}'^2 + b_4' E_{11}' E_{22}' \quad (3.28)$$

From the equation (3.5), we obtain:

$$\begin{Bmatrix} S_{11}' \\ S_{22}' \\ S_{12}' \end{Bmatrix} = B' e^{Q'} \begin{Bmatrix} b_1' & b_4' & 0 \\ b_4' & b_2' & 0 \\ 0 & 0 & 2b_3' \end{Bmatrix} \begin{Bmatrix} E_{11}' \\ E_{22}' \\ E_{12}' \end{Bmatrix} \quad (3.29)$$

Since we don't know the orientation of material symmetry axis, and all strains and stresses are measured with respect to the stretching axis, we have to transform the equation (3.29). If the material symmetry axes x_i' make an angle ϕ with the stretching axes x_i as shown in Figure (12), the stresses can be transformed as the following:

$$\begin{Bmatrix} S_{11} \\ S_{22} \\ S_{12} \end{Bmatrix} = \begin{Bmatrix} \cos^2 \phi & \sin^2 \phi & -2 \sin \phi \cos \phi \\ \sin^2 \phi & \cos^2 \phi & 2 \sin \phi \cos \phi \\ \sin \phi \cos \phi & -\sin \phi \cos \phi & \cos^2 \phi - \sin^2 \phi \end{Bmatrix} \begin{Bmatrix} S_{11}' \\ S_{22}' \\ S_{12}' \end{Bmatrix} \quad (3.30)$$

And similarly, the strains can be transformed. After transformation, the equation (3.29) becomes:

$$\begin{Bmatrix} S_{11} \\ S_{22} \\ S_{12} \end{Bmatrix} = B' e^Q \begin{bmatrix} \beta_1 & \beta_4 & \beta_5 \\ & \beta_2 & \beta_6 \\ & & \beta_3 \end{bmatrix} \begin{Bmatrix} E_{11} \\ E_{22} \\ 2E_{12} \end{Bmatrix} \quad (3.31)$$

where,

$$Q = \frac{1}{2} \beta_1 E_{11}^2 + \frac{1}{2} \beta_2 E_{22}^2 + 2 \beta_3 E_{12}^2 + \beta_4 E_{11} E_{22} + 2 \beta_5 E_{11} E_{12} + 2 \beta_6 E_{22} E_{12} \quad (3.32)$$

$$\begin{aligned} \beta_1 &= b_1' \cos^4 \phi + 2(b_4' + 2b_3') \sin^2 \phi \cos^2 \phi + b_2' \sin^4 \phi \\ \beta_2 &= b_1' \sin^4 \phi + 2(b_4' + 2b_3') \sin^2 \phi \cos^2 \phi + b_2' \cos^4 \phi \\ \beta_3 &= (b_1' + b_2' - 2b_4' - 2b_3') \sin^2 \phi \cos^2 \phi + b_3' (\sin^4 \phi + \cos^4 \phi) \\ \beta_4 &= (b_1' + b_2' - 4b_3') \sin^2 \phi \cos^2 \phi + b_4' (\sin^4 \phi + \cos^4 \phi) \\ \beta_5 &= (b_1' - b_4' - 2b_3') \sin \phi \cos^3 \phi + (b_4' - b_2' + 2b_3') \sin^3 \phi \cos \phi \\ \beta_6 &= (b_1' - b_4' - 2b_3') \sin^3 \phi \cos \phi + (b_4' - b_2' + 2b_3') \sin \phi \cos^3 \phi \end{aligned} \quad (3.33)$$

The strain energy functions similar to the equation (3.16) were also used to fit the biaxial test data of the skin [Tong and Fung, 1976] and the pericardium [Yin et al., 1986]. Therefore, we try the equation (3.16) as a second choice for an orthotropic material:

$$W = \left(\frac{1}{2} A_1' E_{11}'^2 + \frac{1}{2} A_2' E_{22}'^2 + 2 A_3' E_{12}'^2 + A_4' E_{11}' E_{22}' \right) + B' (e^{Q'} - 1) \quad (3.34)$$

$$Q' = \frac{1}{2} b_1' E_{11}'^2 + \frac{1}{2} b_2' E_{22}'^2 + 2 b_3' E_{12}'^2 + b_4' E_{11}' E_{22}' \quad (3.35)$$

From the equation (3.5), we obtain:

$$\begin{Bmatrix} S_{11}' \\ S_{22}' \\ S_{12}' \end{Bmatrix} = \left(\begin{bmatrix} A_1' & A_4' & 0 \\ & A_2' & 0 \\ & & A_3' \end{bmatrix} + B' e^{Q'} \begin{bmatrix} b_1' & b_4' & 0 \\ & b_2' & 0 \\ & & b_3' \end{bmatrix} \right) \begin{Bmatrix} E_{11}' \\ E_{22}' \\ 2E_{12}' \end{Bmatrix} \quad (3.36)$$

After performing transformation, the equation (3.36) becomes:

$$\begin{Bmatrix} S_{11} \\ S_{22} \\ S_{12} \end{Bmatrix} = \left(\begin{bmatrix} \alpha_1 & \alpha_4 & \alpha_5 \\ & \alpha_2 & \alpha_6 \\ & & \alpha_3 \end{bmatrix} + B' e^Q \begin{bmatrix} \beta_1 & \beta_4 & \beta_5 \\ & \beta_2 & \beta_6 \\ & & \beta_3 \end{bmatrix} \right) \begin{Bmatrix} E_{11} \\ E_{22} \\ 2E_{12} \end{Bmatrix} \quad (3.37)$$

where, α has the same form as the equation (3.33).

Therefore, we can use the two equations (3.31) and (3.37) to fit the biaxial test data. Note that the equations (3.31) and (3.37) are same form with the equations (3.25) and (3.26), respectively. That is, if we don't know the angle ϕ prior to test, it brings same difficulty as treating the general anisotropic material. However, we can get some information about the angle ϕ by assuming that the angle ϕ is constant throughout

the deformation process. Generally, the angle ϕ cannot be regarded as constant under large deformation of soft tissues. Even the preferred fiber orientation in pericardium can vary with deformation. Furthermore, the material symmetry properties are depend not only on the preferred fiber directions, but also on the crimped geometry of fibers in each direction. However, we can regard ϕ as constant under suitably chosen conditions such as small loading region or narrow incremental region.

From the equation (3.33), we can get following relationships:

$$\begin{aligned}\beta_1 - \beta_2 &= b_1' (\cos^4\phi - \sin^4\phi) + b_2' (\sin^4\phi - \cos^4\phi) \\ &= (b_1' - b_2') \cos 2\phi\end{aligned}\quad (3.38)$$

$$\beta_5 + \beta_6 = 1/2 (b_1' - b_2') \sin 2\phi \quad (3.39)$$

$$\beta_3 - \beta_4 = b_3' - b_4' \quad (3.40)$$

$$\beta_1 + \beta_2 + 2\beta_4 = b_1' + b_2' + 2b_4' \quad (3.41)$$

If the material is orthotropic, $(\beta_1 + \beta_2 + 2\beta_4)$ and $(\beta_3 - \beta_4)$ are invariant under rotation about the x_3 -axis as shown in equations (3.40) and (3.41). Also, from the above two equations (3.38) and (3.39), we obtain:

$$\tan 2\phi = \frac{2(\beta_5 + \beta_6)}{\beta_1 - \beta_2} \quad (3.42)$$

$$\phi = \frac{1}{2} \tan^{-1} \left[\frac{2(\beta_5 + \beta_6)}{\beta_1 - \beta_2} \right] \quad (3.43)$$

Similarly,

$$\phi = \frac{1}{2} \tan^{-1} \left[\frac{2(d_5 + d_6)}{d_1 - d_2} \right] \quad (3.44)$$

Once the parameters of the function that best fit the data are obtained, we can approximately determine the angle ϕ . For example, if the equation (3.25) fits the biaxial data reasonably well, then we can approximately determine the material symmetry axis from the material parameters b_1, b_2, b_5, b_6 as below:

$$\phi = \frac{1}{2} \tan^{-1} \left[\frac{2(b_5 + b_6)}{b_1 - b_2} \right] \quad (3.43)$$

Also, the strain energy function form of the equation (3.22) can be converted to the form of equation (3.27) by using the relationship (3.33).

3.4 Data Analysis Method.

The central-region dimensions, the outer-edge dimensions and thickness of specimen at its undeformed state were measured using the methods described in section 2.4. As explained in section

2.5, we obtained the stress-strain data in the central-region of specimen. These biaxial stress-strain data were fitted to the constitutive models (equation (3.25); equation (3.26)). The material constants were determined by minimizing the sum-of-the-squares of the errors between the observed stresses and those predicted by the fitted model, using the Marquardt-Levenberg non-linear optimization technique [Patitucci,1983].

4. Microstructure Observation

4.1. Objective of Microstructure Observation

The mechanical behavior of the soft tissue depends primarily on the response of its constituents. Hence, if the constituents' structure, their mechanics and interactions are known, then the overall structural response can be evaluated.

Once the mechanical properties are known, they can be used in diagnosis or treatment, because disease is nothing but deviation from the normal. Using measurements of the mechanical properties of the tissues to decide whether the tissues are normal or not can be very helpful for diagnosis. If the relationship of microstructure to function is known, the cause of deviation from normal can be figured out. This may provide more helpful information to the medicine and surgery.

For these reasons, attempts to correlate mechanical properties with microstructure have been made [e.g.; Apter,1966; Lanir,1979a,b,1980]. One basic approach is to selectively digest either the collagen or elastin prior to mechanical testing [Apter ,1966]. Although this procedure is good to understand the mechanical properties of each constituent, it destroys the structure. Another approach is the simultaneous measurement of both mechanical and structural variables [Broom,1978]. However, this approach has to be combined with the stereology to quantify the microstructure.

Up to now, the correct material symmetry for the pericardium is unknown. It may be that the microscopic observation can be used to obtain the correct material symmetry and the constitutive equation. The immediate objective of the microscopic observation is to get the information of the preferred orientation of fibers in the pericardium. Hence, the number, orientation, waviness, and volume fraction of each fibers will be measured at various stress levels. And these measurements will be presented as the functions of stresses. The material symmetry axes inferred from this observation will be compared with those determined from the pseudoelastic approach. Also, some explanation will be given to the relationship between the material constants and the microscopic measurements. The long term goal is to correlate observations of microstructure of the pericardium to the state of disease such as pericarditis, especially as reflected by changes in the mechanical properties of pericardium.

4.2 Specimen Preparation for the Light Microscopy

The same pericardial tissues used in the biaxial test, will be used in the microscopic observation. After performing the biaxial tests, the pericardium will be fixed, dehydrated, embedded in paraffin, sectioned and stained. The pericardial tissues will be fixed at various stress levels. Buffered neutral formalin (formaldehyde: 100.0ml, distilled water: 900.0ml, sodium acid phosphate, $\text{NaH}_2\text{PO}_4 \cdot \text{H}_2\text{O}$: 4.0g, anhydrous disodium phosphate, Na_2HPO_4 : 6.5g) will be used as a fixative. After performing the fixation in the laboratory at Georgia Tech., the fixed tissues

will be transferred to Emory Univ. The dehydrating, embedding, sectioning and staining will be done by the experienced staff at Emory Univ. They have the fully automatic equipment for these procedures. The slides prepared for the light microscopy will be used for the microscopic observations. To quantify the microstructure, a series of the randomly-sectioned slides are needed with the orientations of the sections clearly marked. If the material is orthogonally anisotropic, cross-sections which are parallel to the x_1x_2 -, x_2x_3 -, and x_3x_1 -planes as shown in Figure (13) can be used for the slides [Kanatani,1985].

4.3 Stereological Analysis

a) The Volume Fraction

The human pericardium is composed of several layers; the mesothelial cell layer, several layers of collagen fibers, small thin-walled vessels, and a few scattered connective tissue cells [Ishihara et al.,1980]. Also, the multilayered network of collagen fibers exists in canine pericardium [Wiegner and Bing, 1981]. The volume fraction of fiber may be closely related to the elastic stiffness. Thus, it is important to know the volume fraction of each layer. Stereologically, the volume fraction can be measured by the point-counting method or by the lineal integration method. The lineal integration method may be a good choice for estimating the volume fractions of layered structure. That is, the ratio between the sum of line segments for any particular layer and total line length form a valid estimate of the volume fraction of that layer [Guyton,1984]. For example, Figure (14) shows a section through entire thickness of parietal pericardium (schematic drawing of the picture taken by Ishihara et al.,1980). The volume fraction of the layer iv can be obtained as the following:

$$(V_V)_{iv} = (L_L)_{iv} = \frac{L_I}{L_T} \quad (4.1)$$

L_T is the test line length. L_L is the lineal fraction. L_I is the length of lineal intercepts. V_V is the volume fraction. If the thickness of specimen is 0.20mm and the length of lineal intercepts with test line 1,2,...,5 are 0.033mm, 0.030mm, 0.035mm, 0.037mm, 0.018mm, respectively as shown in Figure (14), then the volume fraction of layer iv is

$$(V_V)_{iv} = \frac{0.033 + 0.030 + 0.035 + 0.037 + 0.018}{0.20 \times 5} = 0.153 = 15.3 \%$$

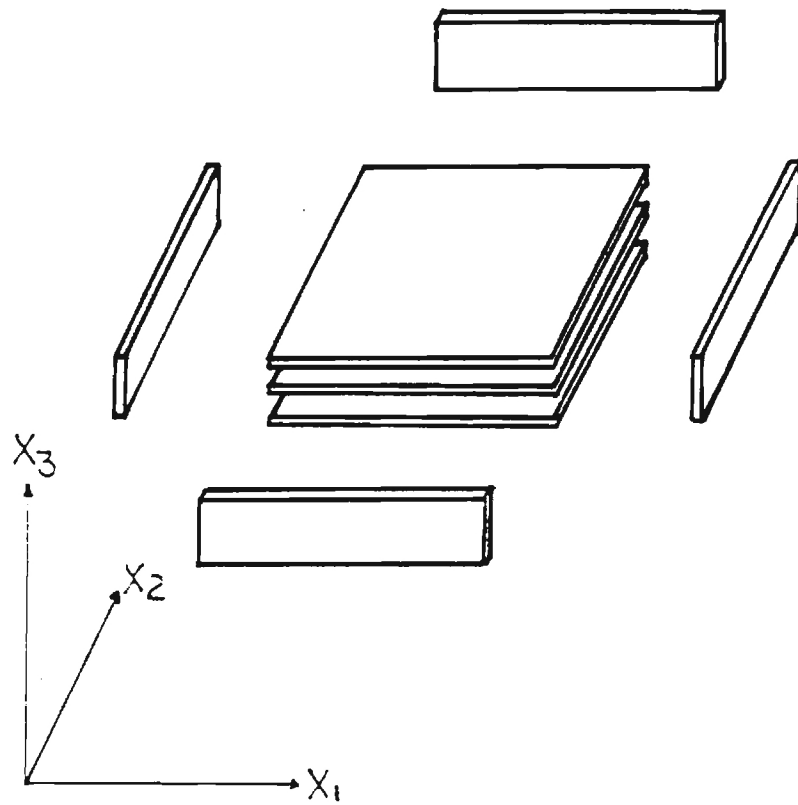


Figure (13) Specimen-sectioning for the microscopic slides.

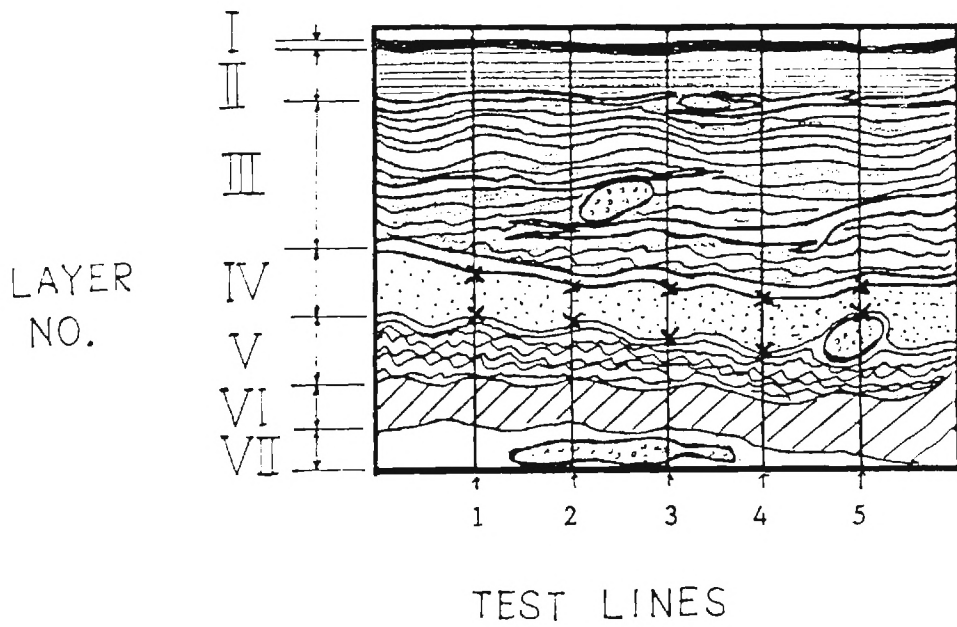


Figure (14) Cross-section of layered structure ; example for the stereological analysis.

b) Waviness of Fiber Bundles

Collagen fibers are seen under the microscope to progress in various directions through the pericardium as wavy bands. Collagen may impart elasticity to the tissue by virtue of its crimped geometry. The waviness of collagen, its distribution density, and its orientation were chosen as the variables in the microstructural models [e.g., Lanir,1983]. Thus quantification of waviness is important. We can express the waviness in several ways, e.g. the number of wave per unit length, the amplitude and pitch of wave. If the collagen fiber is regarded as a long sinusoidal beam as shown in Figure (15), it can be described by the following equation :

$$x_2' = a \sin bx_1' \quad (4.2)$$

By observing the slides fixed at different stress level, we may express a,b as functions of stresses.

$$\begin{aligned} a &= f_1(S_{11}, S_{22}) \\ b &= f_2(S_{11}, S_{22}) \end{aligned} \quad (4.3)$$

The anisotropic characteristics may be explained by the orientation of the collagen bundles. In stereology, these collagen fibers can be regarded as the curves distributed in a three dimensional material. The distributions of such internal structures are characterized by appropriately defined 'distribution densities'. By measuring the length of intersections of the structure with randomly placed cutting planes, it may be possible to determine the 'distribution densities'. The anisotropic characteristics may be inferred from these measured 'distribution densities' [kanatani,1985]. Also, the average preferred fiber orientation can be observed.

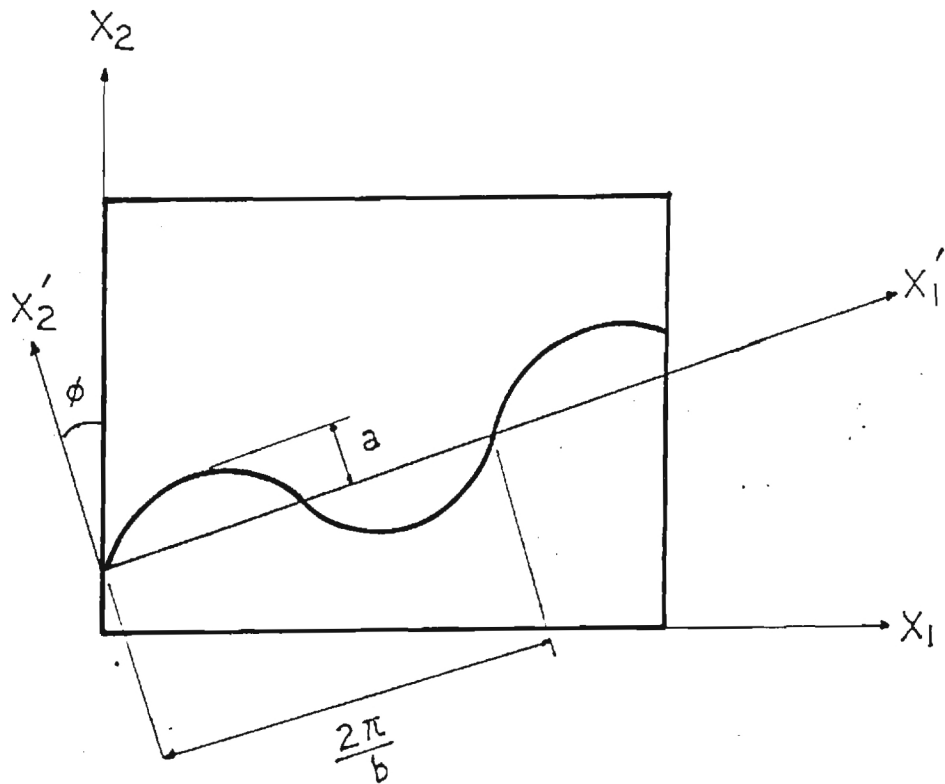


Figure (15) Geometry of collagen fiber bundles.

5. Preliminary Results

5.1 Thickness Measurement

Thickness measurement for the pericardium is one of the difficult task, since the pericardium is soft material and consist of 75% by weight of water. To measure the thickness at its reference state, we have to avoid squeezing and drying of tissue. The micrometer cannot be used alone, because the jaws of micrometer will squeeze the specimen. The small squeezing force, even if it cannot be felt during the measurement, will result in lower value than the true value. To avoid this difficulty, the electrical resistance method was employed. However, this method gives the value combined of tissue thickness and surface saline film thickness, and results in higher thickness value.

To get a true thickness value at its reference state, the new technique 'Two Stage Reading Value Extrapolation Technique' was developed. This technique gave highly reliable and repeatable results in our preliminary experiments. As aforementioned, when the two stage reading values become close enough, the contact stage reading value may be taken as the thickness value (Figure 7). However, it is inconvenient to spend 20-30 min. to measure the thickness at one point. Actually, we recorded two-stage reading values at one point in 0 to 6-8 min., and extrapolated these data using a linear-regression method to get a true thickness value (the value at the cross-point of two straight lines). After remoistening, the same procedures was applied at another point of the specimen. By repeating this procedure several times, the average value was taken as a tissue thickness. During our preliminary tests, the deviations of thickness value at different positions in the same specimen did not exceed 0.02mm (10% of thickness). The results obtained by this technique are given in Table (2) and Table (3).

5.2 Uniform Bi-axial Test

A typical mechanical response of normal pericardium (specimen #03) under the uniform biaxial stretching test is shown in Figure (16). The ordinate is the P-K stress and the abscissa is the Green strain. Two curves in Figure (16) are S_{xx} versus E_{xx} , and S_{yy} versus E_{yy} . This figure demonstrates several characteristic features. First, the strain-stress curve is highly nonlinear, showing a considerable tissue compliance at low loads but a rapid stiffening at higher loads. Second, there is considerable amount of hysteresis, i.e. the curves in loading and unloading are different. Third, the strain-stress relationship in one direction is different from that in other direction (

Table (2). Thickness measurement data for the specimen #01.

Point No.		# 1		# 2	
Stage		Contact	Lost-contact	Contact	Lost-contact
(min.)		(mm)	(mm)	(mm)	(mm)
T i m e	0.0	0.3048	0.4623	0.2565	0.3835
	1.5	0.2946	0.4166	0.2413	0.3429
	3.0	0.2870	0.4039	0.2388	0.3149
	4.5	0.2769	0.3658	0.2210	0.2718
	6.0	0.2642	0.3429	0.2159	0.2515
Linear regression $h = -\alpha t + \beta$		$\alpha = 0.006593$ $\beta = 0.3053$	$\alpha = 0.019307$ $\beta = 0.4560$	$\alpha = 0.006767$ $\beta = 0.2550$	$\alpha = 0.022340$ $\beta = 0.3799$
Thickness		0.227 mm		0.201 mm	

Table (2). Thickness measurement data for the specimen #01.

Point No.		# 1		# 2	
Stage		Contact	Lost-contact	Contact	Lost-contact
	(min.)	(mm)	(mm)	(mm)	(mm)
T i m e	0.0	0.3048	0.4623	0.2565	0.3835
	1.5	0.2946	0.4166	0.2413	0.3429
	3.0	0.2870	0.4039	0.2388	0.3149
	4.5	0.2769	0.3658	0.2210	0.2718
	6.0	0.2642	0.3429	0.2159	0.2515
Linear regression $h = -\alpha t + \beta$		$\alpha = 0.006593$ $\beta = 0.3053$	$\alpha = 0.019307$ $\beta = 0.4560$	$\alpha = 0.006767$ $\beta = 0.2550$	$\alpha = 0.022340$ $\beta = 0.3799$
Thickness		0.227 mm		0.201 mm	

Table (3). Thickness measurement data for the specimen #03.

Point No.		# 1		# 2	
Stage		Contact	Lost-contact	Contact	Lost-contact
	(min.)	(mm)	(mm)	(mm)	(mm)
T	0.0	0.3734	0.5715	0.3175	0.6045
	2.0	0.3708	0.5258		
i	2.5			0.3073	0.5410
	3.5	0.3454	0.5105		
m	4.5			0.3022	0.5080
	5.5	0.3302	0.4623		
e	6.5			0.2819	0.4927
	8.0	0.3124	0.4166		
	8.25			0.2743	0.4217
Linear regression $h = -\alpha t + \beta$		$\alpha = 0.008265$ $\beta = 0.3778$	$\alpha = 0.019208$ $\beta = 0.5703$	$\alpha = 0.005413$ $\beta = 0.3202$	$\alpha = 0.020149$ $\beta = 0.6012$
Thickness		0.232 mm		0.217 mm	

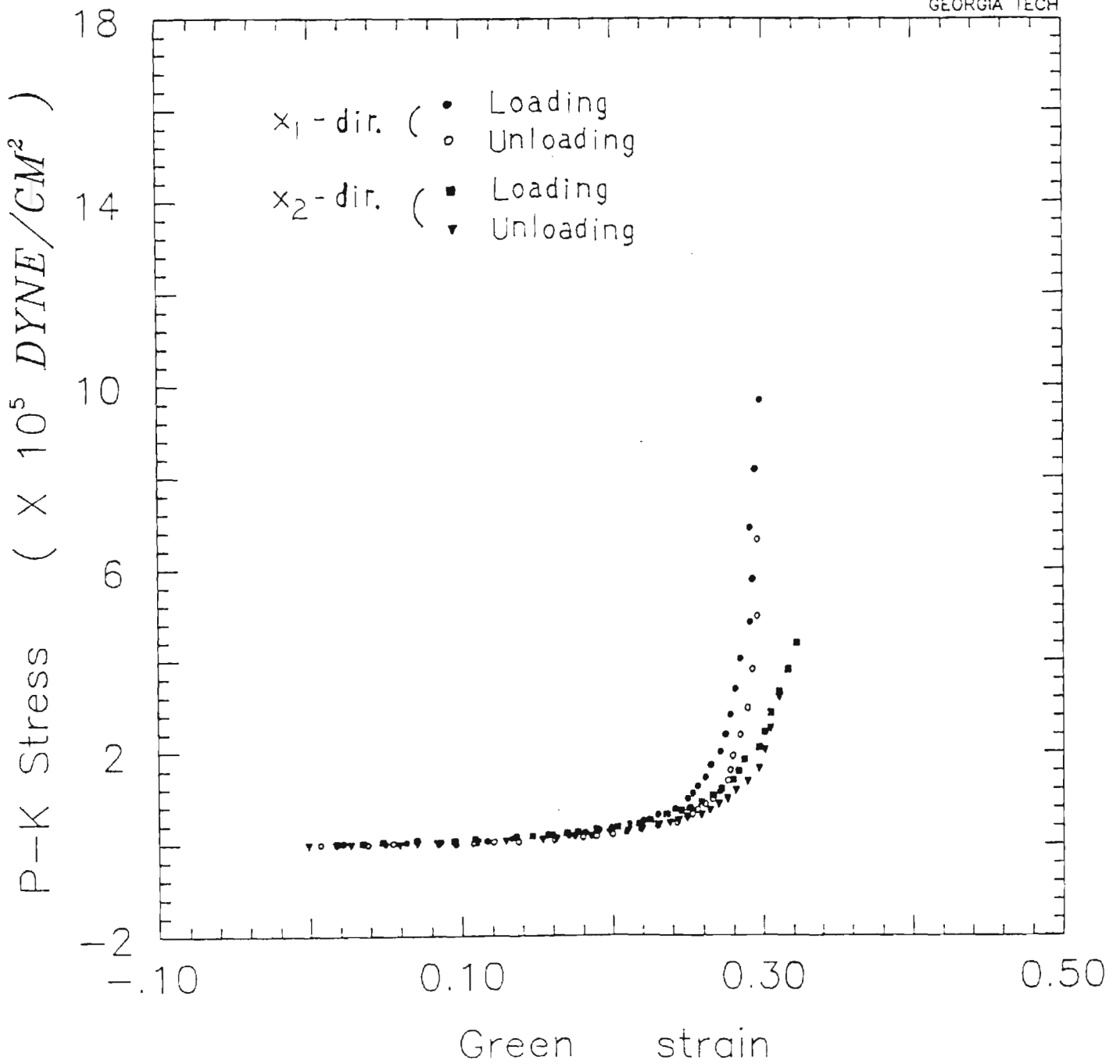


Figure (16) Strain-stress curve of uniform stretching test on specimen #03.

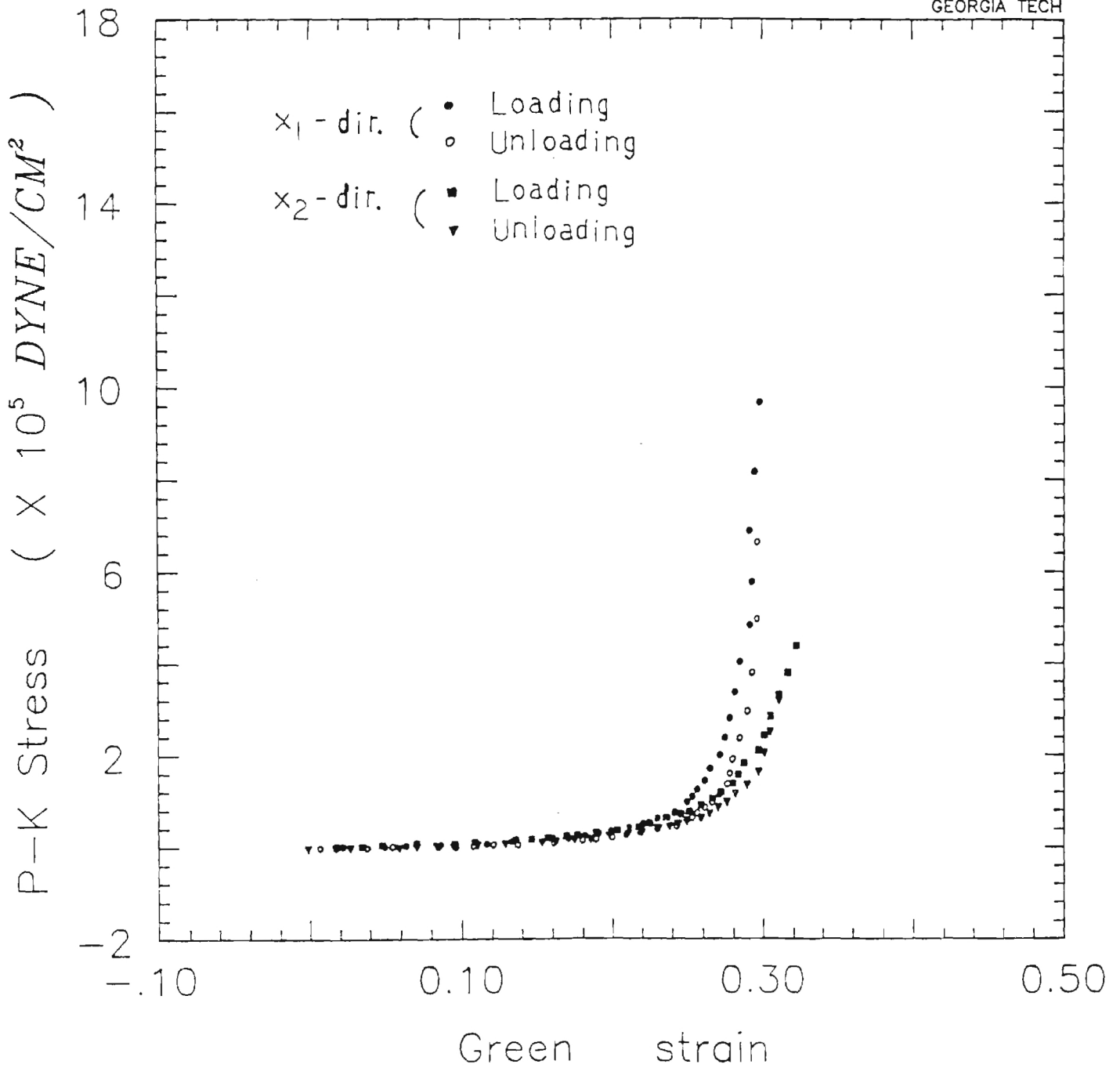


Figure (16) Strain-stress curve of uniform stretching test on specimen #03.

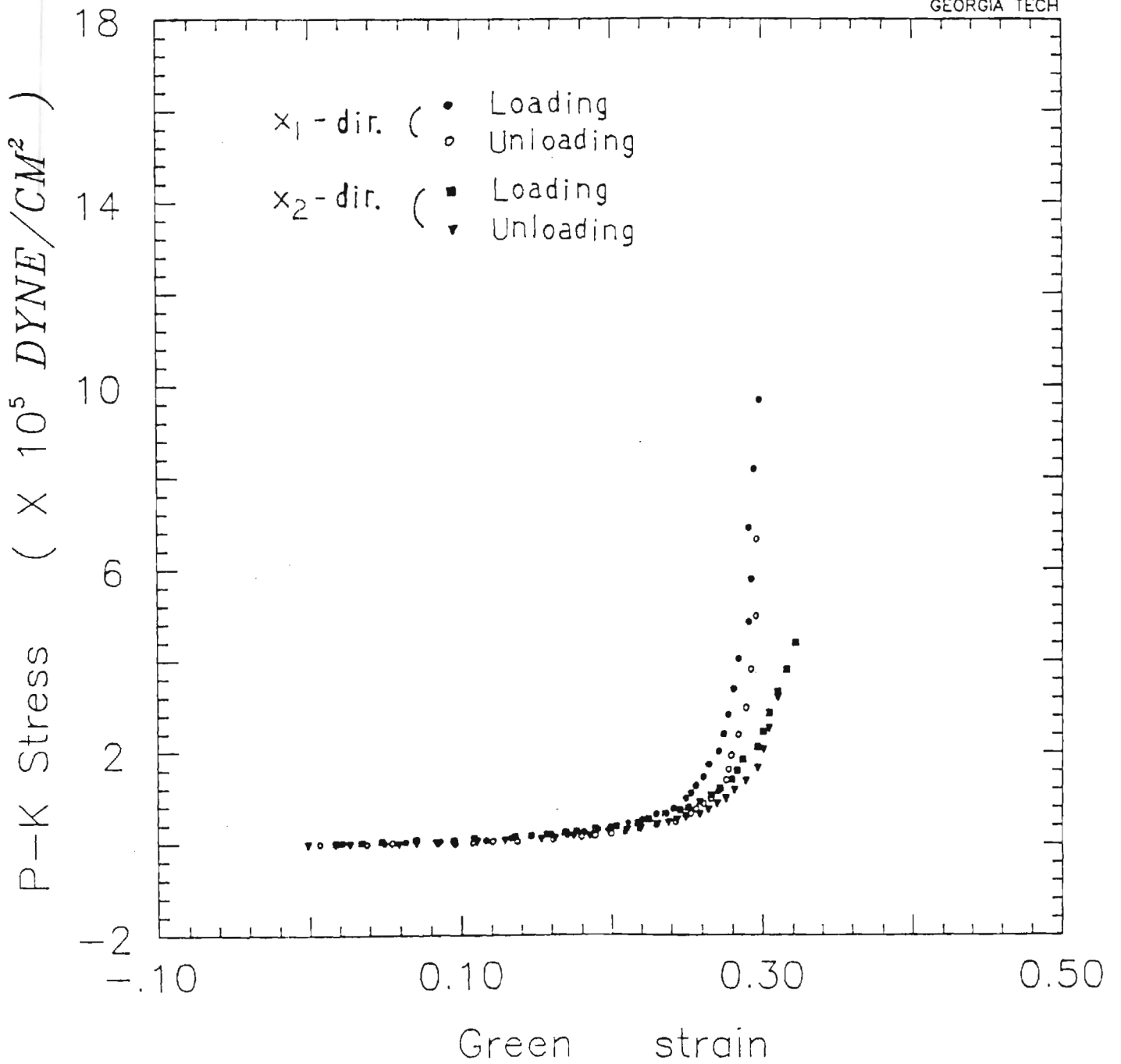


Figure (16) Strain-stress curve of uniform stretching test on specimen #03.

i.e., anisotropic behavior). Note that the maximum obtained Green strains are $E_{11}=0.30$ and $E_{22}=0.32$, and the corresponding P-K stresses are $S_{11}=9.68 \times 10^5$ dynes/cm² and $S_{22}=4.37 \times 10^5$ dynes/cm², due to the material anisotropy. In addition to these behavior, the strain rate has no significant effect on the strain-stress relationship, as shown in Figure (17). Except the anisotropic behavior, these general characteristics are common to other soft tissues.

Figure (18) shows the Green strains imposed on the target region under uniform biaxial stretching test. The extensional strains are almost equal with each other, and the shear strains are relatively small (max. 0.028). Also, the actual deformation histories during uniform biaxial stretching test are shown in Figure (19). Although the equal amounts of stretchings are imposed on the specimen boundary in both directions, the tensile strains (E_{11}, E_{22}) at the central tracking region are slightly different from with each other as shown in Figure (18) and Figure (19). It may be due to several factors such as nonhomogeneous deformation, material anisotropy, off-centered central tracking region and the errors included in the reference state dimension. However, the strongest factor among them is not verified yet.

To verify the possibility of data quantification using the strain energy function as equation (3.25), the same data with Figure (16) is plotted as $\text{Log}_e S/E$ versus E^2 , shown in Figure (20). We may expect the better result for quantification, as straight as the line is. The data of compliant direction (x_2 -dir.) shows no significant transition characteristics. But the data of stiff direction (x_1 -dir.) shows significant transition from one straight line to another straight line. An microstructural explanation may be that more fibers run in one direction (x_1 -dir.) than the other (x_2 -dir.), and the straightening of fibers occurs in a more gradual fashion in the compliant direction than in the stiff direction. Although the strain energy density function as equation (3.25) can fit the data at low strains and at high strains separately, it may not be adequate to fit the whole data simultaneously. Therefore, the strain energy density function as equation (3.26) or other function form have to be tried to fit the data.

5.3 Non-uniform Bi-axial Test.

The response shown in Figure (21). is for the same specimen #03 which was cyclically stretched along two axes at different stretching rates (non-uniform biaxial stretching). This figure shows the anisotropic behavior more apparently. Note that the maximum obtained Green strains are $E_{11}=0.25$ and $E_{22}=0.40$, and the corresponding P-K stresses are $S_{11}=11.23 \times 10^5$ dynes/cm² and $S_{22}=7.29 \times 10^5$ dynes/cm². Still S_{11} is much bigger than S_{22} , but E_{11} is much smaller than E_{22} because of material anisotropy.

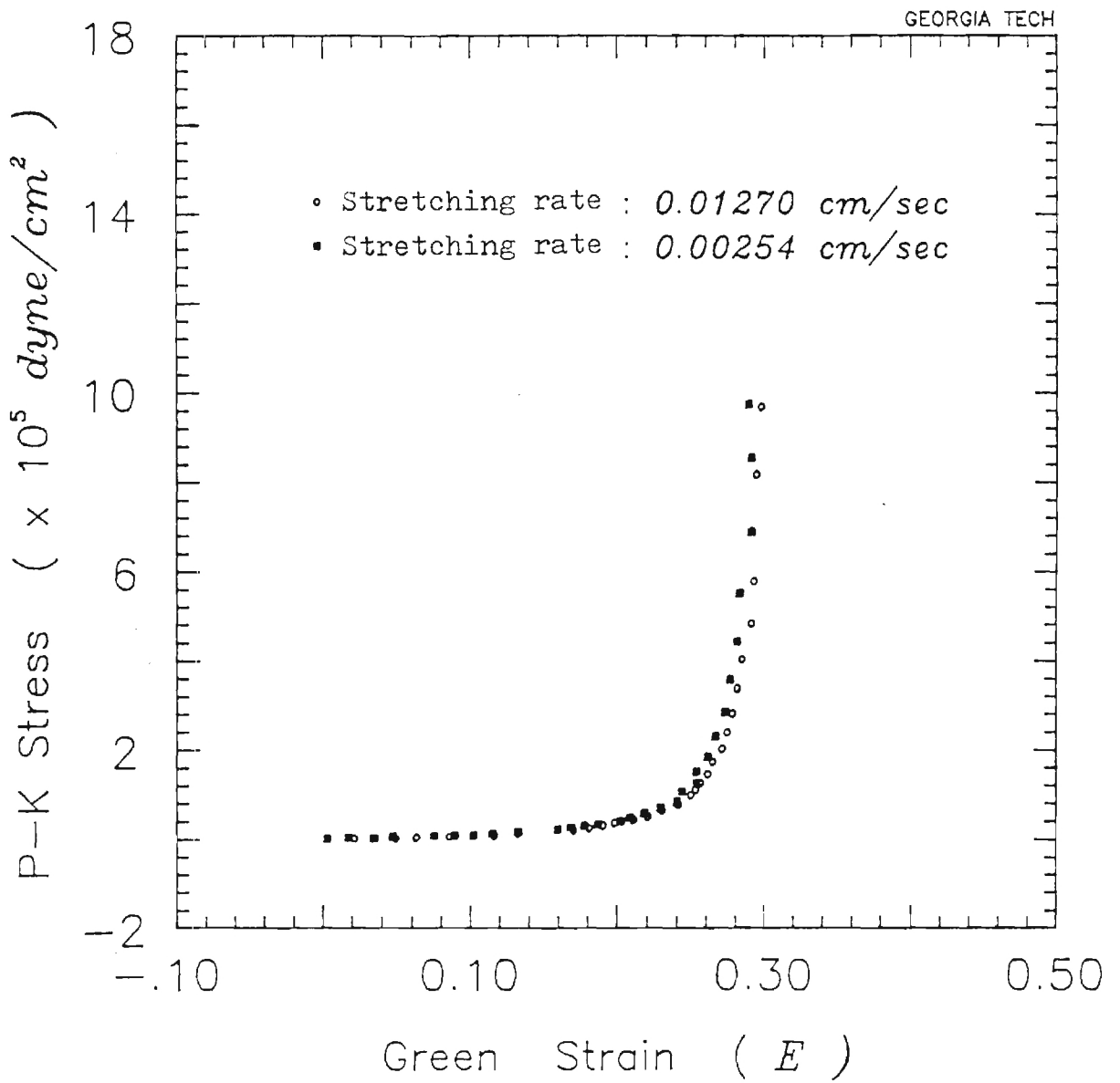


Figure (17) Strain rate insensitivity.

X_1 -direction

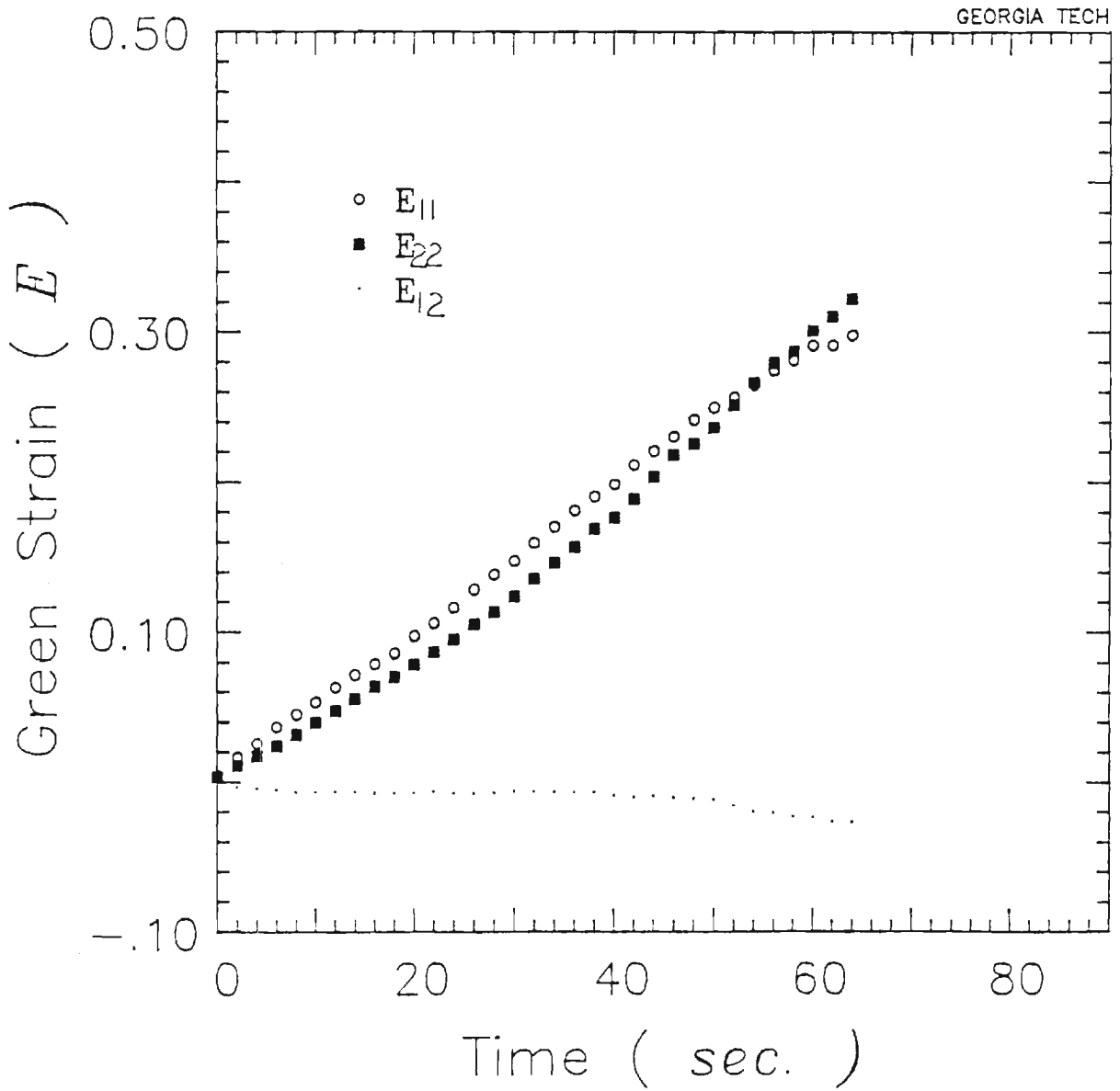


Figure (18) Strains imposed on target region under uniform bi-axial stretching test.

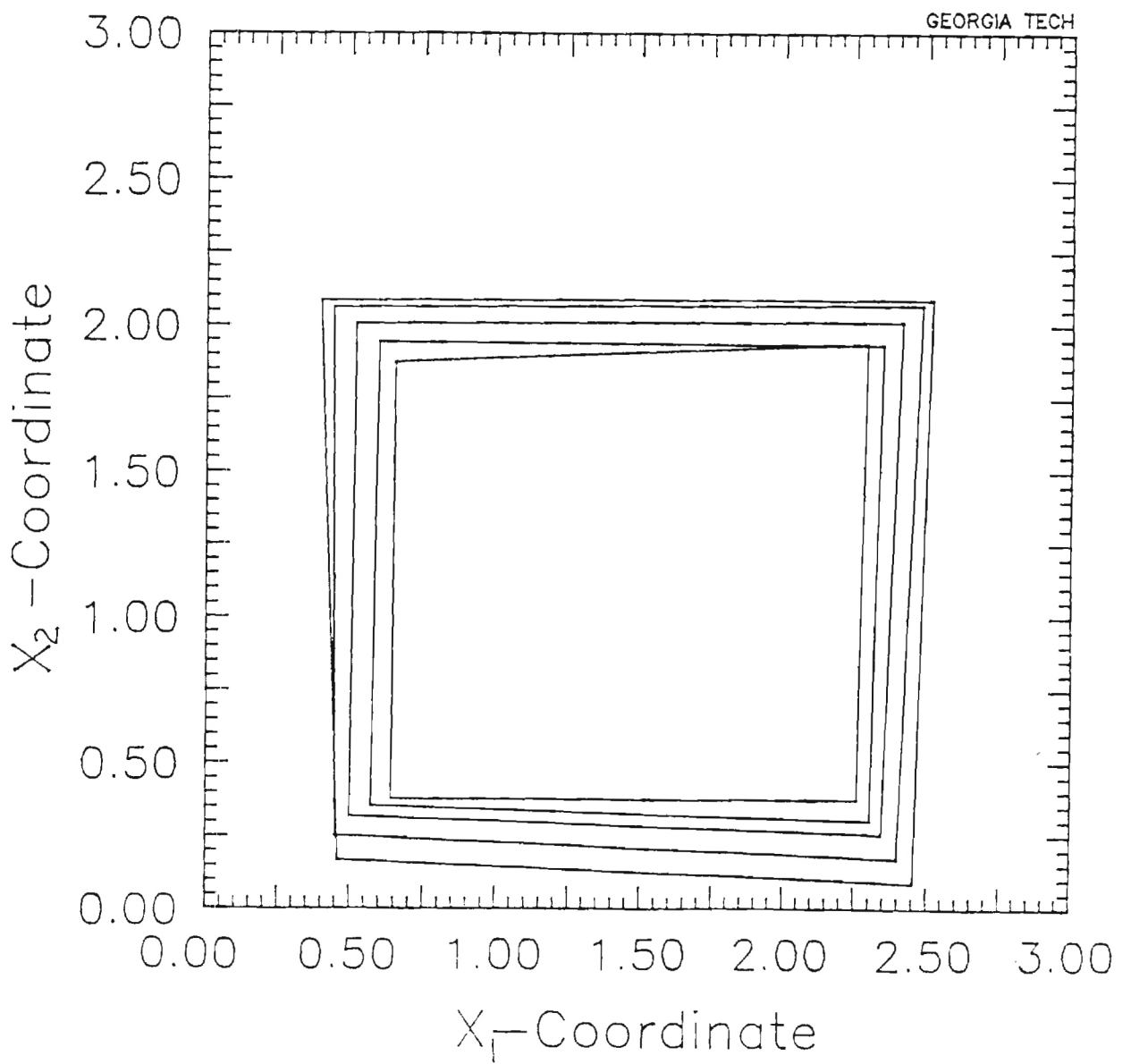


Figure (19) Actual particle histories during uniform bi-axial stretching test.

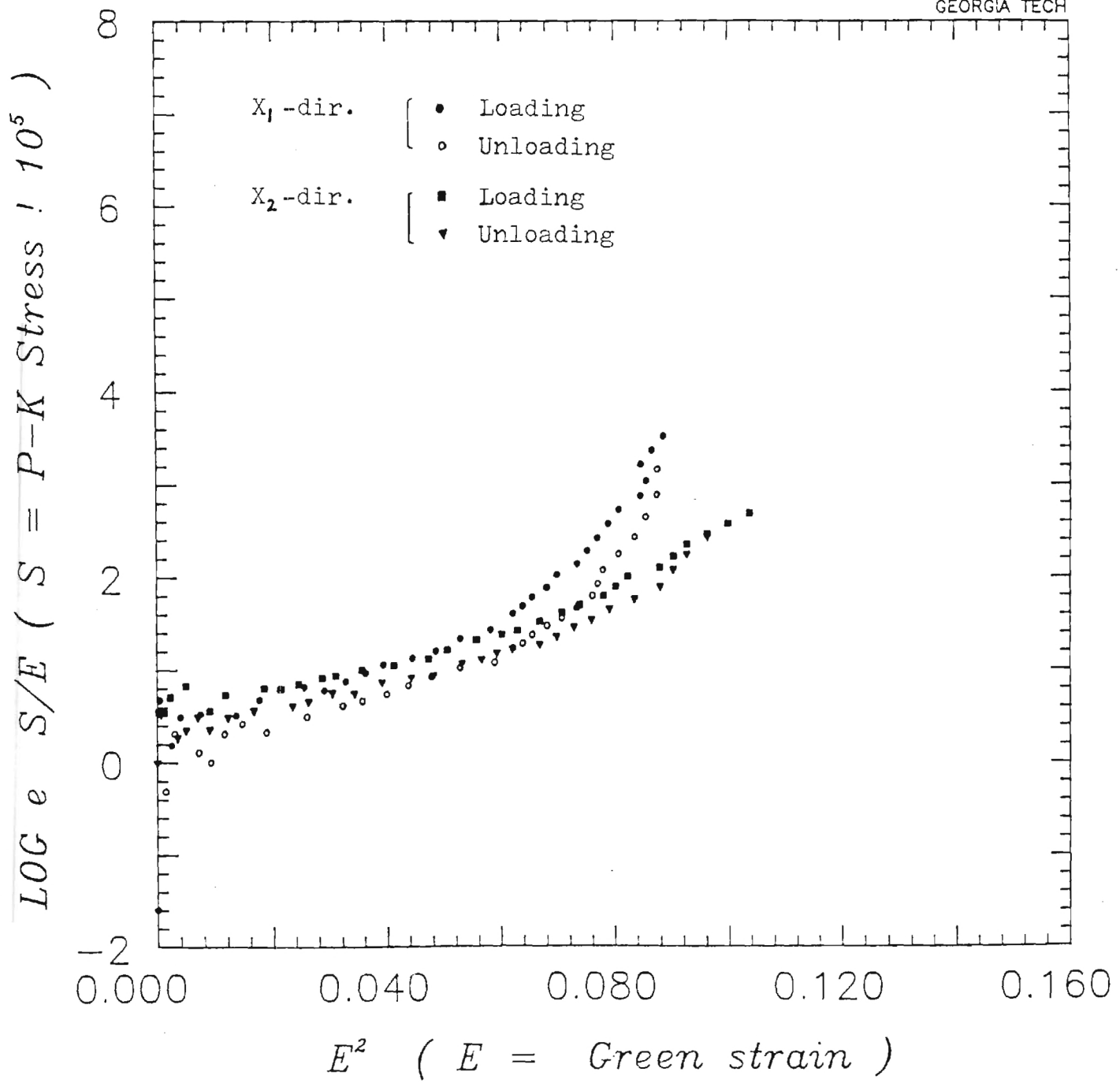


Figure (20) The log function plot of Figure (16).

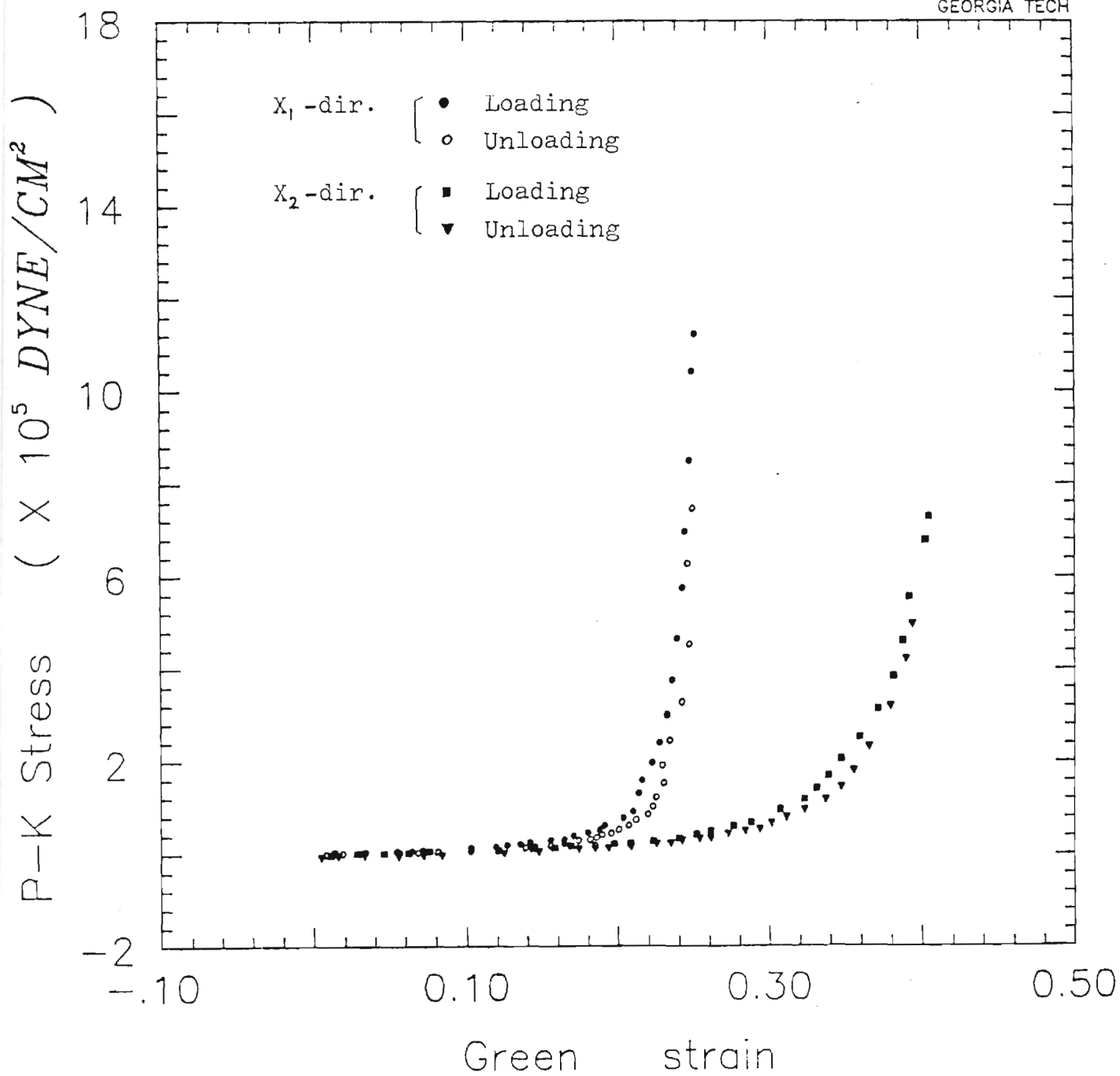


Figure (21) Strain-stress curve of nonuniform stretching test on specimen #03.

Comparing Figure (21). with Figure (16), the strain-stress curves show some amounts of shift. Two curves shift reversely with each other. It means the strain-stress relationships cannot be treated separately in each direction. Figure (22) shows the strains imposed on the central target region under non-uniform biaxial stretching test. Also, the actual deformation histories of target region are shown in Figure (23). The shear strain (max. 0.072) is greater than that (max. 0.028) of uniform stretching test. It implies that the material axis may have some angle with the stretching axis.

5.4 Constant Lateral Displacement Test.

A series of the constant lateral displacement tests were conducted on the specimen #02. In these tests, one axis(x_2 -axis) was cyclically stretched at a constant rate (approximately 0.0038 cm/sec) while the dimension in the second direction (x_1 -axis) was held constant. Figure (24) shows the response when the lateral dimension was held constant at $E_{11}=0.185$. We can see the non-linear characteristics and hysteresis.

The three (E_{22} - S_{22}) curves in Figure (25) show the responses during constant lateral displacement tests in which the lateral dimension in x_1 direction was held approximately constant at $E_{11}=0, 0.185$ and 0.198 respectively, as shown in Figure (26). For clarity, only the responses of loading portion are shown. Notice that increasing the constant-lateral-displacement tended to stiffen the tissue along the stretching axis.

Figure (27) and Figure (28) show the actual particle histories of the central tracking region when the lateral displacement was held constant at $E_{11}=0$, and $E_{11}=0.185$ respectively

The dashed line represents the initial dimension, and the solid lines represent the dimension at each time increment after holding the lateral dimension constant. In Figure (28), notice the difference between the initial dimension and the subsequent dimension immediately after imposing the constant-lateral-displacement of $E_{11}=0.185$. By imposing the constant-lateral-displacement in x_1 -direction, the dimension in x_2 -direction was contracted.

We also notice the translation of central tracking region in Figure (27) and Figure (28). It may be due to the fact that the central tracking region was slightly off-centered from the stretching axis. However, the translation does not affect to the strain measurements.

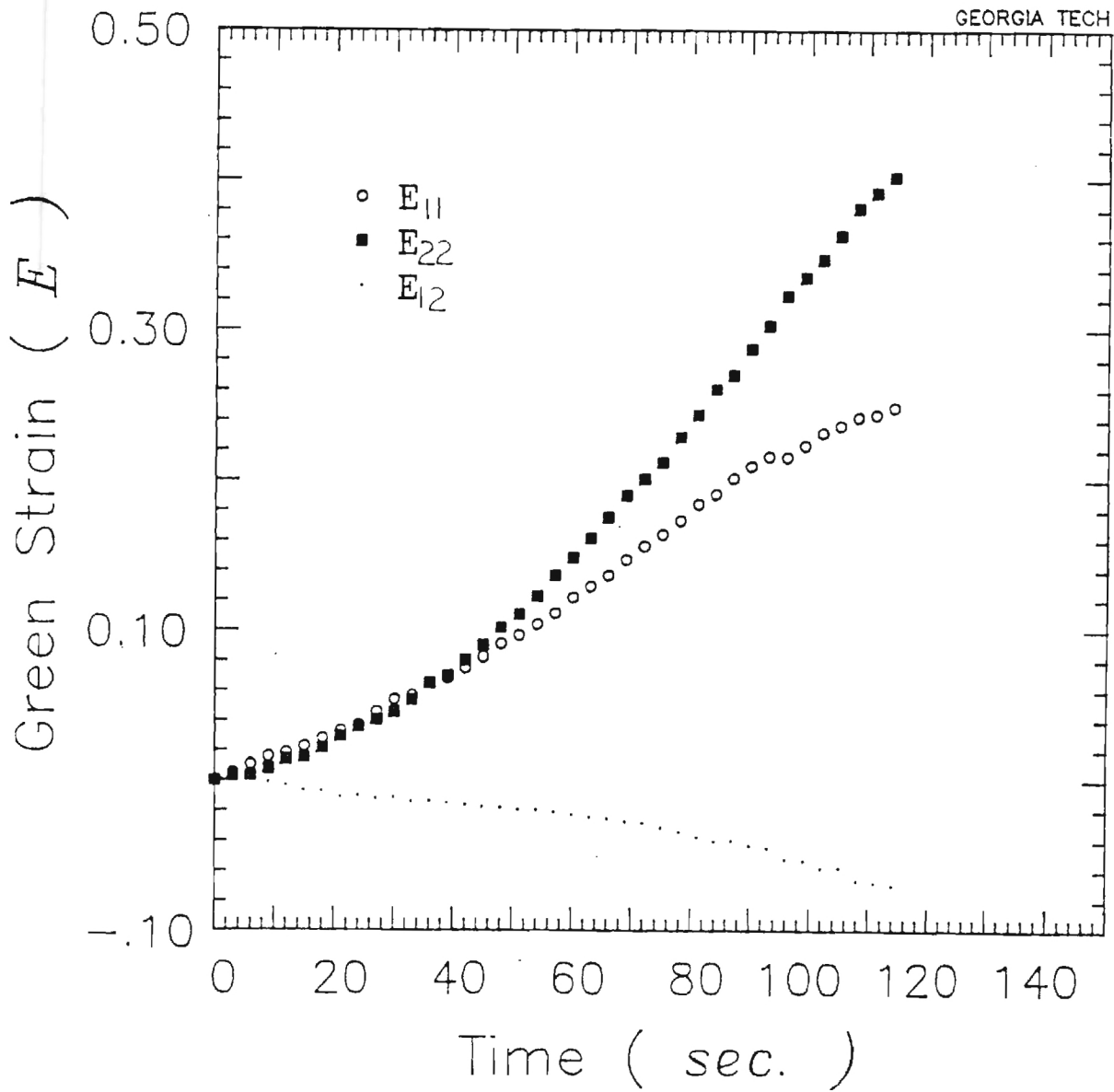


Figure (22) Strain imposed on target region under non-uniform bi-axial stretching test.

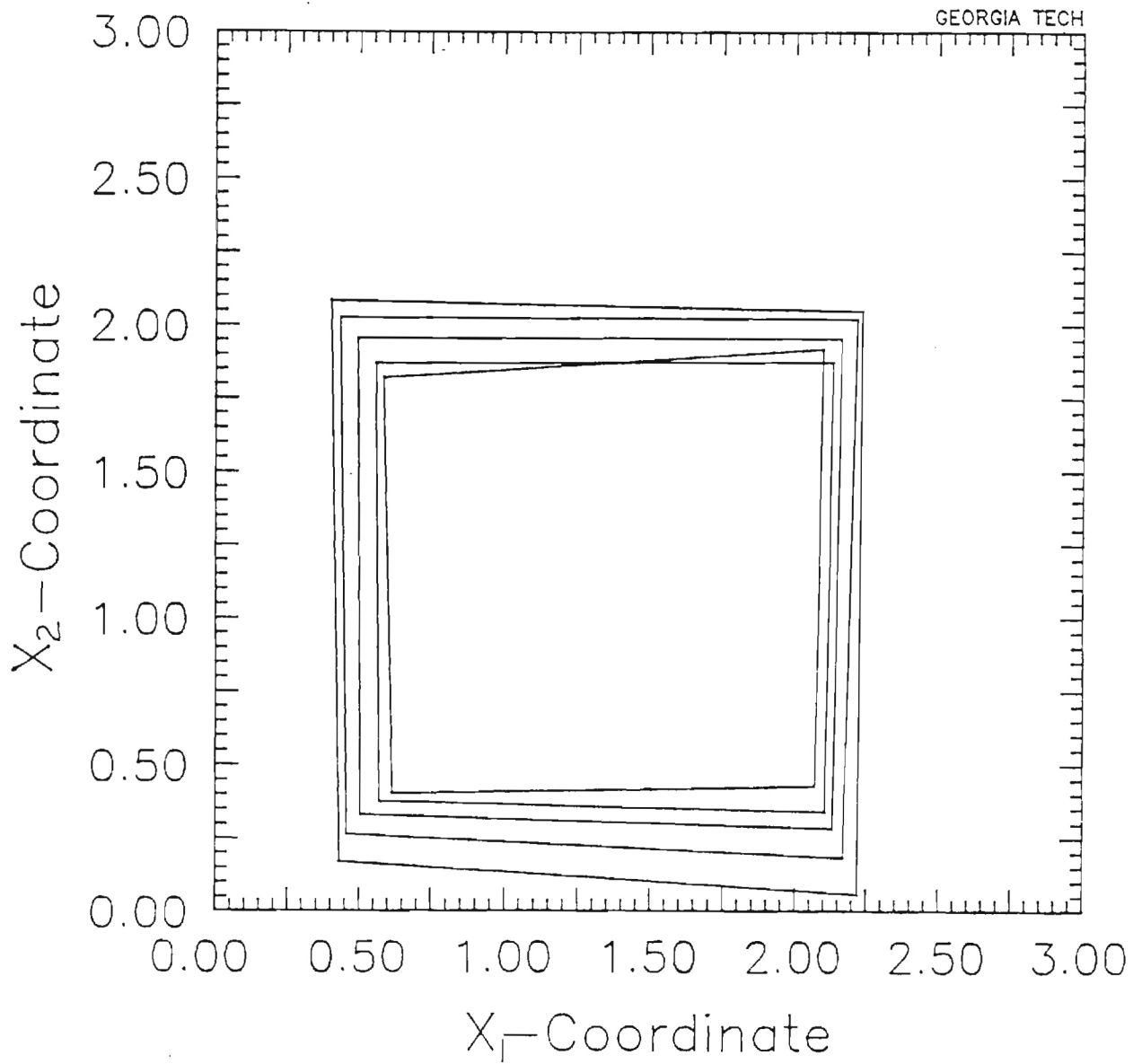


Figure (23) Actual particle histories during non-uniform bi-axial stretching test.

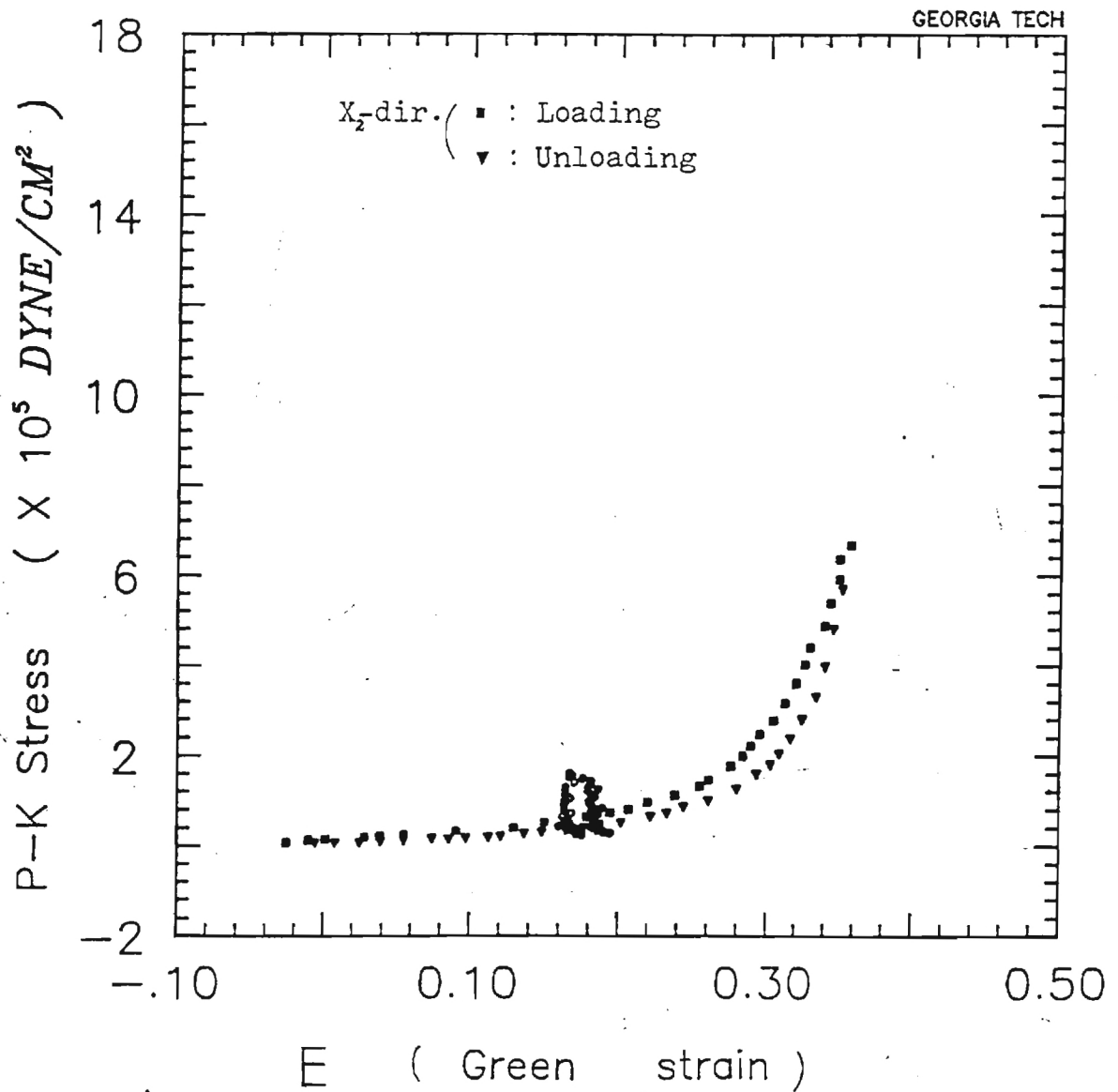


Figure (24) Strain-stress curve of the constant lateral displacement test on specimen #02.

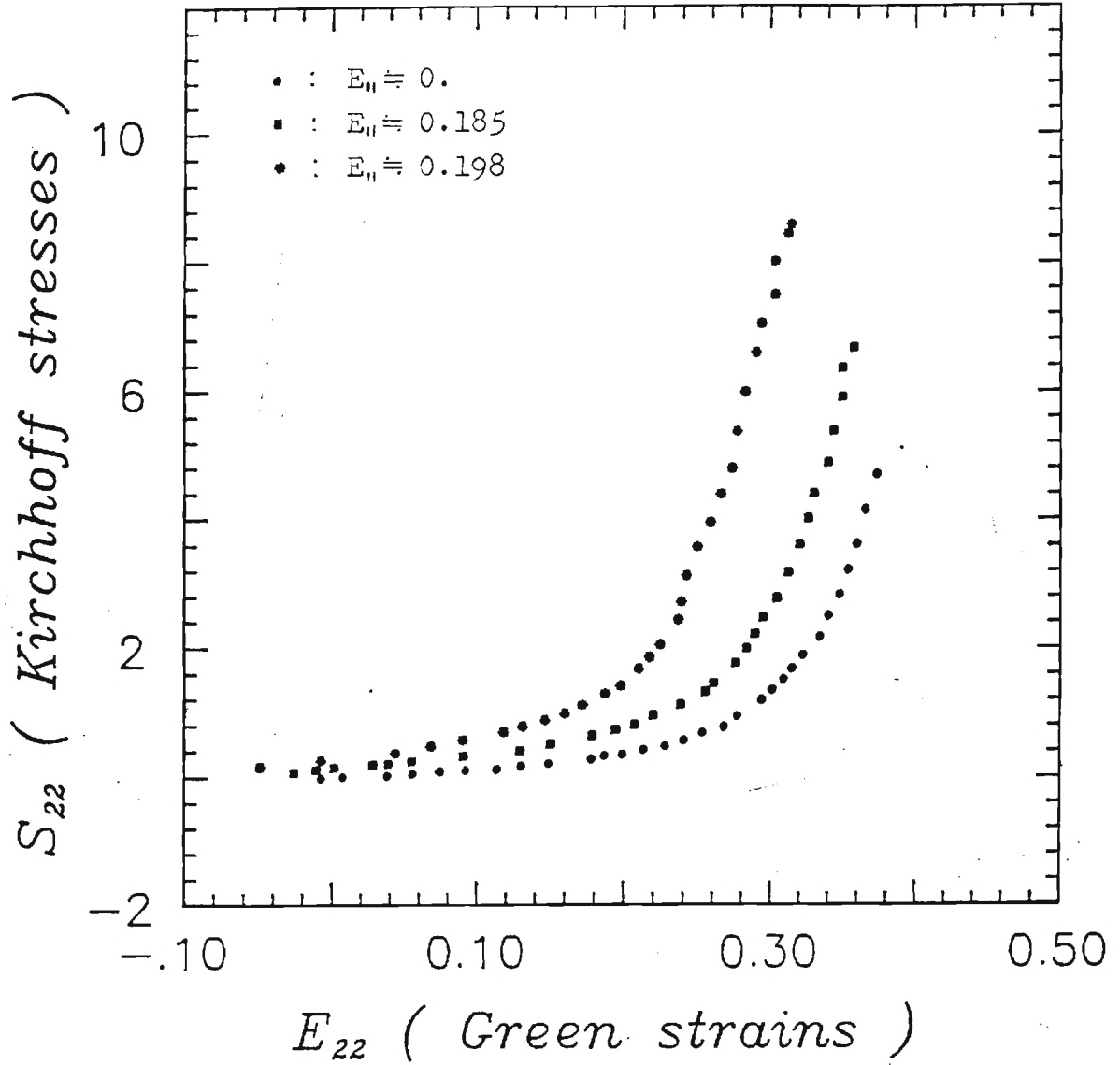


Figure (25) Constant lateral displacement test results when the lateral dimension was held approximately constant at $E_{11} = 0, 0.185, 0.198$ respectively.

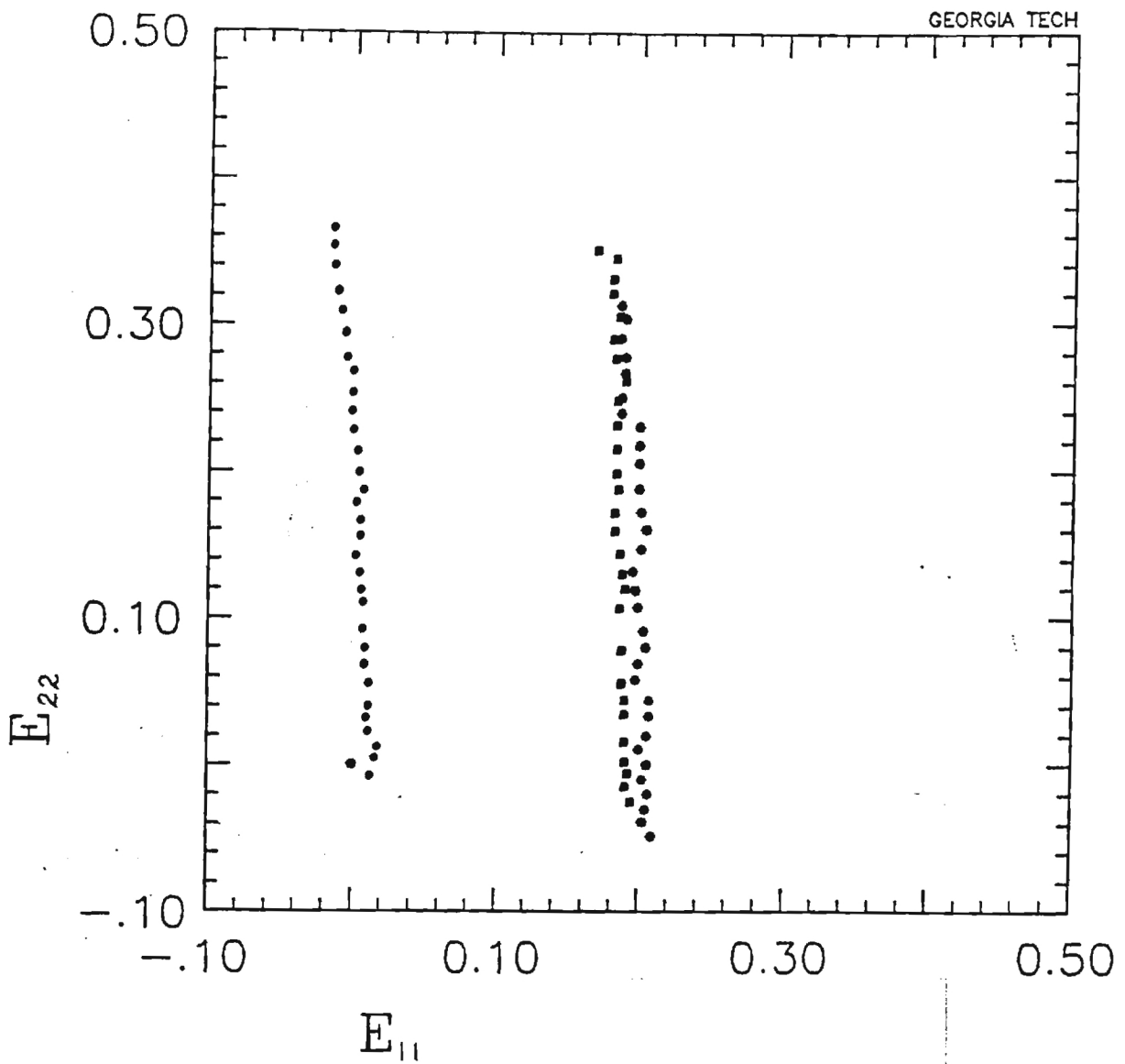


Figure (26) E_{22} versus E_{11} in the constant lateral displacement tests shown in Figure (25).

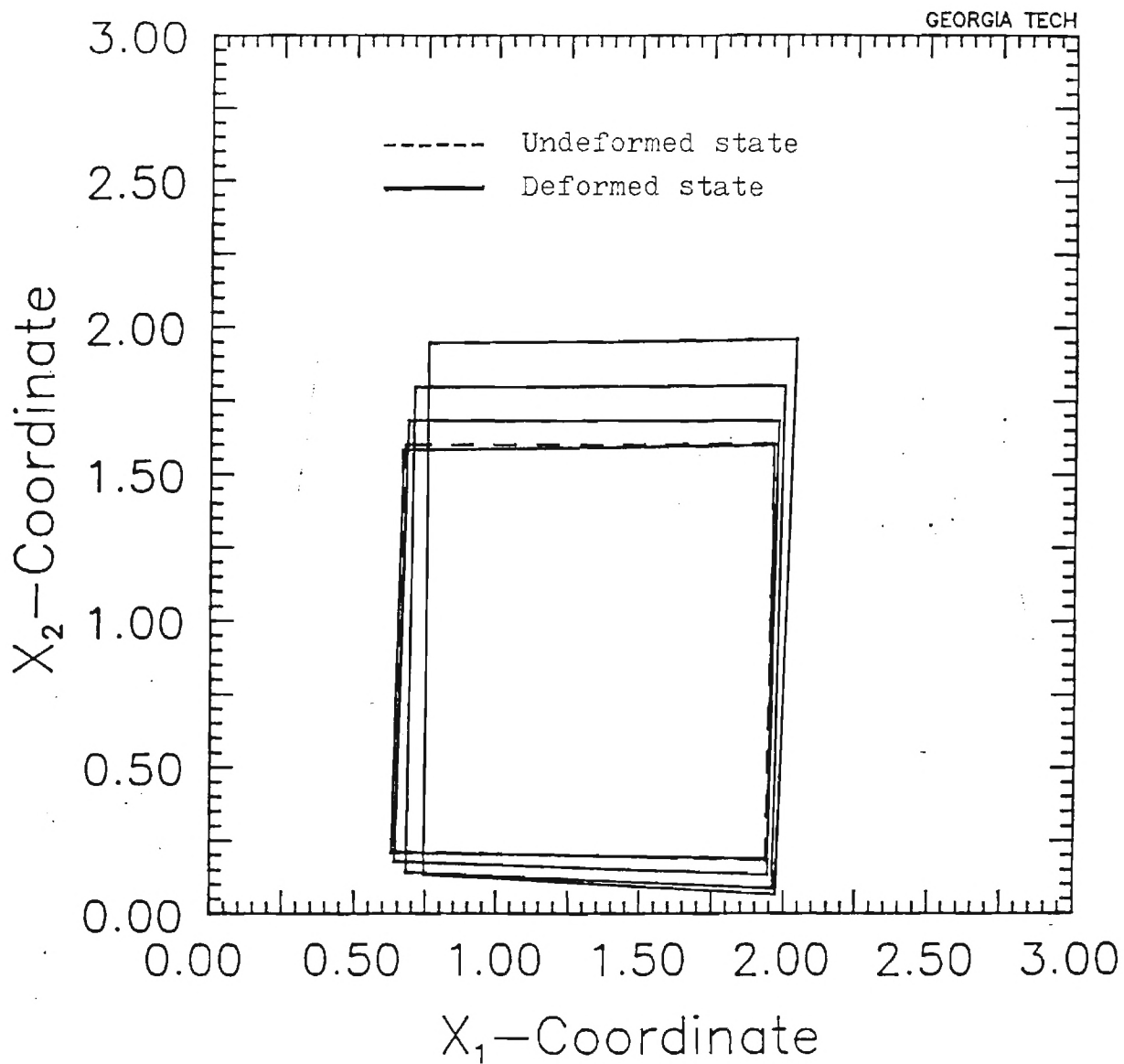


Figure (27) Actual particle histories during the constant lateral displacement test. (The lateral direction was constrained at $\epsilon_{11} = 0$.)

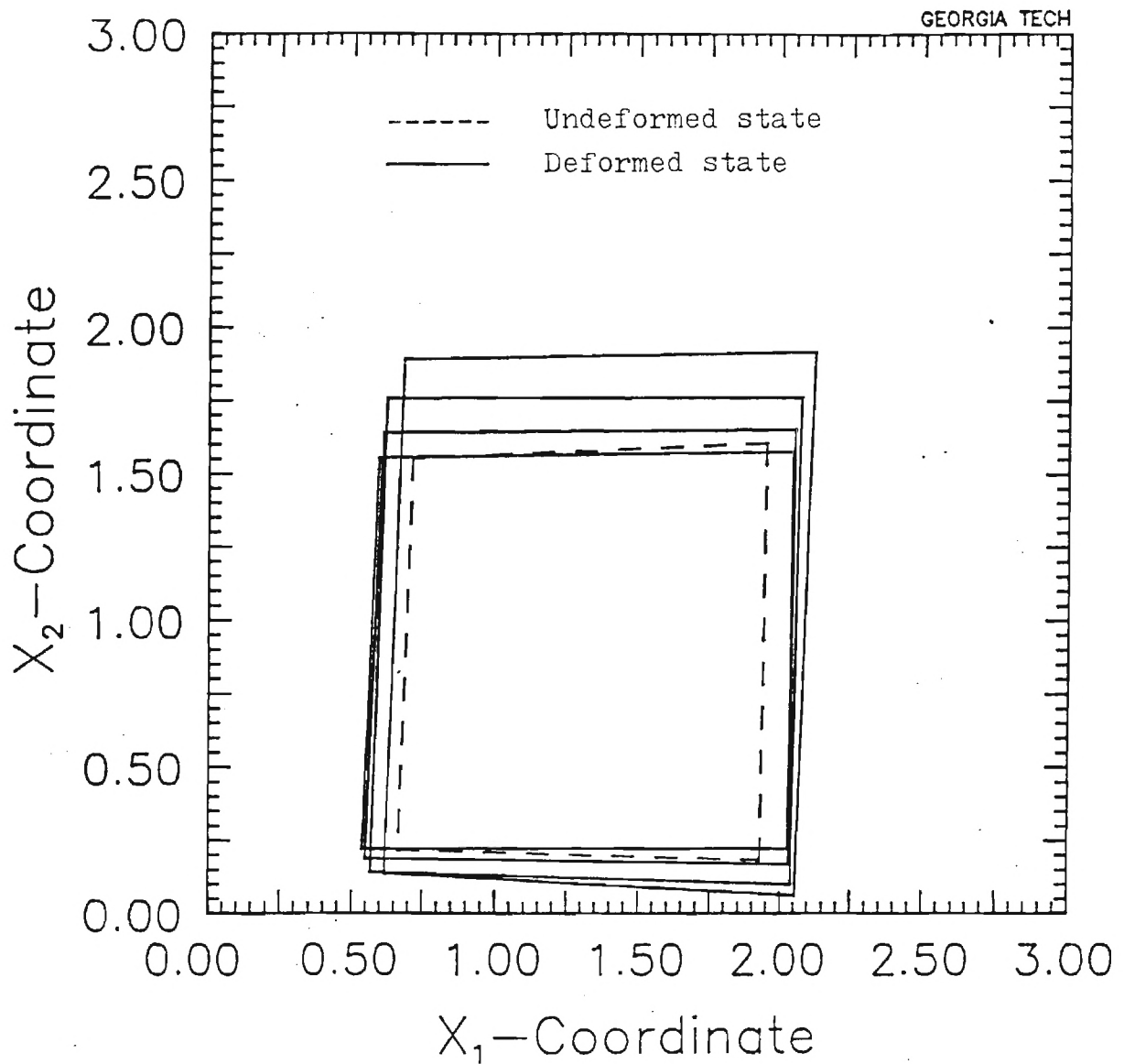


Figure (28) Actual particle histories during the constant lateral displacement test. (The lateral direction was constrained at $\epsilon_{11} = 0.185$)

APPENDIX 1
Symmetry Arguments for Material Constants

The number of material constants A_{ijkl} and b_{ijkl} in equation (3.10) and (3.11) can be reduced by using the symmetry arguments.

$$S_{ij} = \frac{\partial W}{\partial E_{ij}} = A_{ijkl} E_{kl} + B (b_{ijkl} E_{kl}) e^Q \quad (3.10)$$

$$Q = 1/2 b_{ijkl} E_{ij} E_{kl} \quad (3.11)$$

The symmetry arguments are following :

(i) The Kirchhoff stresses (S_{ij}) are symmetric, that is

$$S_{ij} = S_{ji} \quad (A.1)$$

$$S_{ji} = \frac{\partial W}{\partial E_{ji}} = A_{jikl} E_{kl} + B (b_{jikl} E_{kl}) e^{Q^*} \quad (A.2)$$

$$Q^* = 1/2 b_{jikl} E_{ji} E_{kl} \quad (A.3)$$

Since E_{ij} is also symmetric, by comparing equation (3.10) with equation (A.2), we obtain

$$A_{ijkl} = A_{jikl} \quad , \quad \text{and} \quad b_{ijkl} = b_{jikl} \quad (A.4)$$

(ii) The A_{ijkl} (and b_{ijkl}) can be decomposed into a symmetric and a skew-symmetric part [Sokolnikoff, 1956],

$$A_{ijkl} = A_{ijkl}^{(s)} + A_{ijkl}^{(ss)} \quad (A.5)$$

in which (s) and (ss) denote symmetric and skew-symmetric part with respect to k and l . Then equation (3.10) can be represented as following :

$$S_{ij} = \left\{ \begin{array}{l} A_{ijkl}^{(s)} E_{kl} + B (b_{ijkl}^{(s)} E_{kl}) e^Q \\ + \left\{ \begin{array}{l} A_{ijkl}^{(ss)} E_{kl} + B (b_{ijkl}^{(ss)} E_{kl}) e^Q \end{array} \right\} \end{array} \right\} \quad (A.6)$$

Since $A_{ijkl}^{(ss)} = -A_{ijlk}^{(ss)}$, $b_{ijkl}^{(ss)} = -b_{ijlk}^{(ss)}$, and $E_{kl} = E_{lk}$, the double sum in the second term of equation (A.6) vanishes. That is,

$$S_{ij} = A_{ijkl}^{(s)} E_{kl} + B (b_{ijkl}^{(s)} E_{kl}) e^Q \quad (A.7)$$

where $A_{ijkl}^{(s)}$ and $b_{ijkl}^{(s)}$ are symmetric with respect to k and l . Hence we obtain,

$$A_{ijkl} = A_{ijlk} \quad , \quad \text{and} \quad b_{ijkl} = b_{ijlk} \quad (A.8)$$

(iii) We may write $A_{ijkl} E_{ij} E_{kl}$ as $A_{mn} E_m E_n$, where $m, n = 1, 2, \dots, 6$, and $E_1 = E_{11}$, $E_2 = E_{22}$, \dots , $E_6 = E_{31}$. Then equation (3.10) becomes,

$$S_m = \frac{\partial W}{\partial E_r} = A_{mq} E_q + B (b_{mq} E_q) e^Q \quad (A.9)$$

$$S_n = \frac{\partial W}{\partial E_n} = A_{qn} E_q + B (b_{qn} E_q) e^Q \quad (A.10)$$

where m and n are free indices, and q is dummy index. Hence, by changing n in equation (A.10) to m , we obtain $A_{mq} = A_{nq}$. That is,

$$A_{ijkl} = A_{klij} \quad , \quad \text{and} \quad b_{ijkl} = b_{klij} \quad (A.11)$$

From equations (A.4), (A.8) and (A.11), we know that A_{ijkl} and b_{ijkl} satisfy the following symmetry restrictions :

$$A_{ijkl} = A_{jikl} = A_{ijlk} = A_{klij} \quad (A.12)$$

$$b_{ijkl} = b_{jikl} = b_{ijlk} = b_{klij} \quad (A.13)$$

Therefore, each of A_{ijkl} and b_{ijkl} contains only 21 independent material constants . For example, we can write Q in expanded form in terms of these 21 constants:

$$Q = 1/2 b_{ijkl} E_{ij} E_{kl} = 1/2 b_{mn} E_m E_n \quad (\text{where } m, n = 1, 2, \dots, 6) \quad (A.14)$$

That is :

$$\begin{aligned} Q = & \frac{1}{2} b_{11} E_{11}^2 + b_{12} E_{11} E_{22} + b_{13} E_{11} E_{33} + b_{14} E_{11} E_{12} + b_{15} E_{11} E_{23} + b_{16} E_{11} E_{31} \\ & + \frac{1}{2} b_{22} E_{22}^2 + b_{23} E_{22} E_{33} + b_{24} E_{22} E_{12} + b_{25} E_{22} E_{23} + b_{26} E_{22} E_{31} \\ & + \frac{1}{2} b_{33} E_{33}^2 + b_{34} E_{33} E_{12} + b_{35} E_{33} E_{23} + b_{36} E_{33} E_{31} \\ & + \frac{1}{2} b_{44} E_{12}^2 + b_{45} E_{12} E_{23} + b_{46} E_{12} E_{31} \\ & + \frac{1}{2} b_{55} E_{23}^2 + b_{56} E_{23} E_{31} \\ & + \frac{1}{2} b_{66} E_{31}^2 \end{aligned}$$

If the medium is elastically symmetric in certain directions, then the number of independent constants A_{ijkl} and b_{ijkl} in equations (3.10) and (3.11) can be further reduced. It is obvious from equation (3.10) that coefficients A_{ijkl} and b_{ijkl} depend on the chosen reference frame. For certain media the coefficients A_{ijkl} and b_{ijkl} may remain invariant under a given transformation of coordinates, which determines the elastic symmetry of the medium under consideration.

(iv) Consider the monoclinic material which is symmetric with respect to $x_1 x_2$ -plane. This symmetry is expressed by the statement that A_{ijkl} and b_{ijkl} are invariant under the transformation :

$$x_1 = x_1^* \quad , \quad x_2 = x_2^* \quad , \quad x_3 = -x_3^* \quad (A.15)$$

Under this transformation, stresses and strains become,

$$\begin{aligned} S_{11}^* &= S_{11} \quad , \quad S_{22}^* = S_{22} \quad , \quad S_{33}^* = S_{33} \\ S_{12}^* &= S_{12} \quad , \quad S_{23}^* = -S_{23} \quad , \quad S_{31}^* = -S_{31} \end{aligned} \quad (A.16)$$

$$\begin{aligned} E_{11}^* &= E_{11} \quad , \quad E_{22}^* = E_{22} \quad , \quad E_{33}^* = E_{33} \\ E_{12}^* &= E_{12} \quad , \quad E_{23}^* = -E_{23} \quad , \quad E_{31}^* = -E_{31} \end{aligned} \quad (A.17)$$

From equation (3.10), we obtain

$$\begin{aligned} S_{11} = & (A_{11} + B b_{11} e^{\alpha}) E_{11} + (A_{12} + B b_{12} e^{\alpha}) E_{22} + (A_{13} + B b_{13} e^{\alpha}) E_{33} \\ & + (A_{14} + B b_{14} e^{\alpha}) E_{12} + (A_{15} + B b_{15} e^{\alpha}) E_{23} \\ & + (A_{16} + B b_{16} e^{\alpha}) E_{31} \end{aligned} \quad (A.18)$$

$$S_{ii}^* = (A_{11} + B b_{11} e^{\alpha^*}) E_{11}^* + (A_{12} + B b_{12} e^{\alpha^*}) E_{22}^* + (A_{13} + B b_{13} e^{\alpha^*}) E_{33}^* \\ + (A_{14} + B b_{14} e^{\alpha^*}) E_{12}^* + (A_{15} + B b_{15} e^{\alpha^*}) E_{23}^* + (A_{16} + B b_{16} e^{\alpha^*}) E_{31}^* \quad (A.19)$$

$$\text{where } Q^* = 1/2 b_{ijkl} E_{ij}^* E_{kl}^* \quad (A.20)$$

Comparison between equation (A.18) and (A.19), with the condition (A.16) and (A.17), gives the following conditions :

$$A_{15} = A_{16} = 0 \quad (A.21)$$

$$b_{15} = b_{16} = 0 \quad (A.22)$$

$$Q^* = Q \quad (A.23)$$

Referring to equations (A.14), (A.16), (A.17) and (A.20), the condition (A.23) renders the following conditions :

$$b_{15} = b_{25} = b_{35} = b_{16} = b_{26} = b_{36} = b_{46} = b_{45} = 0 \quad (A.24)$$

The condition (A.24) already includes the condition (A.22). Similarly, by considering S_{22}^* , S_{33}^* , S_{12}^* , S_{23}^* and S_{31}^* , we find that

$$A_{15} = A_{25} = A_{35} = A_{16} = A_{26} = A_{36} = A_{46} = A_{45} = 0 \quad (A.25)$$

$$b_{15} = b_{25} = b_{35} = b_{16} = b_{26} = b_{36} = b_{46} = b_{45} = 0 \quad (A.24)$$

For the monoclinic material, the number of material constants A_{ijkl} (and b_{ijkl}) are reduced to 13 from 21. The coefficients b_{ijkl} (= b_{mn}) are expressed in matrix form as below :

$$\begin{bmatrix} b_{11} & b_{12} & b_{13} & b_{14} & 0 & 0 \\ & b_{22} & b_{23} & b_{24} & 0 & 0 \\ & & b_{33} & b_{34} & 0 & 0 \\ & & & b_{44} & 0 & 0 \\ & & & & b_{55} & b_{56} \\ & & & & & b_{66} \end{bmatrix} \quad (A.26)$$

(v) Consider the orthotropic material which has three mutually orthogonal planes of elastic symmetry. Besides the symmetry with respect to x_1x_2 -plane as expressed by equation (A.15), the material constants A_{ijkl} and b_{ijkl} are invariant under the transformation (x_2x_3 -plane of symmetry) :

$$x_1 = -x_1^*, \quad x_2 = x_2^*, \quad x_3 = x_3^* \quad (A.27)$$

By using similar argument as (iv), we obtain:

$$A_{14} = A_{24} = A_{34} = A_{56} = 0 \quad (A.28)$$

$$b_{14} = b_{24} = b_{34} = b_{56} = 0 \quad (A.29)$$

For orthotropic material, the number of constants A_{ijkl} (and b_{ijkl}) can be reduced to 9 from 13. The matrix form is:

$$\begin{bmatrix} b_{11} & b_{12} & b_{13} & 0 & 0 & 0 \\ & b_{22} & b_{23} & 0 & 0 & 0 \\ & & b_{33} & 0 & 0 & 0 \end{bmatrix} \quad (A.30)$$

References

- Abe, H., Nakamura, T., Motomiya, M., Konn, K., and Arai, S., "Stresses in left ventricular wall and biaxial stress-strain relation of the cardiac muscle fiber for the potassium-arrested heart," J. of Biomechanical Eng., 1978; vol. 100 : pp.116-121.
- Adkins, J.E., "Cylindrically symmetrical deformations of incompressible elastic materials reinforced with inextensible cords", J. Rat. Mech. Analysis, 1956; vol. 5 : pp. 198-202.
- Adkins, J.E., and Rivlin, R.S., "Large elastic deformations of isotropic materials", Phil. Trans. R. Soc., 1955; vol. (A)248 : pp.201-223.
- Anversa, P., Olivetti, G., Melissari, M., and Loud, A.V., "Morphometric study of myocardial hypertrophy induced by abdominal aortic stenosis", Lab. Invest., 1979; vol. 40 : pp.341-349.
- Apter, J.T., "Correlation of viscoelastic properties of large arteries with microscopic structure", Circ. Res., 1966; vol. 19 : pp.104-121.
- Avasthey, P., and Wood, E.H., "Intrathoracic and venous pressure relationships during responses to changes in body position", J. of Appl. Physiol., 1974; vol. 37 : pp.166
- Banga, I., "Structure and function of elastin and collagen", Akademiai Kiado, Budapest, 1966.
- Barbenel, J.C., Evans, J.H., and Finlay, J.B., "Stress-strain-time relations for soft connective tissues", in Perspectives in Biomedical Engineering, ed. Kenedi, R.M., 1973 ; pp. 165.
- Barnard, H.L., "The function of the pericardium", Proc. of the Physiological Society, 1898 ; pp. 43-48.
- Belsely, D., Kuh, E., and Welsch, R., "Regression analysis : Identifying influential data and sources of colinearity", John Wiley, New York, 1980.
- Bhargava, V., Shabetai, R., Ross, J., Jr., et al., "The effect of pericardium on pressure-segment length relationship in canine left ventricle in acute volume overload", Am. Heart J., 1983; vol. 105 : pp. 995
- Bingham, D.N., and Dehoff, P.H., "A constitutive equation for the canine anterior cruciate ligament," J. of Biomechanical Eng. 1979; vol. 101 : pp. 15-22.
- Blatz, P.J., "On the mechanical behavior of elastic animal tissue," Trans. of the Society of Rheology, 1969; vol. 13(1) : pp. 83-102.

- Broom, N.D., "Simultaneous morphological and stress-strain studies of the fibrous components in wet heart valve leaflet tissue", *Connective Tissue Research*, 1978 ; vol. 6 : pp. 37-50.
- Broom, N.D., "The stress-strain and fatigue behavior of glutaraldehyde preserved heart valve tissue", *J. of Biomechanics*, 1977; vol. 10 : pp. 707-724.
- Chen, Y.L., and Fung, Y.C., "Stress-strain history relations of rabbit mesentery in simple elongation", *Biomechanical Symposium, ADM-2, ASME*, 1973; pp. 9-10.
- Chuong, C.J. and Fung, Y.C., "Compressibility and constitutive equation of arterial wall in radial compression experiments," *J. Biomechanics*, 1984; vol. 17(1) : pp. 35-40.
- Chuong, C.J., and Fung, Y.C., "Three-dimensional stress distribution in arteries," *J. of Biomechanical Eng.*, 1983; vol. 105 : pp. 268-274.
- Comninou, M., and Yannas, I.V., "Dependence of stress-strain nonlinearity of connective tissues on the geometry of collagen fibers," *J. of Biomechanics*, 1976; vol. 9 : pp. 429-433.
- Decraemer, W.F., Maes, M.A., and Vanhuyse, V.J., "An elastic stress-strain relation for soft biological tissues based on a structural model," *J. of Biomechanics*, 1980; vol. 13 : pp. 463-468.
- Decraemer, W.F., Maes, M.A., Vanhuyse, V.J., and Vanpeperstraete, P., "A non-linear viscoelastic constitutive equation for soft biological tissues, based upon a structural model," *J. of Biomechanics*, 1980; vol. 13 : pp. 559-564.
- Dehoff, P.H., "On the nonlinear viscoelastic behavior of soft biological tissues," *J. of Biomechanics*, 1978; vol. 11: pp. 35-40.
- Demer, L.L., and Yin, F.C.P., "Passive biaxial mechanical properties of isolated canine myocardium," *J. Physiol.*, 1983; vol. 339 : pp. 615-630.
- Demiray, H., "A note on the elasticity of soft biological tissues", *J. of Biomechanics*, 1972; vol. 5 : pp. 309-311.
- Demiray, H., "On the constitutive equations of biological materials", *Trans. of ASME , J. of Appl. Mech.*, 1975; vol. 241(E) : pp. 242-243.
- Demiray, H., "Stresses in ventricular wall", *Trans. of ASME , J. of Appl. Mech.*, 1976; vol. 242 : pp. 194-197.

- Demiray, H., "Incremental elastic modulus for ventricles in diastole," J. of Biomechanics, 1984; vol. 17(8) : pp. 621-626.
- Demiray, H., "Incremental elastic modulus for isotropic elastic bodies with application to arteries," J. of Biomechanical Eng., 1983; vol. 105 : pp. 308-309.
- Demiray, H., "Large deformation analysis of some basic problems in biophysics," Bulletin of Mathematical Biology, 1976; vol. 38 : pp. 701-712.
- Demiray, H., "Large deformation analysis of some soft biological tissues," J. of Biomechanical Eng., 1981; vol. 103 : pp. 73-78.
- Demiray, H., and Vito, R.P., "On large periodic motions of arteries," J. Biomechanics, 1983; vol. 16(8) : pp. 643-648.
- Efron, B., "Computers and the theory of statistics : thinking the unthinkable", S.I.A.M. Rev., 1979; vol. 21 : pp. 460-479.
- Eisenberg, B.R., Kuda, A.M., and Peter, J.B., "Stereological analysis of mammalian skeletal muscle : soleus muscle of adult guinea pig", J. Cell Biol., 1974; vol. 60 : pp. 732-754.
- Elias, H., and Hyde, D.H., "A guide to practical stereology", National Library of Medicine, Krager, N.Y., 1983.
- Ferrans, V.J., Spray, T.C., Billingham, M.E., and Roberts, W.C., "Structural changes in glutaraldehyde-treated porcine heterografts used as substitute cardiac valves", Am. J. of Cardiology, 1978; vol. 41 : pp. 1159-1184.
- Fowler, N.O., "Disease of the pericardium" , Part V. in the Heart (ed. Hurst, J.W., and Bruce, R.), McGraw Hill, 1970; pp. 1254-1269.
- Fowler, N.O., "The pericardium in health and disease", Futura Publishing Company, Inc., N.Y., 1985.
- Freeman, G.L., LeWinter, M.M., "Pericardial adaptations during chronic cardiac dilation in dogs," Circ. Res. 1984; vol. 54(3) : pp. 294-300.
- Freeman, G.L., LeWinter, M.M., "Role of parietal pericardium in acute, severe mitral regurgitation in dogs," Am. J. Cardiol. 1984; vol. 54 : pp.217-219.
- Fung, Y.C., "Elasticity of soft tissues in simple elongation", Am. J. of Physiology, 1967; pp. 1532-1544.
- Fung, Y.C., Perrone, N., and Anlinker, M. (ed.), "Biomechanics-Its foundations and objectives", Prentice-Hall, Inc., Englewood. Cliffs, N.J., 1972.

- Fung, Y.C., "Biorheology of soft tissues", Biorheology, 1973; vol. 10 :
- Fung Y.C., "Inversion of a class of nonlinear stress-strain relationships of biological soft tissues," J. of Biomechanical Eng., 1979; vol. 101 : pp. 23-27.
- Fung, Y.C., "The lung - a perspective of biomechanics development," J. of Biomechanical Eng., 1981; vol. 103 : pp. 91-96.
- Fung, Y.C., Fronek, K., and Patitucci, P., "Pseudoelasticity of arteries and the choice of its mathematical expression," Am. Physiological Society, 1979; pp. H620-631.
- Fung, Y.C., "Biomechanics-Mechanical properties of living tissues", Springer-Verlag, N.Y., 1981.
- Fung, Y.C., "Perspectives of soft tissue mechanics", Biomechanics ; Principle and applications.(ed. Huijkes,R., Van Campen,D., and De Wijn,J.), Martinus Nijhoff Publishers, 1982.
- Fung, Y.C., "On the foundations of biomechanics", J. of Appl. Mech., 1983; vol. 50 : pp. 1003-1009.
- Galford, J.E., and McElhaney, J.H., "A viscoelastic study of scalp, brain, and dura", J. of Biomechanics, 1970; vol. 3 : pp. 211-221.
- Ghista, D.N., and Sandler, H., "An analytic elastic-viscoelastic model for the shape and the forces in the left ventricle", J. of Biomechanics, 1969; vol. 2 :
- Goldberger, A.L., Shabetai, R., Bhargava, V., West, B.J. and Mandell, A.J., "Nonlinear dynamics, electrical alternant, and pericardial tamponade," Am. Heart J., 1984; vol. 107(6) : pp. 1297-1299.
- Gottesman, T., and Hashin, Z., "Analysis of viscoelastic behavior of bones on the basis of microstructure," J. of Biomechanics, 1980; vol. 13 : pp. 89-96.
- Gou, P.F., "Strain energy function for the biological tissues", J. of Biomechanics, 1970; vol. 3 : pp. 547-550.
- Gould, P., Ghista, D., Brombolich, L., and Mirsky, I., "In vivo stresses in the human left ventricular wall : Analysis accounting for the irregular 3-dimensional geometry and comparison with idealized geometry analyses", J. of Biomechanics, 1972; vol. 5 : pp. 521-539.
- Green, A.E., and Adkins, J.E., "Large elastic deformations" (2nd. ed.) Clarendon Press, Oxford, 1970.
- Green, A.E., and Zerna, W., "Theoretical elasticity", Clarendon Press, Oxford, 1968.

- Guyton, J.R., "Locational stereology performed with sampling fields in rat aortic wall, a polarized tissue", *J. of Microscopy*, 1984; vol. 135 : pp. 103-114.
- Hart-Smith, L.J., and Crisp, J.D.C., "Large elastic deformation of thin rubber membranes", *Int. J. Eng. Sci.*, 1967; vol. 5 : pp. 1-24.
- Haut, R.C., and Little, R.W., "Rheological properties of canine anterior cruciate ligaments ", *J. of Biomechanics*, 1969; vol. 2 : pp. 289-298.
- Haut, R.C., and Little, R.W., "A constitutive equation for collagen fibers", *J. of Biomechanics*, 1972; vol. 5 : pp. 423-430.
- Hayes, W.C., and Mockros, L.F., "Viscoelastic properties of human articular cartilage", *J. of Appl. Physiology*, 1971; vol. 31 : pp. 562-568.
- Hayes, W.C., Keer, L.M., Herrmann, G., and Mockros, L.F., "A mathematical analysis for indentation tests of articular cartilage", *J. of Biomechanics*, 1972; vol. 5 : pp. 541-551.
- Hess, O.M., Bhargava, V., Ross, J., Jr., and Shabetai, R., "The role of the pericardium in interactions between cardiac chambers." *Am. Heart J.*, 1983; vol. 106 : pp. 1377-1383.
- Hildebrandt, J., Fukaya, H., and Martin, C.J., "Simple uniaxial and uniform biaxial deformation of nearly isotropic incompressible tissues," *Biophysical Journal*, 1969; vol. 9 : pp. 781-791.
- Hildebrandt, J., Fukaya, H., and Martin, C.J., "Stress-strain relations of tissue sheets undergoing uniform two-dimensional stretch," *J. of Applied Physiology*, 1969; vol. 27(5) : pp. 758-762.
- Hoffman, A.H., and Grigg, P., "A method for measuring strains on soft tissue," *J. Biomechanics*, 1984; vol. 17(10) : pp. 795-800.
- Holt, J.P., "The normal pericardium," *The American Journal of Cardiology*, 1970; vol. 26 : pp. 455-465.
- Hudetz, A.G., "Incremental elastic modulus for orthotropic incompressible arteries," *J. of Biomechanics*, 1979; vol. 12 : pp. 651-655.
- Humphrey, J.D., "Mechanical behavior of excised visceral pleura", Ph.D. thesis, 1985 : Georgia Institute of Technology.
- Hurst, J.W., *The Heart (6th Ed.)*, McGraw-Hill Book Company, New York, 1985.

- Guyton, J.R., "Locational stereology performed with sampling fields in rat aortic wall, a polarized tissue", *J. of Microscopy*, 1984; vol. 135 : pp. 103-114.
- Hart-Smith, L.J., and Crisp, J.D.C., "Large elastic deformation of thin rubber membranes", *Int. J. Eng. Sci.*, 1967; vol. 5 : pp. 1-24.
- Haut, R.C., and Little, R.W., "Rheological properties of canine anterior cruciate ligaments", *J. of Biomechanics*, 1969; vol. 2 : pp. 289-298.
- Haut, R.C., and Little, R.W., "A constitutive equation for collagen fibers", *J. of Biomechanics*, 1972; vol. 5 : pp. 423-430.
- Hayes, W.C., and Mockros, L.F., "Viscoelastic properties of human articular cartilage", *J. of Appl. Physiology*, 1971; vol. 31 : pp. 562-568.
- Hayes, W.C., Keer, L.M., Herrmann, G., and Mockros, L.F., "A mathematical analysis for indentation tests of articular cartilage", *J. of Biomechanics*, 1972; vol. 5 : pp. 541-551.
- Hess, O.M., Bhargava, V., Ross, J., Jr., and Shabetai, R., "The role of the pericardium in interactions between cardiac chambers." *Am. Heart J.*, 1983; vol. 106 : pp. 1377-1383.
- Hildebrandt, J., Fukaya, H., and Martin, C.J., "Simple uniaxial and uniform biaxial deformation of nearly isotropic incompressible tissues," *Biophysical Journal*, 1969; vol. 9 : pp. 781-791.
- Hildebrandt, J., Fukaya, H., and Martin, C.J., "Stress-strain relations of tissue sheets undergoing uniform two-dimensional stretch," *J. of Applied Physiology*, 1969; vol. 27(5) : pp. 758-762.
- Hoffman, A.H., and Grigg, P., "A method for measuring strains on soft tissue," *J. Biomechanics*, 1984; vol. 17(10) : pp. 795-800.
- Holt, J.P., "The normal pericardium," *The American Journal of Cardiology*, 1970; vol. 26 : pp. 455-465.
- Hudetz, A.G., "Incremental elastic modulus for orthotropic incompressible arteries," *J. of Biomechanics*, 1979; vol. 12 : pp. 651-655.
- Humphrey, J.D., "Mechanical behavior of excised visceral pleura", Ph.D. thesis, 1985 : Georgia Institute of Technology.
- Hurst, J.W., *The Heart (6th Ed.)*, McGraw-Hill Book Company, New York, 1985.

- Hwang, N.H.C., and Nan, X.Z., "Prosthetic heart valve replacements," CRC Critical Reviews in Biomedical Engineering, 1982; vol. 9(2) : pp. 99-132.
- Ishihara, T., Ferrans, V.J., Jones, M., Boyce, S.W. Kawanami, O., and Roberts, W.C., "Histologic and Ultrastructural features of normal human parietal pericardium," Am. J. Cardiol., 1980; vol. 46 : pp. 744-753.
- Jenkins, R.B., and Little, R.W., "A constitutive equation for parallel-fibered elastic tissue ", J. of Biomechanics, 1974; vol. 7 : pp. 397-402.
- Kanatani, K.I., "Procedures for stereological estimation of structural anisotropy", International J. of Engineering Science, 1985; vol. 23(5) : pp. 587-598.
- Kenedi, R.M., Gibson, T., Evans, J.H., and Barbenel, J.C., "Tissue mechanics", Phys. Med. Biol., 1975; vol. 20(5) : pp. 699-717.
- Lanir, Y., and Fung, Y.C., "Two dimensional mechanical properties of rabbit skin I.-Experimental system ", J. of Biomechanics, 1974; vol. 7 : pp. 29-34.
- Lanir, Y., and Fung, Y.C., "Two dimensional mechanical properties of rabbit skin II.-Experimental results", J. of Biomechanics, 1974; vol. 7 : pp. 171-182.
- Lanir, Y., "The rheological behavior of the skin", Biorheology, 1979; vol. 16 : pp. 191-202.
- Lanir, Y., "A microstructure model for the rheology of mammalian tendon", J. of Biomechanical Eng., 1980; vol. 102 : pp. 332-339.
- Lanir, Y., "Constitutive equations for fibrous connective tissues," J. of Biomechanics, 1983; vol. 16(1) : pp. 1-12.
- Lanir, Y., "Constitutive equations for the lung tissue," J. of Biomechanical Eng., 1983; vol. 105 : pp. 374-380.
- Lanir, Y., "A structural theory for the homogeneous biaxial stress-strain relationship in flat collagenous tissues," J. of Biomechanics, 1979; vol. 12 : pp. 423-436.
- Lau, I.V., "Effect of timing and velocity of impact on ventricular myocardial rupture," J. of Biomechanical Eng., 1983; vol. 105 : pp. 1-5.
- Lee, J.M., and Boughner, D.R., "Mechanical properties of human pericardium," Circ. Res., 1985; vol. 57(3) : pp. 475-481.
- Lee, J.M., and Boughner, D.R., "Tissue mechanics of canine pericardium in different test environments," Circ. Res., 1981; vol. 49(2) : pp. 533-544.

- Lee, M.C. LeWinter, M.M., Freeman, G.L., Shabetai, R., and Fung, Y.C., "Biaxial mechanical properties of the pericardium in normal and volume overload dogs," *Am.J. Physiol.*, 1985; vol. 249 (2 pt 2) : pp H222-230.
- Lekhnitskii, S.G., "Theory of elasticity of anisotropic body", Mir. Publishers, 1981.
- Lianis, G., "Constitutive equations of viscoelastic solids under finite deformations", A&ES Report No. 63-11, Purdue University, 1963.
- Lianis, G., "Application of thermodynamics of viscoelastic materials with fading memory : Integral constitutive equations", *International J. of Non-linear Mechanics*, 1970 ; vol. 5 : pp. 23-34.
- Ligas, J.R., "A non-linearly elastic, finite deformation analysis applicable to the static mechanics of excised lungs," *J. Biomechanics* 1984; vol.17(8) : pp. 549-552.
- Lockett, F.J., "Nonlinear viscoelastic solids", Academic Press, N.Y., 1972.
- Luna, L.G.,(ed.), "Manual of histologic staining methods of the Armed Forces Institute of Pathology", 3rd. ed., McGraw-Hill Book Company, N.Y., 1968.
- Manak, J.J., "The two-dimensional in vitro passive stress-strain elasticity relationships for the steer thoracic aorta blood vessel tissue," *J. of Biomechanics*, 1980; vol. 13 : pp. 637-646.
- Maruyama, Y., Ashikawa, K., Isoyama, S., Knatsuka, H., Ino-oka, E., and Takishima, T., "Mechanical interactions between four heart chambers with and without the pericardium in canine hearts," *Circ. Res.*, 1982; vol. 50(1) : pp. 86-100.
- Mchale, P.A., and Greenfield, J.C., Jr., "Evaluation of several geometrical models for estimation of left ventricular circumferential wall stress", *Circ. Res.*, 1973; vol. 33 : pp. 303.
- Mirsky, I., "Left ventricular stresses in the intact heart", *Biophysics J.*, 1969; vol. 9 : pp. 189-208.
- Mirsky, I., "Ventricular and arterial wall stresses based on large deformation analyses", *Biophysics J.*, 1973; vol. 13 : pp. 1141-1159.
- Mirsky, I., and Rankin, J.S., "The effects of geometry, elasticity, and external pressures on the diastolic pressure-volume and stiffness-stress relations," *Circ. Res.*, 1979; vol. 44(5) : pp. 601-611.

- Mooney, M., "The theory of large elastic deformation", J. Appl. Physics, 1940; vol. 11 : pp. 582-592.
- Moskowitz, S.E., "Constitutive stress-strain relations for the myocardium in diastole," J. Biomechanics, 1985; vol.18(No.3) : pp. 179-189.
- Moskowitz, S.E., "Passive stress-strain relation for the right ventricle in diastole," J. of Biomechanics, 1982; vol. 15(4) : pp. 249-256.
- Mow, V.C., Kuei, S.C., Lai, W.M., and Armstrong, C.G., "Biphasic creep and stress relaxation of articular cartilage in compression : Theory and experiments", ASME J. of Biomechanical Eng., 1980; vol. 102 : pp. 73-84.
- Nelemans, F.A., "Die Funktion Des Perikards", Arch. Neerl. Physiol., 1940; vol. 24 : pp. 337-390.
- Nishimura, R.A., Kazmier, F.J., Smith, H.C., and Danielson, G.K., "Right ventricular outflow obstruction caused by constrictive pericardial disease," Am. J. Cardiol. 1985; Vol. 55 : pp. 1447-1448.
- Patel, D.J., and Vaishnav, R.N., "The rheology of large blood vessels", Chapter 2. in Cardiovascular Fluid Dynamics (ed. Bergel, D.H.), vol.2 : pp. 1-64., Academic Press, N.Y.
- Patitucci, P., "Computer programs for fitting pseudo-strain energy functions of soft tissues experimental stress and strain data", DECUS, One Iron Way, MR23/E55, Marlboro, MA 01752, 1983.
- Pinto, J.G., and Fung, Y.C., "Mechanical properties of heart muscle in the passive state", J. of Biomechanics, 1973; vol. 6 : pp. 597-616.
- Pinto, J.G., and Patitucci, P.J., "Visco-elasticity of passive cardiac muscle", J. of Biomechanical Eng., 1980; vol. 102 : pp. 57-61.
- Portmans, L.J.M.G., Sauren, A.A.H.J, and Rousseau, E.P.M., "Parameter estimation using the quasi-linear viscoelastic model proposed by Fung," J. of Biomechanical Eng., 1984; vol. 106 : pp.198-203.
- Price, J., Patitucci, P., and Fung, Y.C., "Mechanical properties of resting tenia coli smooth muscle", American J. of Physiology, 1979; vol. 236(5) : pp. C211-C220.
- Rabkin, S., Berghause, D.G., and Bauer, H.F., "Mechanical properties of the isolated canine pericardium," J. of Applied Physiology, 1974; vol. 36(1) : pp. 69-73.

- Rabkin, S.W., and Hsu, P.H., "Mathematical and mechanical modeling of stress-strain relationship of pericardium," *Am. J. of Physiology*, 1975; vol. 299(4) : pp. 896-900.
- Radegran, K., and Bjork, V.O., "Use of glutaraldehyde treated bovine pericardium in cardiac surgery", *Proceedings Shiley European Cardiovascular Conference, Chamonix, France, 1979.*
- Rousseau, E.P.M., Sauren, A.A.H.J., van Hout, M.C., and Steenhoven, A.A., "Elastic and viscoelastic material behavior of fresh and glutaraldehyde-treated porcine aortic valve tissue," *J. of Biomechanics*, 1983; vol. 16(5) : pp. 339-348.
- Sabbah, H.N., Hamid, M.S., and Stein, P.D., "Estimation of mechanical stresses on closed cusps of porcine bioprosthetic valves," *Am. J. Cardiol.*, 1985; vol. 55 : pp. 1091-1096.
- Sahay, K.B., "On the choice of strain energy function for mechanical characterization of soft biological tissues," *Engineering in Medicine*, 1984; vol. 13(1) : pp. 11-13.
- Sanjeevi, R., "A viscoelastic model for the mechanical properties of biological materials," *J. of Biomechanics*, 1982; vol. 15(2) : pp. 107-110.
- Sanjeevi, R., Somanathan, N., and Ramaswamy, D., "A viscoelastic model for collagen fibers," *J. of Biomechanics*, 1982; vol. 15(3) : pp. 181-184.
- Sauren, A.A.H.J., and Rousseau, E.P.M., "A concise sensitivity analysis of the quasi-linear viscoelastic model proposed by Fung," *J. of Biomechanical Eng.*, 1983; vol.105 : pp.92-95.
- Sauren, A.A.H.J., van Hout, M.C., van Steenhoven, A.A., Veldpaus, F.E., and Janssen, J.D., "The mechanical properties of porcine aortic valve tissues," *J. of Biomechanics*, 1983; vol. 16(5) : pp. 327-338.
- Schmid-Schonbein, G.W., and Woo, S.L.Y., and Zweifach, B.W., (ed.), "Frontiers in biomechanics", 1986; Springer-Verlag., N.Y.
- Schoen, F.J., Titus, J.L., and Lawrie, G.M., "Bioengineering aspects of heart valve replacement," *Annals of Biomedical Engineering*, 1982; vol. 10 : pp. 97-128.
- Scholtens, B.J.R., Booij, H.C., and Leblans, P.J.R., "Nonlinear viscoelastic analysis of uniaxial stress-strain measurements of elastomers at constant stretching rates," *J. of Rheology*, 1986; vol. 302(2) : pp. 301-312.
- Shabetal, R., "The function of the pericardium", Chapter 2. in *Pericardium in Health and Disease*, (ed. Fowler, N.O.), 1985; Futura Publishing Company, Inc.

- Shoemaker, P.A., "Irreversible thermodynamics, the constitutive law, and a constitutive model for two-dimensional soft tissues", Ph.D. thesis, 1984; Univ. of California, San Diego.
- Simon, R.R., Coats, R.S., and Woo, S. L-Y., "Relaxation and creep quasilinear viscoelastic models for normal articular cartilage," J. of Biomechanical Eng., 1984; vol. 106 : pp. 159-164.
- Slutsky, R.A., Peck, W.W., Mancini, G.B.J., and Shabetai, R., "Intravascular and extravascular pulmonary fluid volumes during acute experimental pericardial tamponade," Am. Heart J. 1984; vol. 108(1) : pp. 90-96.
- Smiseth, O.A., Refsum, H. and Tyberg, J.V.,; "Pericardial pressure assessed by right atrial pressure," Am. Heart J., 1984; vol. 108(3 pt 1) : pp. 603-605.
- Sokolnikoff, I.S., "Mathematical theory of elasticity" (2nd. ed.) , McGraw-Hill Book Company, INC., New York, 1956.
- Spencer, A.J.M., "Deformations of fiber-reinforced materials", Clarendon Press, Oxford, 1972.
- Spotnitz, H.M., and Kaiser, G.A., "The effect of pericardium on pressure-volume relations in the canine left ventricle," J. of Surgical Research, 1971; vol. 11(7) : pp. 375-380.
- Stamenovic, D., and Wilson, T.A., "A strain energy function for lung parenchyma," J. of Biomechanical Eng., 1985; vol.107 : pp. 81-86.
- Stokes, I. and Greenapple, D.M., "Measurement of surface deformation of soft tissue," J. Biomechanics, 1985; vol. 18(1) : pp. 1-7.
- Stokland, O., Miller, M.M., Lekven, J., Ilebakk, A., "The significance of the intact pericardium for cardiac performance in the dog," Circ. Res. 1980; vol.47(1) : pp 27-32.
- Thubrikar, M., and Eppink, R.T., "A method for analysis of bending and shearing deformations in biological tissue," J. of Biomechanics, 1982; vol. 15(7) : pp. 529-536.
- Tong, P., and Fung, Y.C. "The stress-strain relationship for the skin," J. of Biomechanics, 1976; vol. 9 : pp. 649-657.
- Trowbridge, E.A., Black, M.M., and Daniel, C.L., "The mechanical response of glutaraldehyde-fixed bovine pericardium to uniaxial load", J. of Material Science, 1985; vol. 20 : pp. 114-140.
- Trowbridge, E.A., and Crofts, C.E., "Evidence that deformation which occur during mechanical conditioning of bovine

- pericardium are not permanent", *Biomaterials*, 1986; vol. 7 : pp. 49-54.
- Trowbridge, E.A., and Crofts, C.E., "The standardization of gauge length: Its influence on the relative extensibility of natural and chemically modified pericardium", *J. of Biomechanics*, 1986; vol. 12 : pp. 1023-1033.
- Tyson, G.S., Maier, G.W., Olsen, C.O., Davis, J.W., Rankin, J.S. "Pericardial influences on ventricular filling in the conscious dog," *Circ. Res.* 1984; Vol. 54(2) : pp. 173-184.
- Underwood, E.E., "Quantitative stereology", Addison Wesley, 1970.
- Vaishnav, R.N., "Mathematical Characterization of the nonlinear rheological behavior of the vascular tissue", *Biorheology*, 1980; vol. 17 : pp. 219-226.
- Vaishnav, R.N., and Vossoughi, J., "Incremental formulations on vascular mechanics," *J. of Biomechanical Eng.*, 1984; vol. 106 : pp. 105-111.
- Valanis, K.C., and Landel, R.F., "The strain energy function of a hyperelastic material in terms of the extension ratio", *J. of Appl. Physiology*, 1967; vol. 38 : pp. 2997-3002.
- Vawter, D.L., "Poisson's ratio and incompressibility," *J. of Biomechanical Eng.*, 1983; vol. 105 : pp. 194-195.
- Vawter, D.L., Fung, Y.C., and West, J.B., "Constitutive equation of lung tissue elasticity," *J. of Biomechanical Eng.*, 1979 : vol. 101, pp.38-45.
- Veronda, D.R., and Westman, R.A., "Mechanical characterization of skin : Finite deformations", *J. of Biomechanics*, 1970; vol. 3 : pp. 111-124.
- Viidik, A., and Ekholm, R., "Light and electron microscopic studies of collagen fibers under strain", *Z. Anat. Entwickl. Gesch.*, 1968; vol. 127 : pp. 154-164.
- Vito, R.P., "A note on arterial elasticity", *J. of Biomechanics*, 1973; vol. 6 : pp. 561-564.
- Vito, R.P., "The role of the pericardium in cardiac mechanics", *J. of Biomechanics*, 1979; vol. 12 : pp. 587-592.
- Vito, R.P., "The mechanical properties of soft tissues - I: a mechanical system for biaxial testing," *J. of Biomechanics*, 1980; vol. 13(11) : pp. 947-950.
- Vito, R.P., and Hickey, J., "The mechanical properties of soft tissues - II: the elastic response of arterial segments" *J. of Biomechanics*, 1980; vol. 13(11) : pp. 951-958.

- Vito, R.P., and Demiray, H., "The mechanics of pericardium : Pericardial effusion", Proc. 8th. Northeast Bioengineering Conference, 1980.
- Vogel, S., and Papanicolaou, M.N., "A constant stress creep testing machine," J. of Biomechanics, 1983; vol. 16(2) : pp. 153-156.
- Voukydis, P.C., "The myocardium as a composite material : Analysis", Bull. Math. Biol., 1972; vol. 34 : pp. 173-204.
- Voukydis, P.C., "Geometrical parameters of the individual myocardial fibers", Bull. Math. Biol., 1972; vol. 34 : pp. 205-211.
- Voukydis, P.C., "Fiber stress profile in the left ventricle of the heart during diastole : Effects of distension and hypertrophy", Bull. Math. Biol., 1972; vol. 34 : pp. 379-392.
- Wang, C.Y., and Sonnenblick, E.H., "Dynamic pressure distribution inside a spherical ventricle", J. of Biomechanics, 1979; vol. 12 : pp. 9-12.
- Weibel, E.R., "Principle and methods for the morphometric study of lung", Lab. Inv., 1963; vol. 12 : pp. 131-155.
- Weibel, E.R., and Eliad, H., "Quantitative methods in morphology", Springer-Verlag, N.Y., 1967.
- Weibel, E.R., "Stereological method. I.-Practical methods for biological morphometry", Academic Press, London, 1979.
- Wiegner, A.W., and Bing, O.H.L., "Mechanical and structural correlates of canine pericardium," Circ. Res., 1981; vol. 49(3) : pp. 809-814.
- Wiegner, A.W., and Bing, O.H.L., "Mechanics of myocardial relaxation: application of model to isometric and isotonic relaxation of rat myocardium," J. of Biomechanics, 1982; vol. 15(11) : pp. 831-840.
- Wong, A.Y.K., and Rautaharju, D.M., "Stress distribution within the left ventricular wall approximated as a thick ellipsoidal shell", Am. Heart J., 1968; vol. 75 : pp. 649-662.
- Woo, S. L-Y., Gomez, M.A., and Akeson, W.H., "The time and history-dependent viscoelastic properties of the canine medial collateral ligament," J. of Biomechanical Eng., 1981; vol. 103 : pp. 293-298.
- Woo, S. L-Y., Simon, B.R., Kuei, S.C., and Akeson, W.H., "Quasi-linear viscoelastic properties of normal articular cartilage", J. of Biomechanical Eng., 1980; vol. 102 : pp. 85-90.

- Woodroof, E.A., "The use of glutaraldehyde and formaldehyde for processing tissue heart valves", in Tissue Heart Valves (ed. Ionescu, M.I.), 1979; London.
- Wu, H.C., and Yao, R.F., "Mechanical behavior of the human annulus fibrosus," J. of Biomechanics, 1976; vol. 100 : pp. 44-48.
- Wu, S.G. and Lee, G.C., "On nonlinear viscoelastic properties of arterial tissue," J. of Biomechanical Eng., 1984; vol. 106 : pp. 42-49.
- Wu, S.G., Lee, G.C. and Tseng, N.T., "Nonlinear elastic analysis of blood vessels," J. of Biomechanical Eng., 1984; vol. 106 : pp. 376-383.
- Yin, F.C.P., Chew, P.H., and Zeger, S.L., "An approach to quantification of biaxial tissue stress-strain data," J. Biomechanics, 1986; vol. 19(No.1) : pp.27-37.
- Young, J.T., Vaishnav, R.N., and Patel, D.J., "Nonlinear anisotropic viscoelastic properties of canine arterial segments," J. of Biomechanics, 1977; vol. 10 : pp. 549-559.

Captions for Figures

- Figure (1) The pericardium and heart wall.
- Figure (2) Flow chart of the bi-axial test system.
- Figure (3) Sideview of the bi-axial test equipment.
- Figure (4) Flowchart of the video digitizing system.
- Figure (5) Electrical resistance thickness measuring device.
- Figure (6) Schematic diagram of two reading stage for thickness measurement: (a) contact stage (b) lost-contact stage.
- Figure (7) Thickness measurement - the change of two stage reading values with time for specimen #02.
- Figure (8) Specimen mounting.
- Figure (9) Mapping of tracking particle position from global coordinates to natural coordinates.
- Figure (10) Schematic diagram of a bi-axially stretched specimen for stress measurement.
- Figure (11) Bi-axial stretching of the specimen.
- Figure (12) The orientation of the coordinate systems.
- Figure (13) Specimen sectioning for the microscopic slides.
- Figure (14) Cross-section of layered structure ; example for the stereological analysis.
- Figure (15) Geometry of collagen fiber bundles.
- Figure (16) Strain-stress curve of uniform stretching test on specimen #03.
- Figure (17) Strain rate insensitivity.
- Figure (18) Strains imposed on target region under uniform bi-axial stretching test.
- Figure (19) Actual particle histories during uniform bi-axial stretching test.
- Figure (20) The log function plot of Figure (16).
- Figure (21) Strain-stress curve of nonuniform stretching test on specimen #03.

- Figure (22) Strain imposed on target region under non-uniform bi-axial stretching test.
- Figure (23) Actual particle histories during non-uniform bi-axial stretching test.
- Figure (24) Strain-stress curve of the constant lateral displacement test on specimen #02.
- Figure (25) Constant lateral displacement test results when the lateral dimension was held approximately constant at $E_{11} = 0, 0.185$ and 0.198 , respectively.
- Figure (26) E_{22} versus E_{11} in the constant lateral displacement tests.
- Figure (27) Actual particle histories of the central tracking region during the constant lateral displacement test. (The constrained E_{11} is approximately 0.)
- Figure (28) Actual particle histories of the central tracking region during the constant lateral displacement test. (The constrained E_{11} is approximately 0.185)

Headings for Tables

Table (1) The previously suggested strain energy function forms.

Table (2) Thickness measurement data for the specimen #01.

Table (3) Thickness measurement data for the specimen #03.